Illuminating Dark Energy Fluctuations

A study of spatial correlations in dark energy and their effect on the luminosity distance

by

Casper J.G. Vedder

Daily supervisor: dr. E. Belgacem
First supervisor: dr. N. E. Chisari
Second supervisor: dr. T. Prokopec

Institute for Theoretical Physics
Utrecht University

September, 2022

Utrecht University

Abstract

The origin of dark energy driving the accelerated expansion of the universe is still mysterious. In this thesis we explore the possibility that dark energy fluctuates, resulting in spatial correlations. Due to these fluctuations, the Hubble rate itself becomes a fluctuating quantity. We discuss the effect this has on measurements of type Ia supernovae, which are used to constrain the luminosity distance. We show that the luminosity distance is affected by spatial correlations in several ways. First, the luminosity distance becomes dressed by the fluctuations, thereby differing from standard ΛCDM. Second, angular correlations become visible in the two-point correlation function of the luminosity distance. To investigate the latter we construct the angular power spectrum of luminosity distance fluctuations. We then perform a forecast for two supernova surveys, the ongoing Dark Energy Survey (DES) and the upcoming Legacy Survey of Space and Time (LSST), and compare this effect with relativistic lensing effects from perturbed ΛCDM. We find that the signal can rise above the lensing effects and that LSST could test this effect for a large part of the parameter space. As an example, a specific realisation of such a scenario is that quantum fluctuations of some field in the early universe imprint spatial correlations with a predictable form in the dark energy density today. In this case, the Hubble rate fluctuates due to the intrinsic quantum nature of the dark energy density field. We study whether the signal of this specific model would be measurable, and conclude that testing this model with LSST would be challenging. However, taking into account a speed of sound $c_s < 1$ of the dark energy fluid can make this model observable.

Contents

1 Introduction

Cosmology is the study of the universe as a whole. To make predictions, both a theory for gravity and a theory of matter are needed. The most well known theory of gravity is general relativity, which links the matter content of the universe to its geometry, while the current best theory of matter consists in the Standard Model of particle physics. Both these theories have passed numerous tests over the years. However, cosmological observations [1–5] tell us that we are missing a fundamental piece of the puzzle, as we are forced to introduce several ingredients that go beyond the Standard Model of particle physics to accommodate these observations. This has led to the currently accepted ΛCDM model, whose main components are cold dark matter (CDM) and a cosmological constant Λ. Despite both components lacking a fundamental theoretical underpinning, ΛCDM has been in agreement with a large number of observational data. Therefore its theoretical understanding has provided one of the most profound challenges in current physics and astronomy research. We will focus on the component driving the accelerated expansion of the universe, which in ΛCDM is the cosmological constant Λ, but is more generally referred to as *dark energy*. Dark energy is needed to explain cosmic acceleration, which was discovered using type Ia supernovae measurements in 1998 [6, 7] and later corroborated by, among others, measurements of the cosmic microwave background (CMB) [1]. The physical origin of dark energy is shrouded in mystery, its substance should exert a negative repulsive pressure and its energy density should not dilute under the expansion of the universe. A natural explanation would be the vacuum energy known from quantum field theory, yet its predictions for the vacuum energy are much

too large [8]. This has motivated researchers to investigate a wide range of other ways of explaining cosmic acceleration. Possible explanations go from modifying gravity to adding extra matter condensates; several of these are explored in [9–13].

Adding to the conundrum, recently there have been signs of tensions between parameters probed at several scales. Most notable are the measurements of the Hubble constant H_0, where the tension has now overcome 4σ [14, 15]. Recently the σ_8 tension, between the CMB measurements (*Planck*, [1]) and cosmic shear measurement (*e.g.* KiDS [4], DES [5]), has also gotten more attention. This tension is estimated to be around $2.5\ \sigma$. A large part of the community hopes that these tensions are cracks in the ΛCDM model and will lead to new physics. In light of this, considerable work has been done on models of dark energy that attempt to resolve these tensions. Predictions usually focus on the dynamical aspects of dark energy. For example, modifying dark energy at late time [16–19], or by altering the early universe [20–23].

We pursue another route, focusing on the spatial correlations dark energy may exhibit. Spatial correlations can be seen all over the universe, ranging from the temperature anisotropies in the cosmic microwave background [1] to the distribution of galaxies throughout the universe [24]. The origin of these fluctuations is quantum mechanical. These quantum fluctuations appear during inflation and are then imprinted in the gravitational potential, forming the sources of the wonderful structure we observe in the universe [25]. This indicates that it is possible for quantum effects to play an important role in the large scale behaviour of the universe, and we need to take them seriously.

From this perspective it is not a stretch to assume dark energy might have spatial correlations imprinted in it or, more boldly, that dark energy itself is quantum mechanical. The latter is the scenario that we are interested in. A specific realisation of this was explored by [26–31], where the scenario was explored that dark energy is sourced by the quantum fluctuations of a very light scalar field that is spectator during inflation. In this model dark energy fluctuates due to the spatial correlations inherited from inflation. It has been shown that due to these spatial correlations, which lead to a fluctuating Hubble rate, this model can alleviate the Hubble tension towards 1σ [30].

In the near future telescopes such as the Rubin Observatory, which will deliver the *Legacy Survey of Space and Time* (LSST) [32], will obtain maps of the sky with unprecedented detail. This will allow us to discriminate in the wide range of models currently available. It is therefore of importance to have predictions of a certain class of models containing these spatial fluctuations.

To this end we propose a phenomenological model of dark energy with spatial fluctuations, causing the background to fluctuate. This leads to a fluctuating Hubble rate, where at each point the effect of dark energy is such that the Hubble rate obeys the following operator Friedmann equation,

$$\boxed{3M_P^2\hat{H}^2(z,\hat{n}) = \rho_C(z)\hat{\mathrm{I}} + \hat{\rho}_Q(z,\hat{n}).} \tag{1.1}$$

Here, $M_P = 2.435 \times 10^{18}\ \mathrm{GeV}/c^2$ is the reduced Planck mass, ρ_C is the energy density of classical matter and $\hat{\rho}_Q$ is the energy density operator containing the dark energy field, $\hat{\mathrm{I}}$ is the identity operator. These operators can be understood as acting on a Hilbert space of quantum states and describe the fluctuating fields. $\hat{H}, \rho_c$ and $\hat{\rho}_Q$ are functions of the redshift z, the operators also depend on the unit vector on the celestial sphere $\hat{n}$. For the correlations we use a phenomenological power

law ansatz, which is described in more detail in Chapter 3, but in Chapter 9 and 10 we study the previously mentioned inflationary model [26–31] where a scalar field produces such spatial correlations [30, 31].

A fluctuating Hubble rate would induce correlations in a wide variety of large scale structure observables. In this thesis we focus on its imprint on the luminosity distance. Observationally, the luminosity distance is obtained from the 'known' luminosity of a standard candle and the observed flux. Theoretically, this distance can be expressed in terms of the spacetime geometry. In ΛCDM this leads to the well known expression in terms of the Hubble rate, $d_L(z) = (1+z)\int_0^z dz' H(z')^{-1}$ (see Appendix A). However, our Hubble parameter is a fluctuating quantity determined by (1.1), therefore $d_L(z)$ also becomes a fluctuating quantity. Consequently we turn the luminosity distance into an operator:

$$\boxed{\hat{d}_L(z,\hat{n}) = (1+z)\int_0^z dz' \hat{H}^{-1}(z',\hat{n}).} \tag{1.2}$$

We make predictions for the correlations our model produces and assess its detectability, comparing it with the expected noise and with effects that would be expected to be seen in perturbed ΛCDM, where these fluctuations come from relativistic effects such as convergence and the Doppler effect.

These relativistic effects on the luminosity distance have been well studied [33–37], with some work also having been done on these fluctuations in theories with dynamical dark energy/modified gravity [36] or in the case of inhomogeneous dark energy [37]. In the latter case the convergence effect of inhomogeneities was studied for a phenomenological model of dark energy. These papers, however, do not study the effects of a fluctuating Hubble parameter, but rather the effect of density perturbations between the emitter and the observer. Both effects result in a non zero power spectrum for the luminosity distance fluctuations.

This thesis is organised as follows. In Chapter 2 we give a brief overview of the current status of cosmology, a reader acquainted with cosmology could skip this section. In Chapter 3 we describe the phenomenological model of spatial correlations in dark energy, Chapter 4 is then devoted to calculating the effects of the fluctuations on the luminosity distance, which is used to evaluate its angular power spectrum in Chapter 5. Chapter 6 is devoted to the contaminant signal coming from relativistic effects, which is expected to be seen in ΛCDM. In Chapter 7 we describe the supernovae surveys and forecasting methods needed to assess the measurability. We present the main results of our phenomenological model in Chapter 8, where we compare its power spectrum with the relativistic effects and our estimated noise contributions. Hereafter we switch gears and discuss a specific model. This model is described in Chapter 9 and we discuss the prospects for its measurability in Chapter 10. We then conclude with a summary, conclusion and outlook in Chapter 11. In the Appendices we offer some additional (background) material and calculations that are either too long to include in the main text, or lie outside the main scope of this thesis.

Lastly, we point out that an article based on the work of this thesis is currently submitted to the *Journal of Cosmology and Astroparticle Physics (JCAP)*: "C.J.G. Vedder, E. Belgacem, N.E. Chisari, T. Prokopec. Fluctuating Dark Energy and the Luminosity Distance, arXiv:2209.00440, *submitted to JCAP*, 2022." [38]

2

The current state of cosmology

Cosmology has set itself the task of understanding the entire universe and all its content. This might sound like a daunting task, but nonetheless research in cosmology has been extraordinarily lively over the last decades. Progress has been made on all fronts of cosmology. Observationally, several missions have mapped the universe very well. For example, the Cosmic Microwave Background (CMB), the relic radiation that is remnant from earlier epochs of the universe, has been mapped with immense precision by the *Planck* satellite [1]. Later epochs of the universe are also well constrained by distance measurements of Type Ia supernovae [3] or mappings of the Large Scale Structure [4, 5]. These observations have led to a so-called 'standard model of cosmology', which currently fits the data very well. Be that as it may, cosmology is far from done as there are still several open questions: the physical origin of both dark matter and dark energy is currently unknown, as is the physical origin of inflation, the hypothetical period of very rapid acceleration in the very early universe. On top of this, there is increased evidence of tension between cosmological parameters probed at different scales [14, 15].

2.1 The standard model of Cosmology

Observations point towards a spatially flat universe that is homogeneous and isotropic on very large scales. Since the observations by Edwin Hubble [39], it is also known that the universe is expanding. These observations are well captured by the

Friedmann-Lemaître-Robertson-Walker (FLRW) space-time, which is defined by the following invariant line element,

$$ds^2(x) = g_{\mu\nu}(x)dx^\mu dx^\nu = -dt^2 + a^2(t)\delta_{i,j}dx^i dx^j, \tag{2.1}$$

where t denotes the cosmological time and x^i spatial variables, denoting the comoving position. The dynamics of the expansion of space is then encoded in the time dependent function $a(t)$, known as the scale factor.

This expansion has as a direct consequence that the wavelength λ of light emitted by some astrophysical object at time t_{emit} is stretched by the scale factor a before it is observed on earth. It is convenient to define this stretching factor as the redshift z:

$$1 + z \equiv \frac{\lambda_{\text{obs}}}{\lambda_{\text{emit}}} = \frac{a_{\text{obs}}}{a_{\text{emit}}} = \frac{1}{a_{\text{emit}}}, \tag{2.2}$$

where, without loss of generality, the current value of the scale factor (a_{obs}) has been set to one. In an expanding universe the scale factor can be mapped to time, therefore redshift z can be used as a time coordinate.

The dynamics of the scale factor $a(t)$ is determined by the matter content of the Universe, according to Einstein's theory of relativity. The gravitational part of this theory can be written nicely in the Einstein-Hilbert action,

$$S_{EH} = \frac{1}{16\pi G_N}\int d^4\sqrt{-g}R. \tag{2.3}$$

Here, $g = \det[g_{\mu\nu}]$ and R is the Ricci curvature scalar. This can then be coupled to a matter action S_m, with the total action reading $S = S_{EH} + S_m$. When extremizing this action one obtains the Einstein field equations,

$$G_{\mu\nu}(x) = R_{\mu\nu}(x) - \frac{1}{2}g_{\mu\nu}(x)R(x) = 8\pi G_N T_{\mu\nu}(x). \tag{2.4}$$

Here, $T_{\mu\nu}$ is the energy momentum tensor, $G_{\mu\nu}$ is the Einstein tensor, given in terms of the Ricci tensor $R_{\mu\nu}$ and Ricci scalar R. The Einstein equations relate the energy budget, entering via the energy momentum tensor, to the geometry of the universe, which is described by the Einstein tensor. The Energy-Momentum tensor $T_{\mu\nu}$ is defined as

$$T_{\mu\nu}(x) = \frac{-2}{\sqrt{-g(x)}}\frac{\delta S_m}{\delta g^{\mu\nu}(x)}. \tag{2.5}$$

When specified to a FLRW metric (2.1) and assuming the matter fields to be ideal classical fluids, in which case $T_i{}^\mu{}_\nu = \text{diag}(-\rho_i, p_i, p_i, p_i)^\mu{}_\nu$, with ρ_i the energy density and p_i the pressure, the Einstein equations reduce to the Friedmann equations,

$$\boxed{\begin{aligned} H^2(t) &= \frac{8\pi G_N}{3}\sum_i \rho_i(t), && (2.6)\\ \frac{\ddot{a}}{a}(t) &= -4\pi G_N \sum_i \left(\rho_i(t) + 3p_i(t)\right). && (2.7) \end{aligned}}$$

Here, the index i runs over all fluid species. Now the relation between the geometry and the universe is clear as the param-

eter H denotes the Hubble parameter $\frac{\dot{a}}{a}$, describing the expansion rate of the universe. The second equation describes the acceleration of the expansion rate of the universe, hence it is also known as the acceleration equation.

Ideal fluids are characterised by their equation of state, which for simple fluids takes the form $p = w\rho$. For cosmology, the relevant species have $w = 0$ (dust, dark matter), $w = \frac{1}{3}$ (relativistic matter) and $w = -1$ (cosmological constant). These fluids independently satisfy a conservation equation,

$$\dot{\rho}_i(t) + 3H(t)(\rho_i(t) + p_i(t)) = 0. \tag{2.8}$$

When assuming the previously discussed species, we can then write the Friedmann equations as follows:

$$\frac{H^2(t)}{H_0^2} = \Omega_M a(t)^{-3} + \Omega_R a(t)^{-4} + \Omega_\Lambda, \tag{2.9}$$

H_0 denotes the Hubble parameter at current time and $\Omega_i = \frac{8\pi G_N \rho_i}{3H_0^2}$ is the energy density fraction today. At late times the radiation part is negligible. The *Planck* satellite has measured these values, giving $\Omega_M = 0.315$ and $\Omega_\Lambda = 1 - 0.315 = 0.685$ with great precision [1]. This sets the stage of our universe. However, while we may understand the stage relatively well, the actors playing in this stage are largely ill understood. Only 5 percent (baryonic matter) is known at a fundamental level (the Standard Model of particle physics). Despite a tantalising amount of astronomical evidence, dark matter still eludes us in the laboratory. Even more shrouded in mystery is the remaining part of the energy budget. In the previously discussed ΛCDM model it is modelled as a cosmological constant Λ defined by a constant equation of state parameter $w = -1$, which is currently consistent with all observations. However, a typical physicist feels uneasy with a cosmological constant. At first, it seems not possible for a substance to not dilute under the the expansion of the universe. On the other hand, in Quantum Field Theory empty space also carries energy in the form of particle - anti particle pairs popping up due to the Heisenberg uncertainty relation. Unfortunately, when we quantify this vacuum value, its natural value is much larger than the amount needed to explain the observations. This problem is widely known as the cosmological constant problem [8]. Therefore, the cosmological constant is not only a simple parameter to fit, it is also a profound puzzle for the theoretical physicist. Many physicist have risen to this challenge and constructed several models of dark energy, which do not rely on a cosmological constant to explain the accelerated expansion of the Universe. A convenient way of classifying such models in cosmology is in terms of either modified gravity or as a matter condensate/physical dark energy. Modified gravity encompassing additions to the Einstein-Hilbert actions, while physical dark energy/matter condensates provide additional matter content, in the case of scalar fields possibilities are for example *quintessence* [10] or *k-essence* [13] models. Several reviews on the topic of dark energy are available [9–12].

2.2 Initial conditions and the theory of Inflation

While the previously discussed ΛCDM model works well, it does not tell us anything about the initial conditions and suffers several problems. The solution to this lies in in the theory of inflation [40–42], which is the topic of this section. The

most notable* problem inflation can solve is known as *the horizon problem*. In the late 20th century it was realised that when one considers a period of very rapid acceleration prior to the recombination epoch this problem is solved [40]. Thereafter it was understood that this period of accelerated expansion can also account for the the origin of perturbations in the universe, which might be its greatest triumph. We first briefly discuss the horizon problem and its solution and then move on to the quantum fluctuations that seed the structure formation in the later universe.

From CMB observations we know that the universe, at an age of 380000 years, was very uniform [1], containing temperature fluctuations of roughly 1 part in 10^5. This is actually very surprising, as random initial conditions would result in a highly inhomogeneous universe. An explanation for this uniformity is that large patches of universe were in thermal contact with each other. Unfortunately, in our universe this does not seem to work. Our universe is so large that different parts could not be in causal contact with each other due to the large distances separating them and the universe existing for a finite time. This problem is widely known as the *horizon problem*. It can be quantified by computing the angular separation on the sky for which two patches cannot be in causal contact as the ratio of the horizon distance $d_{\rm hor}$ at last scattering over the angular diameter distance d_A to the last scattering surface:

$$\frac{d_{\rm hor}(z_{\rm ls})}{d_A} = 1.2^\circ. \tag{2.10}$$

This means that patches separated by more than 1.2° could not possible have been in causal contact with each other. To gain some insight we write down the comoving horizon distance:

$$\chi = \int_0^a d\ln a' \frac{1}{a'H(a')}, \tag{2.11}$$

which is the logarithmic integral over the comoving Hubble radius. From this we learn that if there was an epoch where the comoving Hubble radius was decreasing, then the horizon might have received contributions from the very early universe where the comoving Hubble radius was significantly larger. A shrinking factor $\frac{1}{aH}$ corresponds to $\ddot{a} > 0$, which is precisely the condition for an accelerated expansion! This postulated epoch of accelerated expansion is then known as inflation [40–42].

Inflation has even more up its sleeve, as it gives an explanation for the very small deviations from homogeneity in the cosmic microwave background. These deviations later grow to become all the wonderful structures we see in our universe. If the perturbations would be quantum fluctuations imprinted right after the big bang, they could be stretched to super horizon scales due to the rapid expansion during inflation. At these scales the perturbations are then frozen until reentering at a time when the acceleration of the universe is slowing down. This is right on time to produce the temperature anisotropies seen in the Cosmic Microwave Background [1].

*Other problems include: the flatness problem, the monopole problem and the structure formation problem.

As an example, single field slow roll inflation results in the following power spectrum for the field perturbations [43]:

$$\Delta_\varphi(k) = \frac{4\pi k^3 \left\langle \hat{\varphi}_{\mathbf{k}} \hat{\varphi}^\dagger_{\mathbf{k}} \right\rangle}{(2\pi)^3} \propto k^{n_s - 1}. \tag{2.12}$$

Here, $n_s \approx 1 - 2\varepsilon - \eta$, where ε and η are the first and second *slow roll* parameters. It turns out that these perturbations are directly imprinted in the gravitational potential. This happens via the curvature perturbation $\mathcal{R}$. The curvature perturbation is a gauge invariant scalar quantity built from the perturbations of the metric and the field around their background values, its formal definition can be found in ref. [44, p. 57]. Its usefulness resides in its conservation on super Hubble scales, as described by ref. [44, section 7.13, 7.14]. Their spectra are related by

$$\Delta_{\mathcal{R}}(k, \eta) = \frac{1}{2\varepsilon M_{\mathrm{p}}^2} \Delta_\varphi(k, \eta). \tag{2.13}$$

Subsequently the curvature perturbations are linked to the gravitational potential Φ. After inflation, during radiation domination we have $\mathcal{R} \approx \frac{3}{2}\Phi$ [43]. This then sources the temperature fluctuations in the Cosmic Microwave Background and later on the matter perturbations in the Large Scale Structure. A good review on the topic of cosmic inflation is the one by [45].

2.3 A Perturbed Universe and the Large Scale Structure

We established that due to the quantum fluctuations during inflation, the universe deviates slightly from a perfect homogeneous state, this statement is confirmed by the temperature perturbations in the cosmic microwave background [1]. A key question is then, how these inhomogeneities propagate into the late universe. The answer is fascinating, as due to the non linear nature of gravity, these tiny perturbations grow out to form the galaxies and galaxy clusters we can observe on the nights sky.

As we can observe this structure in the late universe, we can study the statistics of these perturbations. The matter perturbations are usually quantified using the matter power spectrum.

$$\langle \delta(\vec{k}, z) \delta^*(\vec{q}, z') \rangle = (2\pi)^3 P_m(k, z, z') \delta^3(\vec{k} - \vec{q}). \tag{2.14}$$

This can be understood as the Fourier transformed correlation function, describing correlations between overdensities as a function of distance. An overdensity is defined as a deviation from the average density $\bar{\rho}$:

$$\delta(\vec{x}) = \frac{\rho(\vec{x}) - \bar{\rho}}{\bar{\rho}} \tag{2.15}$$

At the linear scales that we are mostly interested in, the power spectrum simplifies and takes the following form [43]:

$$P_{\mathrm{L}}(k, z, z') = AT(k)^2 D(z) D(z') k^{n_s}. \tag{2.16}$$

Here, A is an amplitude, $D(z)$ the growth function describing the time evolution of an overdensity, $T(k)$ is a transfer function that modifies the k dependence of the primordial power spectrum. We describe this power spectrum in more detail in section 6.5. This power spectrum depends on the fluctuations inherited from inflation and therefore contains information about the early universe.

2.4 Cosmological tensions

While the current ΛCDM model largely fits the data very well, tensions between different parameters when probed at different scales have emerged. In particular, this is he case when using early universe probes such a the Cosmic Microwave Background in conjunction with late universe probes. Most notably has become the tension on the Hubble parameter H_0, as in this case the tension has overcome 4σ [14, 15]. The values for H_0 most often cited in the literature are either the CMB measurements by *Planck* of (67.4 ± 0.5) km/s Mpc^{-1} [1] or the value obtained by distance ladder measurements using type 1a supernovae from the *SH0ES* collaboration [46] that quote (74.03 ± 1.42) km/s Mpc^{-1}. However, the problem is larger than just reconciling these two measurements, as the tension remains when considering other probes as well. Other early universe probes include for example inverse distance ladder measurements anchored by either the CMB, Baryon Acoustic Oscillations (BAO) or primordial nucleosynthesis (BBN) [47–51], while the late universe is also contrained by *e.g.* time delays of strongly lensed quasars [52], distance ladder calibrations using the tip of the red giant branch (finding a slightly lower value for H_0[†], [53]) or with Mira variables [54].

Many believe that this tension might be caused by new physics. Therefore theorists have taken this opportunity to explore models that can potentially resolve this tension. An extensive list of such models is presented in [15]. We will go over some models. For example, there are several ideas of introducing new physics such that Hubble constant inferred from the cosmic microwave background is larger. Starting with proposals affecting the late universe; one suggestion is to introduce dark energy with $w < -1$, known in the literature as a phantom equation of state [16]. Other ideas range from interacting dark energy [17], metastable dark energy [18] to decaying dark matter [19]. Although it has been demonstrated that these scenarios do indeed result in a higher Hubble constant value when used to match CMB data only, it is challenging to reconcile such models with cosmic chronometers or BAO measurements [55, 56]. Other models alter the physics of the early universe intstead. One of such proposals is the case where a scalar field dilutes faster than dark matter starting from an initial state frozen by Hubble friction [21, 22]. However, these models need to be fine-tuned, typically in one of three areas: their potential, their initial conditions, or when to make the fields (dis)appear. Seperately, such models often fail to accomodate the σ_8 tension [57], mentioned later in this section. Another early dark energy approach is altering the speed of sound during recombination or to try to make recombination happen at an earlier time [23]. Instead of focusing on raising H_0

[†]This measurement is actually not in tension with the early measurements, therefore providing an interesting perspective.

measured by early probes one could also try to alter the local measurements. These, for example, focus on changing the supernova calibration (chameleon dark energy, [58]) or by changing the effective Newton constant at late time [59].

As a completely independent approach, it was shown recently by ref. [30] that spatial correlations in dark energy, resulting in a fluctuating Hubble parameter, can also alleviate the Hubble tension. We discuss this approach more in depth in Chapter 9 of this thesis.

At last, while the community is hoping for new physics, these tensions could also be the result of unknown systematics, instead of the much hoped for new physics [60, 61].

Apart from the Hubble tension, over the last years the tensions on the σ_8 parameter have also received more attention. This tension appears when comparing the *Planck* CMB measurements [1] of this parameter with the measurements of cosmic shear surveys such as the Kilo Degree Survey (KiDS [4]) or the Dark Energy Survey (DES [5]). This tension is currently estimated at about 2.5 σ, and might be releated to the Hubble tension, posing an interesting problem to the cosmology community.

3

Spatial correlations and a phenomenological model

To describe spatial correlations in dark energy we construct a phenomenological model. We propose a model where we base the statistics of the dark energy field on the statistics of the underlying (quantum) field that builds it. This chapter is devoted to the description and motivation for this model.

We assume that dark energy is sourced by an energy density field $\hat{\rho}_Q(t, \vec{x})$, which is a function of both time and position. However, position and time are not readily available in observations, we thus choose to represent the density field in terms of redshift z and unit angle on the celestial sphere $\hat{n}$. We then assume this is a fluctuating quantity with average value $\langle \hat{\rho}_Q \rangle (z)$, where the average $\langle \dots \rangle$ is an ensemble average over a space-like hypersurface of equal time, due to this averaging the angular dependence has disappeared. These fluctuations can have several origins, for example, dark energy could originate from a quantum field that was spectator during inflation, as was explored by a series of papers [26–31].

We assume the fluctuations induce spatial correlations in the dark energy density field. These are not visible in the one-point function as it has no angular dependence, therefore we consider the two-point function $\langle \hat{\rho}_Q(z, \hat{n}) \hat{\rho}_Q(z, \hat{m}) \rangle$. We parameterise this spatial dependence as follows,

$$\boxed{\langle \hat{\rho}_Q(z, \hat{n}) \hat{\rho}_Q(z, \hat{m}) \rangle = \langle \hat{\rho}_Q \rangle (z)^2 s_i(\|\vec{x} - \vec{y}\|).} \tag{3.1}$$

Due to the statistical homogeneity and isotropy the function $s_i(\|\vec{x}-\vec{y}\|)$ depends only on the absolute comoving distance between the comoving coordinates $\vec{x}$ and $\vec{y}$. Fluctuations give rise to a non zero variance $\sigma_Q^2(z, \|\vec{x}-\vec{y}\|)$, which we can write as follows:

$$\sigma_Q^2(z, \|\vec{x}-\vec{y}\|) = \langle \hat{\rho}_Q(z,\hat{n})\hat{\rho}_Q(z,\hat{m})\rangle - \langle \hat{\rho}_Q\rangle(z)^2 = \langle \hat{\rho}_Q\rangle(z)^2\,(s_i(\|\vec{x}-\vec{y}\|)-1)\,. \tag{3.2}$$

We study two separate phenomenological models. In both cases we assume the energy density field is built from a more fundamental Gaussian quantum field, where for simplicity we assume this to be a single field $\hat{\varphi}$. In the first case we assume that this relation is quadratic, $\hat{\rho}_Q \propto \hat{\varphi}^2$. In the second case we assume this relation is linear, $\hat{\rho}_Q \propto \hat{\varphi}$. From these assumptions we motivate two different s-functions, describing the behaviour of the two-point correlations and therefore the variance of the density field $\hat{\rho}_Q$.

3.1 Case I

We first consider the case where the energy density $\hat{\rho}_Q$ depends on the square of the Gaussian field $\hat{\varphi}$, *i.e.* $\hat{\rho}_Q \propto \hat{\varphi}^2$. We assume this fundamental quantum field to be Gaussian and to have a zero vacuum expectation value (vev), $\langle\hat{\varphi}\rangle = 0$. In this case the relevant field theoretical correlator would be $\langle\hat{\varphi}^2(t,\vec{x})\hat{\varphi}^2(t,\vec{y})\rangle$. As we assume the fields to be Gaussian, we can Wick contract them. This then gives us

$$\langle\hat{\varphi}^2(t,\vec{x})\hat{\varphi}^2(t,\vec{y})\rangle = \langle\hat{\varphi}^2(t)\rangle^2 + 2\langle\hat{\varphi}(t,\vec{x})\hat{\varphi}(t,\vec{y})\rangle^2. \tag{3.3}$$

When considering $\|\vec{x}-\vec{y}\| = 0$ we obtain $3\langle\hat{\varphi}^2(t)\rangle$, therefore the s-function should give a factor 3 at coincidence. Meaning that due to Wick's theorem the local variance of the field is twice its density squared. If $\|\vec{x}-\vec{y}\| \to \infty$ we expect $\langle\hat{\varphi}(t,\vec{x})\hat{\varphi}(t,\vec{y})\rangle = \langle\hat{\varphi}\rangle^2(t)$, as over such distances we expect the field to decouple. The vacuum expectation value of this field is assumed to be zero, hence we obtain $\langle\hat{\varphi}(t,\vec{x})\hat{\varphi}(t,\vec{y})\rangle = 0$ in this limit. As a result we only have a single copy of $\langle\hat{\varphi}^2(t)\rangle$ over such distances, therefore the function $s_1(\|\vec{x}-\vec{y}\|)$ should be one after a characteristic length scale r_0. We note that this means that the variance of the density fluctuations is zero after a distance r_0, the field does not fluctuate over such distances.

By this reasoning we expect the function $s_1(\|\vec{x}-\vec{y}\|)$ to go from three at coincidence to one over a characteristic length scale that we denote r_0. For the intermediate regime it is natural to assume power law behaviour that decays with distance. We parameterise the slope of this power law by the spectral index n_{DE}. These arguments then result in the following function $s_1(r)$:

$$s_1(r) = \begin{cases} 3 - 2\left(\frac{r}{r_0}\right)^{n_{\mathrm{DE}}}, & r \le r_0, \\ 1, & r > r_0, \end{cases} \qquad \textit{Case I.} \tag{3.4}$$

Here, we used the short notation $r = \|\vec{x}-\vec{y}\|$. The form of this function for several values of the spectral index is shown in Figure 3.1.

3.1.1 A simple example

The motivation for choosing $\hat{\rho}_Q \propto \hat{\varphi}^2$ resides in the energy momentum tensor. We discuss a simple example. A minimally coupled field φ, with potential $V(\varphi)$ is defined by the Lagrangian,

$$S_\varphi = \int d^4x\sqrt{-g}\left(-\frac{1}{2}g^{\mu\nu}\partial_\mu\varphi\partial_\nu\varphi - V(\varphi)\right). \tag{3.5}$$

The energy momentum tensor is then given by,

$$\begin{aligned} T^\varphi_{\mu\nu}(x) &= -\frac{2}{\sqrt{-g}}\frac{\delta S_\varphi}{\delta g^{\mu\nu}(x)} \\ &= \left(\partial_\mu\varphi\right)\left(\partial_\nu\varphi\right) + g_{\mu\nu}\left[-\frac{1}{2}\left(\partial_\alpha\varphi\right)\left(\partial_\beta\varphi\right)g^{\alpha\beta} - V(\varphi)\right]. \end{aligned} \tag{3.6}$$

Now, we assume the potential to only consists of a mass term, $V(\varphi) = \frac{1}{2}m^2\varphi^2$. On FLRW, the energy momentum tensor is diagonal and takes the perfect fluid form. From this we obtain the density,

$$\rho_Q = -T^0_0 = \frac{1}{2}\left(\partial_0\varphi\right)^2 + \frac{1}{2a^2}(\vec{\nabla}\varphi)^2 + \frac{m^2}{2}\varphi^2 \approx \frac{m^2}{2}\varphi^2. \tag{3.7}$$

The last step can be argued from the behaviour of dark energy: we do not expect it to rapidly vary in time and distance.

A more sophisticated example of such a theory would be a field that is spectator during inflation, the dominant contribution to the 00 element of the Energy-Momentum tensor would in this case be going $\propto \hat{\varphi}^2$. A realisation of such a dark energy candidate is explored by [29, 30], which we discuss in more detail in Chapter 9. Other examples of dark energy models built from scalar fields are *e.g. quintessence* and *k-essence* models [9, 10, 13].

3.1.2 Non Gaussianity

Lastly, we observe that when we assume the (quantum) fields to be Gaussian, the energy density $\hat{\rho}_Q$ will inherently be non Gaussian as the the density depends on the square of the gaussian field. For example, the three-point function of the (quantum) fluctuations $\delta\hat{\rho}_Q = \hat{\rho}_Q - \langle\hat{\rho}_Q\rangle$ would obey the following statistics at coincidence,

$$\langle\delta\hat{\rho}^3_Q\rangle = 8\langle\hat{\rho}_Q\rangle^3 \neq 0. \tag{3.8}$$

In the Gaussian case this would yield zero, which it now clearly does not. A short recap of Gaussian statistics and Wick's theorem can be found in Appendix B.

3.2 Case II

For *Case II* we explore the scenario where we the energy density depends linearly on the gaussian field, $\hat{\rho}_Q \propto \hat{\varphi}$. To have a non zero average energy density we assume the field $\hat{\varphi}$ to have a non zero vacuum expectation value (vev): $\langle\hat{\varphi}\rangle(z) \neq 0$. For

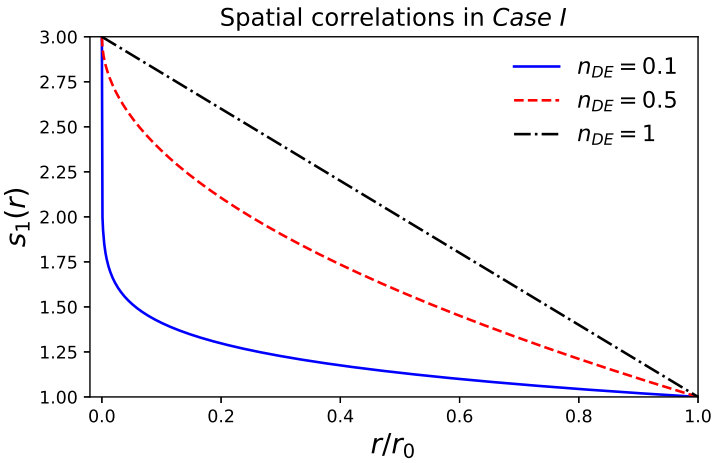

Figure 3.1: The function $s_1(r)$, describing the form of the spatial correlations, given *Case I* for several values of the index n_{DE}. The Figure shows r in units of r_0. Note that apart from a rescaling on the axis, the form of the function does not differ between the two cases. This can be traced back to the scale free behaviour of the power law used to parameterise the function. We expect r_0 to be of order Hubble length H_0^{-1}.

this case we assume the following function $s_2(\|\vec{x}-\vec{y}\|)$:

$$s_2(r) = \begin{cases} \tilde{\sigma}_Q^2 \left[1 - \left(\frac{r}{r_0}\right)^{n_{\mathrm{DE}}}\right] + 1, & r \leq r_0, \\ 1, & r > r_0, \end{cases} \qquad \textit{Case II.} \tag{3.9}$$

Here, $\tilde{\sigma}_Q^2 = \frac{\sigma_Q^2}{\langle\hat{\rho}_Q\rangle^2}$, with σ_Q^2 being the local variance of the energy density field $\hat{\rho}_Q$. Before motivating this function we point out that this is a more general form of the s-function defined in *Case I*, as assuming $\tilde{\sigma}_Q^2 = 2$ recovers (3.4). We stress that these theories are still quite different as this merely states that the two-point energy density function has the same form, however, the higher point correlators will be very different, as *Case I* is a non-Gaussian theory, while *Case II* is Gaussian.

In *Case I* we could derive $\tilde{\sigma}^2 = 2$ from Wick's theorem, as the two-point energy density corresponded to a four point field correlator. But in the case where the energy density relates linearly to the field, Wick's theorem is of no help when predicting this constant, therefore we keep it as a free parameter. Similar to *Case I*, we assume the fields to decouple after some characteristic length scale r_0. But, as opposed to *Case I*, the two-point function $\langle\hat{\varphi}(t,\vec{x})\hat{\varphi}(t,\vec{y})\rangle \overset{r\to\infty}{=} \langle\hat{\varphi}\rangle^2(t)$ does not go to zero due to the non zero vev. Therefore, the function $s_2(r)$ also goes to one as $r \to \infty$. We also assume that at coincidence there is some non zero variance, meaning (3.2) returns a non zero value as coincidence. Therefore $s(0) - 1 = \tilde{\sigma}_Q^2 \neq 0$. When $\tilde{\sigma}_Q^2 \to 0$ both the local and the non local fluctuations disappear, hence this is the classical limit of this theory.

An important distinction from *Case I* is the fact that this variance is not bounded. In principle it can be very close to 0, while in *Case I* the local variance is naturally large due to Wick's theorem, which was a consequence of the non-Gaussianity of $\hat{\rho}_Q$ as it depended on the square of the Gaussian field. In *Case II* the field depends linearly on the Gaussian field, therefore this density has the inherited the Gaussian statistics. The function $s_2(r)$ has a similar shape as the one displayed in Figure 3.1, but goes from $1 + \tilde{\sigma}_Q^2$ at coincidence to 1 at $r = r_0$.

4

Fluctuations in the luminosity distance

The main subject of this thesis is how spatial correlations in dark energy become visible in the luminosity distance. To this end we adopt the previously introduced model and use it to make predictions for the correlations in the luminosity distance. These enter via the Hubble rate, that becomes a fluctuating parameter due to the fluctuations in dark energy. More precisely, at each point the effect of dark energy is such that the Hubble rate obeys the following operator Friedmann equation,

$$\boxed{3M_P^2\hat{H}^2(z,\hat{n}) = \rho_C(z)\hat{\mathrm{I}} + \hat{\rho}_Q(z,\hat{n}).} \tag{4.1}$$

Here, $M_P = 2.435 \times 10^{18}\,\mathrm{GeV}/c^2$ is the reduced Planck mass, ρ_C is the energy density of classical matter and $\hat{\rho}_Q$ is the energy density operator containing the dark energy field, $\hat{\mathrm{I}}$ is the identity operator. These operators can be understood as acting on a Hilbert space of quantum states and describe the fluctuating fields. $\hat{H}, \rho_c$ and $\hat{\rho}_Q$ are functions of the redshift z, the operators also depend on the unit vector on the celestial sphere $\hat{n}$.

To see the effect of a fluctuating Hubble rate we first expand it in fluctuations $\hat{\rho}_Q = \langle\hat{\rho}_Q\rangle + \delta\hat{\rho}_Q$. Here, the brackets $\langle\ldots\rangle$ denote an ensemble average. With this we obtain,

$$3M_P^2\hat{H}^2(z,\hat{n}) = \rho_{\mathrm{tot}}(z) + \delta\hat{\rho}_Q(z,\hat{n}) = \rho_{\mathrm{tot}}(z)\left(1 + \frac{\delta\hat{\rho}_Q(z,\hat{n})}{\rho_{\mathrm{tot}}(z)}\right), \tag{4.2}$$

where $\rho_{\text{tot}}(z) = \rho_c(z) + \langle\hat{\rho}_Q(z)\rangle$ is the total energy budget. Taking the state average of (4.2) reduces it to the Friedmann equation in semi-classical gravity. To be precise, this averaging is a state average over a space-like hypersurface of constant time. Due to causality we can only observe over our past light-cone. This then prohibits us from directly observing the $H(z)$ that is obtained in this way, as we cannot directly observe all of the structure on this hypersurface.

In our treatment we go beyond semi-classical gravity by including the fluctuations in our treatment.

4.1 One-point function

We use the standard definition of the luminosity distance (derived in (A.6)), however, since the Hubble rate is a fluctuating quantity described by (4.1) we need to upgrade the luminosity distance to an operator: $d_L(z) \to \hat{d}_L(z,\hat{n})$, where due to the fluctuations this operator also depends on the unit angle on the celestial sphere $\hat{n}$. Therefore we have:

$$\boxed{\frac{\hat{d}_L(z,\hat{n})}{1+z} = \int_0^z dz' \frac{1}{\hat{H}(z',\hat{n})}.} \tag{4.3}$$

The Hubble rate follows from the operator Friedmann equation (4.2). Taking the state average $\langle\ldots\rangle$ of (4.3) results in:

$$\frac{\langle\hat{d}_L\rangle(z)}{1+z} = \int_0^z dz' \left\langle \frac{1}{\hat{H}(z',\hat{n})} \right\rangle = \int_0^z \frac{dz'}{\bar{H}(z')} \left\langle \frac{1}{\sqrt{1+\frac{\delta\hat{\rho}_Q(z',\hat{n})}{\rho_{\text{tot}}(z')}}} \right\rangle. \tag{4.4}$$

We defined $\sqrt{3}M_P\bar{H} = \sqrt{3}M_P\left(\langle H^2\rangle\right)^{\frac{1}{2}} = \sqrt{\rho_{\text{tot}}}$, which is the root mean squared (RMS) of (4.2). The second equality follows from the Friedmann equation and separating out the RMS H. From observations we know the ratio $\frac{\delta\hat{\rho}_Q}{\rho_{\text{tot}}}$ to be small. Because of this we feel justified in Taylor expanding around zero,

$$\frac{\langle\hat{d}_L\rangle(z)}{1+z} = \int_0^z \frac{dz'}{\bar{H}(z')} \left(1 - \frac{1}{2}\frac{\langle\delta\hat{\rho}_Q(z',\hat{n})\rangle}{\rho_{\text{tot}}(z')} + \frac{3}{8}\frac{\langle\delta\hat{\rho}_Q(z',\hat{n})^2\rangle}{\rho_{\text{tot}}(z')^2}\right). \tag{4.5}$$

However, due to Wick's theorem the higher n-point correlators grow very quickly, leading to a series rapidly diverging. For this reason, we calculated via another route the expansion up to all orders. This is discussed in Appendix D. From this we can conclude that the error made by truncating at quadratic order in quantum fluctuations is reasonable.

By definition, we know that $\langle\delta\hat{\rho}_Q\rangle(z) = 0$. Inserting the definition of $\delta\hat{\rho}_Q$ then gives us,

$$\frac{\langle\hat{d}_L\rangle(z)}{1+z} = \int_0^z \frac{dz'}{\bar{H}(z')} \left(1 + \frac{3}{8}\frac{\langle\hat{\rho}_Q(z',\hat{n})^2\rangle - \langle\hat{\rho}_Q(z')\rangle^2}{\rho_{\text{tot}}(z')^2}\right). \tag{4.6}$$

We can use our phenomenological model to rewrite $\langle\hat{\rho}_Q^2(z)\rangle = \langle\hat{\rho}_Q\rangle(z)^2 s_i(0)$, where the function $s_i(\|\vec{x}-\vec{y}\|)$ was specified in Chapter 3. The subscript i can take values 1 or 2, referring to *Case I* or *Case II* respectively. Using this we obtain,

$$\boxed{\frac{\langle\hat{d}_L\rangle(z)}{1+z} = \int_0^z \frac{dz'}{\bar{H}(z')} \left(1 + \frac{3}{8}\Omega_Q(z')\left(s_i(0)-1\right)\right),} \tag{4.7}$$

where we also defined $\Omega_Q(z) = \frac{\langle\hat{\rho}_Q(z)\rangle}{\rho_{\rm tot}(z)}$. The factor $(s_i(0) - 1)$ is proportional to the local variance of the density field. When $s_i(0) - 1 = 0$, which is the classical limit $\tilde{\sigma}_Q^2 \to 0$ of *Case II*, the local variance is zero and we indeed recover the classical expression for the luminosity distance. Therefore we infer that if the local variance of the field is non zero the luminosity distance becomes dressed by the fluctuations of the dark energy field. An interesting consequence of this is that the observed parameters do not necessarily match the global parameters of the underlying Friedmann-Lemaître-Robertson-Walker (FLRW) universe. We thus need to make the distinction between the local parameters and the global, or bare, parameters. The local parameters are the parameters that are affected by the fluctuations and can therefore, depending on the magnitude of the fluctuations, be quite different. We stress again that these global parameters are in principle not directly measurable, as we always do measurements in our local perturbed part of the universe.

Again, we can make the distinction between the two cases. In *Case II* these local fluctuations are related to the quantity $\frac{\sigma_Q^2}{\rho_{\rm tot}^2}$, where σ_Q^2 is the local variance of $\hat{\rho}_Q$. In this case σ_Q^2 can be anything, thus in principle this contribution could be quite small. A specific model could make a prediction for this quantity. However, in *Case I* the deviation from the classical result is determined by Wick's theorem and is given by $\frac{3}{4}\Omega_Q(z)^2$. This contribution is relatively large and results in a large difference between the bare and local quantities. This is discussed in more detail in section 4.3.

4.2 Two-point function

We now perform a similar analysis for the two-point correlation function of the luminosity distance. We take the state average of two luminosity distance operators as defined in (4.3):

$$\frac{\langle\hat{d}_L(z_1,\hat{n})\hat{d}_L(z_2,\hat{m})\rangle}{(1+z_1)(1+z_2)} = \int_0^{z_1} dz' \int_0^{z_2} dz \left\langle \frac{1}{\hat{H}(z,\hat{n})\hat{H}(z',\hat{m})} \right\rangle . \tag{4.8}$$

Using the Friedmann equation (4.2) we obtain,

$$\frac{\langle\hat{d}_L(z_1,\hat{n})\hat{d}_L(z_2,\hat{m})\rangle}{(1+z_1)(1+z_2)} = \int_0^{z_1} dz \int_0^{z_2} dz' \frac{1}{\bar{H}(z)\bar{H}(z')} \left\langle \left(1+\frac{\delta\hat{\rho}_Q(z,\hat{n})}{\rho_{\rm tot}(z)}\right)^{-\frac{1}{2}} \left(1+\frac{\delta\hat{\rho}_Q(z',\hat{m})}{\rho_{\rm tot}(z')}\right)^{-\frac{1}{2}} \right\rangle . \tag{4.9}$$

Expanding this up to quadratic order then gives the result,

$$\frac{\langle\hat{d}_L(z_1,\hat{n})\hat{d}_L(z_2,\hat{m})\rangle}{(1+z_1)(1+z_2)} = \int_0^{z_1} dz \int_0^{z_2} dz' \frac{1}{\bar{H}(z)\bar{H}(z')} \left[1 + \frac{1}{4}\frac{\langle\delta\hat{\rho}_Q(z,\hat{n})\delta\hat{\rho}_Q(z',\hat{m})\rangle}{\rho_{\rm tot}(z)\rho_{\rm tot}(z')} + \frac{3}{8}\frac{\langle\delta\hat{\rho}_Q(z)^2\rangle}{\rho_{\rm tot}(z)^2} + \frac{3}{8}\frac{\langle\delta\hat{\rho}_Q(z')^2\rangle}{\rho_{\rm tot}(z')^2}\right] , \tag{4.10}$$

where we already used that the linear terms are zero. Apart from the $\frac{3}{8}$ terms that we had already seen before, we now also see the $\frac{1}{4}$ term. This term is especially interesting as this is dependent on the difference between the two angles and thus

induces angular correlations. We can now insert the definition of the fluctuation $\delta\hat{\rho}_Q(z,\hat{n})$ again,

$$\frac{\langle \hat{d}_L(z_1,\hat{n})\hat{d}_L(z_2,\hat{m})\rangle}{(1+z_1)(1+z_2)} = \int_0^{z_1} dz \int_0^{z_2} dz' \frac{1}{\bar{H}(z)\bar{H}(z')}\left[1+\frac{1}{4}\frac{\langle\hat{\rho}_Q(z)\hat{\rho}_Q(z')\rangle - \langle\hat{\rho}_Q(z,\hat{n})\rangle\langle\hat{\rho}_Q(z',\hat{m})\rangle}{\rho_{\rm tot}(z)\rho_{\rm tot}(z')}+\right.$$
$$\left.\frac{3}{8}\left(\frac{\langle\hat{\rho}_Q(z)\rangle^2}{\rho_{\rm tot}(z)^2}\left(s_i(0)-1\right)+\frac{\langle\hat{\rho}_Q(z')\rangle^2}{\rho_{\rm tot}(z')^2}\left(s_i(0)-1\right)\right)\right]. \quad (4.11)$$

The final result can then be obtained by using the expression for the unequal time correlator derived in Appendix E,

$$\boxed{\frac{\langle \hat{d}_L(z_1,\hat{n})\hat{d}_L(z_2,\hat{m})\rangle}{(1+z_1)(1+z_2)} = \int_0^{z_1} dz \int_0^{z_2} dz' \frac{1}{\bar{H}(z)\bar{H}(z')}\left[1+\frac{3}{8}\left(\Omega_Q(z)^2+\Omega_Q^2(z')\right)\left(s_i(0)-1\right)\right.}$$
$$\boxed{\left.+\frac{1}{4}\left(\frac{\bar{H}_0^4}{\bar{H}(z)^2\bar{H}(z')^2}\Omega_{Q,0}^2\left(1+(\Delta t(z)+\Delta t(z'))\frac{\langle\dot{\hat{\rho}}_Q\rangle_0}{\langle\hat{\rho}_Q\rangle_0}\right)s_i(\|\vec{x}-\vec{y}\|)-\Omega_Q(z)\Omega_Q(z')\right)\right], \quad (4.12)}$$

where $\Delta t(z) = t(z) - t_0$, $t(z)$ denotes the cosmological time at redshift z, the subscript 0 means it is evaluated today. $\dot{\hat{\rho}}_Q(t_0)$ denotes the time derivative of $\hat{\rho}_Q$ evaluated today. We can now see that the correlation function $s(\|\vec{x}-\vec{y}\|)$ has appeared, meaning this signal has angular dependence. When $s_i(0) \neq 1$, as in *Case I*, we can also identify another contribution representing the contribution of the local variance.

4.3 Matching the bare quantities

Local fluctuations affect the one-point function of the luminosity distance, the luminosity distance is therefore dressed by these fluctuations, resulting in a prediction for the luminosity distance that is different from the standard ΛCDM. Therefore, the parameters inferred by experiments such as SH0ES [3] or *Planck* [1] are not necessarily the right parameters describing the underlying FLRW universe, but rather the values we observe locally. The underlying 'bare' parameters, would be unobservable directly as they are defined on a global hypersurface of equal time. The idea that parameters measured do not equal the underlying parameters is not a new idea, as it was previously studied in the context of relativistic universes containing inhomogeneities [34, 62]. But to our knowledge it has to this date not yet been studied from our perspective, where the fluctuations arise due to (quantum) fluctuations in the Hubble rate.

In *Case I* these local fluctuations are inevitable, as due to Wick's theorem there are always local fluctuations giving $\langle\hat{\rho}_Q^2\rangle \neq \langle\hat{\rho}_Q\rangle^2$. It is therefore important to estimate the bare parameters $\Omega_{Q,0}$ and H_0 of our model. Ideally, to estimate these bare parameters one would fit our model to current data sets. For example, comparing it with current supernovae samples. We proceed in a similar fashion, we obtain our values by comparing it to the local low redshift distance ladder measurements from the SH0ES collaboration [2]. This gives the following constraint up to cubic order:

$$\langle\hat{d}_L(z)\rangle = \frac{z}{H_L}\left\{1+\frac{1}{2}\left[1-q_L\right]z-\frac{1}{6}\left[1-q_L-3q_L^2+j_L\right]z^2\right\}. \quad (4.13)$$

Here, H_L, q_L and j_L are the locally measured Hubble, deceleration and jerk parameters. Their definitions in an unperturbed

FLRW universe can be found in ref. [63]. The subscript L denotes that these are measured locally. These parameters are model independent and therefore well suited for our approach. We match this equation order by order with (4.7). We assume the background is well described by a flat wCDM model. This gives us $\bar{H} = H_0\sqrt{\Omega_{c,0}(1+z)^3 + \Omega_{Q,0}(1+z)^{3(w_Q+1)}}$ and $\Omega_{c,0} = 1 - \Omega_{Q,0}$.

We want to match the *Case I* bare parameters, therefore we need to expand the following luminosity distance, including the extra term due to the included fluctuations,

$$\langle \hat{d}_L \rangle(z) = \frac{1+z}{H_0}\int_0^z dz' \frac{1+\frac{3}{4}\Omega_Q(z)^2}{\sqrt{\Omega_{c,0}(1+z)^3 + \Omega_{Q,0}(1+z)^{3(w_Q+1)}}}, \tag{4.14}$$

$$\Omega_Q(z) = \frac{\Omega_{Q,0}(1+z)^{3(w_Q+1)}}{\Omega_{c,0}(1+z)^3 + \Omega_{Q,0}(1+z)^{3(w_Q+1)}}. \tag{4.15}$$

Here $\Omega_{c,0} = 1 - \Omega_{Q,0}$. Expanding this and matching it power by power with (4.13) then gives the following three equations:

$$\frac{1}{H_L} = \frac{1}{H_0}\left(1 + \frac{3}{4}\Omega_{Q,0}^2\right) \tag{4.16}$$

$$\frac{1}{2H_L}\left[1 - q_L\right] = \frac{1}{4H_0}\left(1 + \frac{3}{4}\Omega_{Q,0}^2 - \frac{3}{4}w_Q\left(4 - 12\Omega_{Q,0} + 15\Omega_{Q,0}^2\right)\right) \tag{4.17}$$

$$\begin{aligned} -\frac{1}{6H_L}\left[1 - q_L - 3q_L^2 + j_L\right] = &-\frac{1}{8H_0}\left(1 + \frac{3}{4}\Omega_{Q,0}^2 - \frac{w_Q}{2}\left(4 - 12\Omega_{Q,0} + 15\Omega_{Q,0}^2\right)\right. \\ &\left. + \frac{3w_Q^2}{4}\Omega_{Q,0}\left(8 - 60\Omega_{Q,0} + 150\Omega_{Q,0}^2 - 105\Omega_{Q,0}^3\right)\right). \end{aligned} \tag{4.18}$$

Once the local parameters are fixed by measurements, we can numerically solve this system of equations for $\Omega_{Q,0}$, H_0 and w_Q. For the local parameters we use the values found by [2], these are obtained by fitting the low redshift expansion over the redshift range spanning from $z = 0.023$ to $z = 0.15$. They find that $H_L = 74.1 \pm 1.3\ \mathrm{km\ s^{-1}Mpc^{-1}}$, $q_L = -0.55$ and $j_L = 1$. The solutions for the bare parameters are then $H_0 = 118.0\ \mathrm{km\ s^{-1}Mpc^{-1}}$, $\Omega_{Q,0} = 0.89$ and $w_Q = -0.97$.

We stress that this is not a real fit, but merely a way of estimating the quantities to obtain predictions for the measurability.

5

The angular power spectrum

in this chapter we will quantify the angular correlations in terms of the angular power spectrum C_ℓ. The angular power spectrum provides a useful tool to this end [36, 37], it gives the expected power in each mode ℓ derived from an expansion in spherical harmonics $Y_{\ell m}(\hat{n})$, which is a natural basis to expand in on the sphere. This is a projected power spectrum, as the distance or redshift coordinate is integrated over to project the correlations on the celestial sphere. This power spectrum has several advantages; first of all, we will mainly be interested on the largest scales, as the dark energy correlations will be strongest in this regime (which can be traced to the large characteristic length scale coming from inflation: for our specific model, see Chapters 9 and 10). To study this regime consistently, we need a function that can be measured on the full sphere without approximations (*e.g.* the flat sky approximation [43]). The C_ℓ's allow us to calculate the angular power spectrum including wide angle effects. Another advantage of this power spectrum is the fact that it can be measured without assumptions on the specific model, in comparison, the three dimensional power spectrum relies on the conversion from redshift to distance, which is in fact cosmology dependent.

Our observable of interest are the residuals from the mean in the luminosity distance. This is a scalar function, therefore

it can be expanded in spherical harmonics,

$$\Delta(z,\hat{n}) = \frac{\hat{d}_L(z,\hat{n}) - \langle \hat{d}_L \rangle(z)}{\langle \hat{d}_L \rangle(z)} = \sum_{\ell=0}^{\infty} \sum_{m=-\ell}^{\ell} \Delta_{\ell m}(z) Y_{\ell m}(\hat{n}). \tag{5.1}$$

This expansion defines the coefficients $\Delta_{\ell m}$. To obtain an expression for $\Delta_{\ell m}$ we can invert this equation, using that the spherical harmonics form a complete basis we obtain:

$$\Delta_{\ell m}(z) = \int d^2\hat{n} \Delta(z,\hat{n}) Y^*_{lm}(\hat{n}). \tag{5.2}$$

These coefficients $\Delta_{\ell m}$ are stochastic variables, therefore we take an ensemble average over them. This ensemble average would be over an ensemble of universes. However, we only have one universe to sample, this then yields a fundamental uncertainty known as *cosmic variance*. Assuming the process generating the fluctuations is statistically isotropic, the ensemble average takes the form:

$$\langle \Delta_{\ell m}(z) \Delta^*_{\ell' m'}(z') \rangle = C_\ell(z,z') \delta_{\ell\ell'} \delta_{mm'}, \tag{5.3}$$

where C_ℓ is the angular power spectrum and the δ's denote the Kronecker delta. Because of statistical isotropy we can assume that independent m's do not contain individual information and we can average over them. This gives us the following expression for the power spectrum

$$\boxed{C_\ell(z,z') = \frac{1}{2\ell+1} \sum_{m=-\ell}^{\ell} \langle \Delta_{\ell m}(z) \Delta^*_{\ell m}(z') \rangle.} \tag{5.4}$$

We can note that we only have $2\ell+1$ modes m at our disposal for every ℓ to sample our distribution. This quantifies the *cosmic variance*.

We can now insert (5.2) in (5.4) to obtain:

$$C_\ell(z,z') = \frac{1}{2\ell+1} \left\langle \int d^2\hat{n} \int d^2\hat{m} \Delta(z,\hat{n}) \Delta(z',\hat{m}) \sum_{m=-\ell}^{\ell} Y_{\ell m}(\hat{n}) Y^*_{\ell m}(\hat{m}) \right\rangle. \tag{5.5}$$

We can use the well known addition formula for spherical harmonics (see *e.g.* [64]) to simplify this, the addition formula relates the sum over the spherical harmonics to the Legendre polynomials $\mathcal{P}_\ell$ as follows,

$$\frac{1}{2\ell+1} \sum_{m=-\ell}^{\ell} Y_{\ell m}(\hat{n}) Y_{\ell m}(\hat{m}) = \frac{1}{4\pi} \mathcal{P}_\ell(\hat{n} \cdot \hat{m}). \tag{5.6}$$

This then simplifies (5.5),

$$C_\ell(z,z') = \frac{1}{4\pi}\int d^2\hat{n}\int d^2\hat{m}\langle\Delta(z,\hat{n})\Delta(z',\hat{m})\rangle\mathcal{P}_\ell(\hat{n}\cdot\hat{m}) \tag{5.7}$$

$$= 2\pi\int_{-1}^{1} d\mu\langle\Delta(z)\Delta(z')\rangle(\mu)\mathcal{P}_\ell(\mu). \tag{5.8}$$

In the second step we used that due to the isotropy of the background the angular dependence of the correlator $\langle\Delta(z,\hat{n})\Delta(z',\hat{m})\rangle$ appears only through the relative angle. Here, $\mu = \hat{n}\cdot\hat{m} = \cos(\theta)$, where θ is the angle between $\hat{n}$ and $\hat{m}$. So far, this has all been purely mathematical. We can insert our model via the correlation function $\langle\Delta(z)\Delta(z')\rangle(\mu)$, it is convenient to express it in the following way,

$$\langle\Delta(z)\Delta(z')\rangle(\mu) = \frac{\langle\hat{d}_L(z)\hat{d}_L(z')\rangle(\mu)}{\langle\hat{d}_L\rangle(z)\langle\hat{d}_L\rangle(z')} - 1. \tag{5.9}$$

For $\ell \geq 1$ we can exploit the fact that any constant not depending on the angle is proportional to $\mathcal{P}_0(\mu)$ and therefore, due to the orthogonality of the Legendre polynomials, these will not contribute for the power spectra with multipoles $\ell \geq 1$. Then, combining (4.12) and (5.8) gives us the following expression for the angular power spectrum with $\ell \geq 1$*.

$$C_\ell(z,z') = -a_i\pi\frac{\Omega_{Q,0}^2\bar{H}_0^4}{2}\frac{(1+z)(1+z')}{\langle\hat{d}_L\rangle(z)\langle\hat{d}_L\rangle(z')} \times\int_{-1}^{1}d\mu\int_0^{z'}dz_1\int_0^{z}dz_2\frac{\left(1+(\Delta t(z_1)+\Delta t(z_2))\frac{\langle\dot{\hat{\rho}}_Q\rangle_0}{\langle\hat{\rho}_Q\rangle_0}\right)}{\bar{H}(z_1)^3\bar{H}(z_2)^3}\left(\frac{r(z_1,z_2,\mu)^{n_{DE}}}{r_0^{n_{DE}}}\right)\mathcal{P}_\ell(\mu), \tag{5.10}$$

where $\Delta t(z) = t(z) - t_0$, $t(z)$ denotes the cosmological time at redshift z, the subscript 0 means it is evaluated today. $\dot{\hat{\rho}}_Q(t_0)$ denotes the time derivative of $\hat{\rho}_Q$ evaluated today. The factor a_i depends on the case, we define it as.

$$a_i = \begin{cases} 2, & i = 1,\ \textit{Case I}, \\ \tilde{\sigma}_Q^2, & i = 2,\ \textit{Case II}. \end{cases} \tag{5.11}$$

The power spectrum can be simplified some more by commuting the redshift integrals with the angular integral, as the integral over μ can then be solved. This is discussed elaborately in Appendix G. Here we just state the result,

$$C_\ell(z_1,z_2) = -\frac{a_i}{2}\pi^{\frac{3}{2}}\Omega_{Q,0}^2H_0^4\frac{2^{-\ell}\left(-\frac{n_{DE}}{2}\right)_\ell}{\Gamma(\frac{3}{2}+\ell)}\frac{(1+z_1)(1+z_2)}{\langle\hat{d}_L\rangle(z_1)\langle\hat{d}_L\rangle(z_2)}\int_0^{z_1}dz\int_0^{z_2}dz'\frac{\left(1+(\Delta t(z)+\Delta t(z'))\frac{\langle\dot{\hat{\rho}}_Q\rangle_0}{\langle\hat{\rho}_Q\rangle_0}\right)}{\bar{H}(z)^3\bar{H}(z')^3} \times\left(\frac{\chi(z)^2+\chi(z')^2}{r_0^2}\right)^{\frac{n_{DE}}{2}}\mu_0(z,z')^{-\ell}{}_2F_1\left(\frac{\ell}{2}-\frac{n_{DE}}{4},\frac{1}{2}+\frac{\ell}{2}-\frac{n_{DE}}{4};\frac{3}{2}+\ell;\mu_0(z,z')^{-2}\right). \tag{5.12}$$

$\chi(z) = \int_0^z dz'\bar{H}^{-1}(z')$ is the comoving coordinate, we use the unperturbed comoving distance as this comoving distance is

*Here we assumed the regime where the fluctuations saturate is never reached. For our predictions later on this means we will consider $H_0r_0 \geq 2$.

related to comoving coordinate $\vec{x}$. We used the short notation $\mu_0(z,z') = \frac{\chi(z)^2+\chi(z')^2}{2\chi(z)\chi(z')}$. ${}_2F_1$ is Gauss' hypergeometric function and $(a)_\ell = \frac{\Gamma(a+\ell)}{\Gamma(a)}$ is the Pochammer symbol. This power spectrum cannot yet be compared with observations. Observations are done by measuring $\frac{\hat{d}_L(z,\hat{n})-\bar{d}_L(z)}{\bar{d}_L(z)}$, where

$$\bar{d}_L = \int \frac{d^2\hat{n}}{4\pi}\hat{d}_L(z,\hat{n}) \tag{5.13}$$

is the luminosity distance averaged over all directions. If the angular averaging is the same as the ensemble averaging, the field is said to be ergodic. In our case, however, this is not the case. It is possible to relate our power spectrum to the one that would be observationally available. This can be approximated as a simple rescaling of our power spectrum and is derived in detail in Appendix F. The result is

$$\begin{aligned}\tilde{C}_\ell(z_1,z_2) = &-\frac{\frac{a_i}{2}}{1+\frac{C_0(z_1,z_2)}{4\pi}}\pi^{\frac{3}{2}}\Omega_{Q,0}^2\bar{H}_0^4\frac{2^{-\ell}\left(-\frac{n_{\rm DE}}{2}\right)_\ell}{\Gamma(\frac{3}{2}+\ell)}\frac{(1+z_1)(1+z_2)}{\langle\hat{d}_L\rangle(z_1)\langle\hat{d}_L\rangle(z_2)}\\ &\times\int_0^{z_1}dz\int_0^{z_2}dz'\frac{\left(1+(\Delta t(z)+\Delta t(z'))\frac{\langle\hat{\rho}_Q\rangle_0}{\langle\hat{\rho}_Q\rangle_0}\right)}{\bar{H}(z)^3\bar{H}(z')^3}\left(\frac{\chi(z)^2+\chi(z')^2}{r_0^2}\right)^{\frac{n_{\rm DE}}{2}}\\ &\times\mu_0(z,z')^{-\ell}{}_2F_1\left(\frac{\ell}{2}-\frac{n_{\rm DE}}{4},\frac{1}{2}+\frac{\ell}{2}-\frac{n_{\rm DE}}{4};\frac{3}{2}+\ell;\mu_0(z,z')^{-2}\right).\end{aligned} \tag{5.14}$$

Our angular power spectrum is a function of ℓ, z and z'. Observationally, however, the C_l's are split into redshift bins and integrated over some redshift distribution that traces the field

$$C_\ell^{i,j} = \int_0^\infty dz p^i(z)\int_0^\infty dz' p^j(z')\tilde{C}_\ell(z,z'), \tag{5.15}$$

where $p^i(z) = \frac{1}{N^i}\frac{dN^i}{dz}$, is the normalised number distribution as a function of redshift of supernovae used to trace the field. The superscript i denotes the redshift bin that is being used.

Numerically, it is more convenient to express it in a different way. After we switched order of integration ($\int_0^\infty dz\int_0^z dz' \to \int_0^\infty dz'\int_{z'}^\infty dz$), our C_ℓ's take the following form:

$$\boxed{\begin{aligned}C_\ell^{i,j} = &-\frac{a_i}{2}\pi^{\frac{3}{2}}\Omega_{Q,0}^2H_0^4\frac{2^{-\ell}\left(-\frac{n_{\rm DE}}{2}\right)_\ell}{\Gamma(\frac{3}{2}+\ell)}\\ &\times\int_0^\infty dz\int_0^\infty dz'\frac{W^{i,j}(z,z')}{\bar{H}(z)^3\bar{H}(z')^3}\left(1+(\Delta t(z)+\Delta t(z'))\frac{\langle\hat{\rho}_Q\rangle_0}{\langle\hat{\rho}_Q\rangle_0}\right)\left(\frac{\chi(z)^2+\chi(z')^2}{r_0^2}\right)^{\frac{n_{\rm DE}}{2}}\\ &\times\mu_0(z,z')^{-\ell}{}_2F_1\left(\frac{\ell}{2}-\frac{n_{\rm DE}}{4},\frac{1}{2}+\frac{\ell}{2}-\frac{n_{\rm DE}}{4};\frac{3}{2}+\ell;\mu_0(z,z')^{-2}\right),\end{aligned}} \tag{5.16}$$

where $W^{i,j}(z,z')$ is then defined as:

$$W^{i,j}(z,z') = \int_z^\infty dz_1\int_{z'}^\infty dz_2\frac{(1+z)(1+z')p^i(z)p^j(z')}{\langle\hat{d}_L\rangle(z)\langle\hat{d}_L\rangle(z')\left(1+\frac{C_0(z,z')}{4\pi}\right)}. \tag{5.17}$$

We will calculate these power spectra for *Case I* in Chapter 8. Following the discussion in section 4.3 we assume the matched values. The background Hubble rate $\bar{H}$ and the coordinate comoving distance are obtained from the assumed underlying flat wCDM universe,

$$\chi(z) = \int_0^z \frac{dz'}{H_0 E(z')}, \qquad \bar{H} = H_0 E(z), \qquad E(z) = \sqrt{\Omega_{c,0}(1+z)^3 + \Omega_{Q,0}(1+z)^{3(\omega_Q+1)}}. \tag{5.18}$$

These integrals are then solved using a numerical routine in `Python`.

6

Correlations due to relativistic effects

To know whether or not our signal is measurable, it is crucial to compare it with the signal that would be observed in a null experiment, i.e. a universe without spatial correlations in dark energy. In principle any positive measurement of angular correlations in the luminosity would be exciting, as such a measurement has currently not been performed as of today. However, it does not necessarily has to point us to new physics as General Relativity, combined with the perturbations in the gravitational field inherited from inflation also produces a non zero power spectrum for the luminosity distance [33–36]. These fluctuations are intrinsically relativistic effects known as convergence, Doppler, (integrated) Sachs-Wolfe, volume dilation and time delay [33–36, 65–67]. In this chapter we review these effects and derive the angular power spectra for the Doppler and convergence effects in perturbed ΛCDM [34, 67]. Our proposed dark energy model would then need to rise above this signal for it to be measurable. We point out that ideally one would perform this calculation also in the context of our DE model, however, this is beyond the scope of this thesis.

6.1 Luminosity distance in a perturbed relativistic universe

To obtain the formula's describing the correlations we follow the approach by [34], they calculate the convergence of photons due to the gravitational field by solving the Sachs equation [68]. The fully relativistic expression to linear order reads

[33, 34, 67],

$$\Delta_\kappa(z,\hat{n}) = \frac{1}{2\chi}\int_0^\chi d\chi' \frac{\chi-\chi'}{\chi'}\Delta_\perp(\Phi+\Psi) + \left(\frac{1}{\chi\mathcal{H}}-1\right)\vec{v}\cdot\hat{n} - \frac{1}{\chi}\int_0^\chi d\chi'(\Phi+\Psi) + \left(1-\frac{1}{\chi\mathcal{H}}\right)\int_0^\chi d\chi'(\dot{\Phi}+\dot{\Psi}) + \left(1-\frac{1}{\chi\mathcal{H}}\right)\Psi + \Phi. \tag{6.1}$$

Here, Δ_κ is the lensing* contribution to $\Delta = \frac{d_L}{\bar{d}_L} - 1$. Φ and Ψ denote the Bardeen potentials, $\mathcal{H} = aH$ is the conformal Hubble parameter. We can now recognise the several relativistic effects contributing to the signal. The first term is the standard expression for the lensing convergence, the second term is related to peculiar velocities and redshift space distortions and is known as Doppler lensing, the third term describes the effect of time delay. Then on the second line, we have the integrated Sachs-Wolfe effect, volume dilations and the Sachs-Wolfe effect. Apart from being studied in the context of the luminosity distance, these effects have also been studied in the context of galaxy surveys [65–67, 69, 70].

While all terms contribute to the correlations, two of the terms dominate. Namely, Doppler and convergence, which are the first two terms of (6.1). In the following two sections we calculate the auto power spectra for these effects [34, 67, 70]. The cross correlations between these effects are zero, as convergence selects modes perpendicular to the line of sight while the Doppler effect only takes modes along the line of sight into account.

6.2 Doppler

First, we focus on the second term, known in the literature as the Doppler contribution. These stem from the same effect as the more well known redshift space distortions. The peculiar velocity of the supernova changes the redshift one would measure if it was caused by just the Hubble flow. As a result of this the supernovae appears (de)magnified. Its contribution is given by [35, 69, 70],

$$\kappa_v(z,\hat{n}) = \left(\frac{1}{\chi(z)\mathcal{H}(z)}-1\right)\vec{v}\cdot\hat{n}. \tag{6.2}$$

This effect depends on the velocity's direction, $\vec{v}\cdot\hat{n}$, reflecting the fact that the effect is opposite if it is either moving from or towards the observer. At low redshift the first term in (6.2) dominates, due to the small comoving distance χ. If we assume the supernova is moving towards the observer, meaning $\vec{v}\cdot\hat{n} < 0$. Then the Doppler term demagnifies the supernova at low redshift. At high redshift the second term dominates and as a result the supernova is magnified in this regime. This can be explained as follows [67]: when fixing the redshift, a supernova moving towards us is in reality more distant in comoving coordinates than it appears. At low redshift this gives a negative contribution, due to the smaller angle it is observed under. At high redshift, however, this is not the case. In this regime the dominant contribution comes from the universe having a smaller scale factor when the photons were emitted. The bundle of photons is then stretched under the expansion of the universe when moving towards us, increasing the observed magnitude. For a *Planck* cosmology [1] the effects are equal at $z \approx 1.6$ and cancel out. For the values of z that we consider, the low redshift contribution always dominates. This effect

*The nomenclature 'lensing' can be confusing, as the first term in (6.1) is also widely known as lensing (convergence) on its own. However, all these effects change the observed magnitude of the supernova due to the matter perturbations and can be understood as lensing effects. Therefore, when referring to the lensing effects we mean the (dominating) contributions from (6.1).

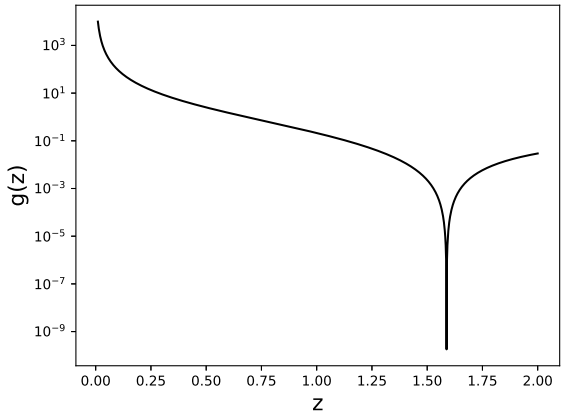

Figure 6.1: The behaviour of the function $g(z) = \left(\frac{1}{\chi\mathcal{H}} - 1\right)^2$, this expression appears in the angular power spectrum of Doppler lensing and largely drives its redshift dependence.

then becomes smaller with redshift. This is clear in Figure 6.1, where the behaviour of the function $g(z) = \left(\frac{1}{\chi\mathcal{H}} - 1\right)^2$ is shown. We square it as this is how it appears in the power spectrum, we indeed see that this term is mainly relevant at very low redshift.

6.2.1 The angular power spectrum

To make quantitative predictions we derive the angular power spectrum for this effect [67, 70]. We start from the expression as given in (6.2),

$$\Delta_v = \left(\frac{1}{\chi\mathcal{H}} - 1\right)\vec{v}\cdot\hat{n} \tag{6.3}$$

To connect the velocity field to the density field, which in turn can be connected to the power spectrum, we need the continuity equation from General Relativity [43],

$$\vec{v}(\vec{k},z) = i\mathcal{H}(z)f(z)\frac{\vec{k}}{k^2}\delta(\vec{k},z). \tag{6.4}$$

Here, $f(z) = \frac{d\ln D(z)}{d\ln a}$ is the growth rate with $D(z)$ being the growth function. This quantity is Fourier transformed, inserting its inverse Fourier transform in (6.1) one obtains,

$$\Delta_v = i\int \frac{d^3k}{(2\pi)^3}\left(\frac{1}{\chi} - \mathcal{H}(z)\right)\frac{\vec{k}\cdot\hat{n}}{k^2}f(z)\delta(\vec{k},z)e^{i\vec{k}\cdot\hat{n}\chi}. \tag{6.5}$$

We write the factor $\vec{k}\cdot\hat{n}e^{i\vec{k}\cdot\hat{n}\chi}$ conveniently in terms of spherical harmonics using the following identity,

$$\vec{k}\cdot\hat{n}e^{i\vec{k}\cdot\hat{n}\chi} = 4\pi k\sum_{\ell m} i^\ell j'_\ell(k\chi)Y_{\ell m}(\hat{k})Y_{\ell m}(\hat{n}). \tag{6.6}$$

Using this we find,

$$\Delta_v = 4\pi \sum_{\ell m} \int \frac{d^3k}{(2\pi)^3} \left(\frac{1}{\chi} - \mathcal{H}(z)\right) f(z) \frac{\delta(\vec{k}, z)}{k} i^{\ell+1} j'_\ell(k\chi) Y_{\ell m}(\hat{k}) Y_{\ell m}(\hat{n}). \tag{6.7}$$

An expansion in spherical harmonics is defined by $\Delta(z, \hat{n}) = \sum_{\ell m} \Delta_{\ell m}(z) Y_{\ell m}(\hat{n})$. Which is precisely the form of (6.7), we can thus read off the expansion coefficients,

$$\Delta_{v,\ell m} = 4\pi i^{\ell+1} \left(\frac{1}{\chi} - \mathcal{H}(z)\right) f(z) \int \frac{d^3k}{(2\pi)^3} \frac{\delta(\vec{k}, z)}{k} j'_\ell(k\chi) Y_{\ell m}(\hat{k}). \tag{6.8}$$

For convenience we state the angular power spectrum again, given as a summation over the modes m, previously given in (5.5),

$$C_\ell(z_1, z_2) = \frac{1}{2\ell + 1} \sum_{m=-\ell}^{\ell} \langle \Delta^*_{\ell m}(z_1) \Delta_{\ell m}(z_2) \rangle. \tag{6.9}$$

We can now readily insert the spherical harmonic coefficients (6.8) in (6.9) to obtain the angular powerspectrum in our case,

$$\begin{aligned} C^v_\ell(z_1, z_2) = \frac{(4\pi)^2}{2\ell + 1} &\left(\frac{1}{\chi(z_1)} - \mathcal{H}(z_1)\right) f(z_1) \left(\frac{1}{\chi(z_2)} - \mathcal{H}(z_2)\right) f(z_2) \\ &\times \int \frac{d^3q}{(2\pi)^3} \int \frac{d^3k}{(2\pi)^3} \frac{\langle \delta(\vec{k}, z_1) \delta^*(\vec{q}, z_2) \rangle}{kq} j'_\ell(k\chi(z_1)) j'_\ell(q\chi(z_2)) \sum_{m=-\ell}^{\ell} Y_{\ell m}(\hat{k}) Y^*_{\ell m}(\hat{q}). \end{aligned} \tag{6.10}$$

We can rewrite the factor $\langle \delta(\vec{k}, z_1) \delta^*(\vec{q}, z_2) \rangle$ in terms of the matter power spectrum P_m. This is defined as,

$$\langle \delta(\vec{k}, z_1) \delta^*(\vec{q}, z_2) \rangle = (2\pi)^3 P_m(k, z, z') \delta^3(\vec{k} - \vec{q}). \tag{6.11}$$

Here, δ^3 is the three dimensional Dirac delta function. Using this definition to solve one of the momentum integrals gives us,

$$\begin{aligned} C^v_\ell(z_1, z_2) = \frac{(4\pi)^2}{2\ell + 1} &\left(\frac{1}{\chi(z_1)} - \mathcal{H}(z_1)\right) f(z_1) \left(\frac{1}{\chi(z_2)} - \mathcal{H}(z_2)\right) f(z_2) \\ &\times \int \frac{d^3k}{(2\pi)^3} \frac{P_m(k, z_1, z_2)}{k^2} j'_\ell(k\chi(z_1)) j'_\ell(k\chi(z_2)) \sum_{m=-\ell}^{\ell} Y_{\ell m}(\hat{k}) Y^*_{\ell m}(\hat{k}). \end{aligned} \tag{6.12}$$

The sum can now be evaluated using the addition formula, which was stated in (5.6). Also using the the fact that the power spectrum only depends on the absolute wave number k allows us to write,

$$C^v_\ell(z_1, z_2) = \frac{2}{\pi} \left(\frac{1}{\chi(z_1)} - \mathcal{H}(z_1)\right) f(z_1) \left(\frac{1}{\chi(z_2)} - \mathcal{H}(z_2)\right) f(z_2) \int_0^\infty dk P_m(k, z_1, z_2) j'_\ell(k\chi(z_1)) j'_\ell(k\chi(z_2)) \tag{6.13}$$

This power spectrum is shown in Figure 6.2 for several redshift values. In Figure 6.2a, we show the power spectrum in the regime where it decreases with redshift, while in Figure 6.2b the regime is shown where the effect increases with redshift.

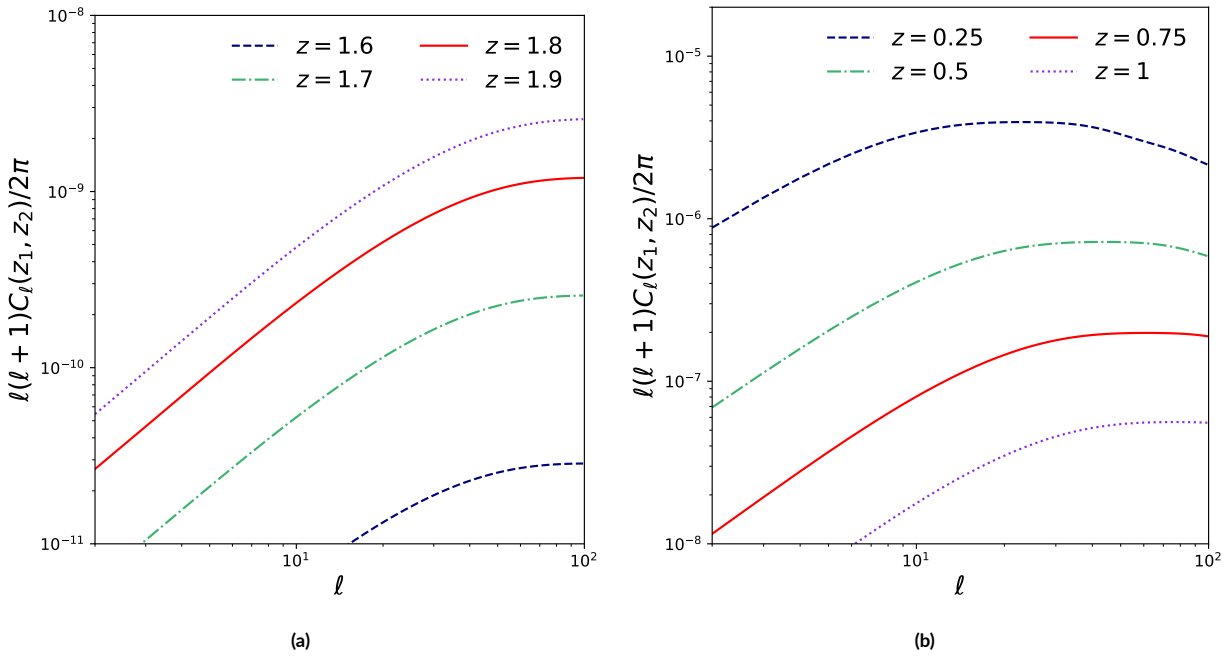

Figure 6.2: The Doppler power spectrum as a function of redshift, given by (6.13). The left panel shows the lower redshift behaviour, which is the most relevant part for this thesis. The right panel shows the higher redshift behaviour. We see that after $z = 1.6$ the power spectrum increases with redshift, while prior to this it decreases with redshift.

We do not show the unequal redshift correlations for the Doppler contribution. The Doppler effect is negligible at unequal redshifts, as it requires two objects to be physically close together in order for their velocities to be correlated.

For the final expression we also need to integrate over a redshift distribution, as in reality measurements are not done on an infinitely thin redshift slice, but over a distribution of sources in redshift space. This gives us,

$$C_\ell^{v,i,j} = \frac{2}{\pi}\int_0^\infty dz_1 p^i(z_1)\left(\frac{1}{\chi(z_1)} - \mathcal{H}(z_1)\right) f(z_1) \int_0^\infty dz_2 p^j(z_2)\left(\frac{1}{\chi(z_2)} - \mathcal{H}(z_2)\right) f(z_2) \times \int_0^\infty dk P_m(k, z_1, z_2) j_\ell'(k\chi(z_1)) j_\ell'(k\chi(z_2)). \tag{6.14}$$

This spectrum is shown in Chapter 8.

6.3 Convergence

The convergence contribution in General Relativity is given by [34],

$$\Delta_c(z,\hat{n}) = \int_0^z \frac{dz'}{H(z')}\frac{\chi(z)-\chi(z')}{\chi(z)\chi(z')}\Delta_\perp\left(\Phi(z,\vec{k}) + \Psi(z,\vec{k})\right), \tag{6.15}$$

where we used the result in (6.1) and swapped $d\chi = \frac{dz}{H(z)}$. $\Delta_\perp$ is the Laplacian evaluated transverse to the line of sight and Φ and Ψ are the Bardeen potentials. The convergence term expresses how certain overdense regions between the observer and the supernova magnify the source, thereby increasing (or decreasing) the supernova's luminosity. We note that this ef-

fect depends on the full line of sight and thus becomes stronger with redshift.

6.3.1 The angular power spectrum

To calculate the angular power spectrum we proceed in similar fashion as for the Doppler spectrum. We write the Fourier transform of the metric potentials Φ and Ψ and the expand the exponent in spherical harmonics,

$$\Phi(z,\hat{n}) + \Psi(z,\hat{n}) = \int \frac{d^3k}{(2\pi)^3}\left(\Phi(z,\vec{k}) + \Psi(z,\vec{k})\right) e^{i\vec{k}\cdot\hat{n}\chi} \tag{6.16}$$

$$= 4\pi \int \frac{d^3k}{(2\pi)^3}\left(\Phi(z,\vec{k}) + \Psi(z,\vec{k})\right) \sum_{\ell m} i^\ell j_\ell(k\chi) Y_{\ell m}(\hat{k}) Y_{\ell m}(\hat{n}). \tag{6.17}$$

We are interested in the Laplacian perpendicular to the line of sight of this function. From considering the previous expression, we see that the angular dependence only appears in the spherical harmonic $Y_{\ell m}(\hat{n})$. The perpendicular Laplacian thus directly works on this function. The spherical harmonics are the eigenfunctions of the angular part of the Laplace equation with eigenvalues $\ell(\ell+1)$, we can thus directly write $\Delta_\perp Y_{\ell m}(\hat{n}) = \ell(\ell+1) Y_{\ell m}(\hat{n})$. Inserting this in (6.15) yields,

$$\Delta_c(z,\hat{n}) = 4\pi \sum_{\ell m} \ell(\ell+1) \int \frac{d^3k}{(2\pi)^3} \int_0^z \frac{dz'}{H(z')} \frac{\chi(z)-\chi(z')}{\chi(z)\chi(z')} \left(\Phi(z,\vec{k}) + \Psi(z,\vec{k})\right) i^\ell j_\ell(k\chi) Y_{\ell m}(\hat{k}) Y_{\ell m}(\hat{n}). \tag{6.18}$$

Analogous to the Doppler case we can now read of the coefficients for the spherical harmonics expansion,

$$\Delta_{c,\ell m}(z) = 4\pi\ell(\ell+1) \int \frac{d^3k}{(2\pi)^3} \int_0^z \frac{dz'}{H(z')} \frac{\chi(z)-\chi(z')}{\chi(z)\chi(z')} \left(\Phi(z,\vec{k}) + \Psi(z,\vec{k})\right) i^\ell j_\ell(k\chi) Y_{\ell m}(\hat{k}). \tag{6.19}$$

We want to express this in terms of an overdensity $\delta(z,\vec{k})$, from the Poisson equation the following transfer function can be derived [43].

$$T_{\Phi+\Psi}(z,\vec{k}) = -\frac{3H_0^2\Omega_M}{k^2 a(z)}. \tag{6.20}$$

We now have all the ingredients to calculate the angular power spectrum. Expressing (6.19) in terms of the overdensity, δ, by using the transfer function and then inserting it in (6.9) gives us,

$$C_\ell^c(z,z') = \frac{(4\pi)^2\ell^2(\ell+1)^2}{2\ell+1} \int_0^z \frac{dz_1}{H(z_1)} \frac{\chi(z)-\chi(z_1)}{\chi(z)\chi(z_1)} \int_0^{z'} \frac{dz_2}{H(z_2)} \frac{\chi(z')-\chi(z_2)}{\chi(z')\chi(z_2)}$$
$$\times \int \frac{d^3k}{(2\pi)^2} \int \frac{d^3q}{(2\pi)^3} T_{\Phi+\Psi}(k,z) T_{\Phi+\Psi}(q,z') \langle \delta(z_1,\vec{k}) \delta^*(z_2,\vec{q}) \rangle j_\ell(k\chi(z_1)) j_\ell(q\chi(z_2)) \sum_{m=-\ell}^{\ell} Y_{\ell m}(\hat{k}) Y^*_{\ell m}(\hat{q}). \tag{6.21}$$

This can be simplified by first using the definition of the Power spectrum to set $\vec{q} = \vec{k}$ and then using the addition formula again to evaluate the sum, yielding,

$$C_\ell^\epsilon(z,z') = \frac{2}{\pi}(\ell(\ell+1))^2 \int_0^z \frac{dz_1}{H(z_1)} \frac{\chi(z)-\chi(z_1)}{\chi(z)\chi(z_1)} \int_0^{z'} \frac{dz_2}{H(z_2)} \frac{\chi(z')-\chi(z_2)}{\chi(z')\chi(z_2)} \times \int_0^\infty dk k^2 T_{\Phi+\Psi}(k,z_1) T_{\Phi+\Psi}(k,z_2) P_m(k,z_1,z_2) j_\ell(k\chi(z_1)) j_\ell(k\chi(z_2)). \quad (6.22)$$

A difference with the Doppler spectrum is that this spectrum has significant contribution at different redshift. This is the result of it being an integrated effect, all structure between the observer and the source contributes. A slice at redshift z and a slice at redshift z' is still correlated, as the photons originating from the sources on these slices partially travel through the same structure. To obtain the full expressions we also need to integrate this over some redshift distribution that traces the field, in our case that is a supernovae distribution.

$$C_\ell^{\epsilon,i,j} = \frac{2}{\pi}(\ell(\ell+1))^2 \int_0^\infty dz p^i(z) \int_0^\infty dz' p^j(z') \int_0^z \frac{dz_1}{H(z_1)} \frac{\chi(z)-\chi(z_1)}{\chi(z)\chi(z_1)} \int_0^{z'} \frac{dz_2}{H(z_2)} \frac{\chi(z')-\chi(z_2)}{\chi(z')\chi(z_2)} \times \int_0^\infty dk k^2 T_{\Phi+\Psi}(k,z_1) T_{\Phi+\Psi}(k,z_2) P_m(k,z_1,z_2) j_\ell(k\chi(z_1)) j_\ell(k\chi(z_2)). \quad (6.23)$$

It is then convenient to switch order of integration in the following way $\int_0^\infty dz \int_0^z dz' \rightarrow \int_0^\infty dz' \int_{z'}^\infty dz$. This then gives the final result,

$$\boxed{C_\ell^{\epsilon,i,j} = \frac{2}{\pi}(\ell(\ell+1))^2 \int_0^\infty \frac{dz_1}{H(z_1)} W_L^i(z_1) \int_0^\infty \frac{dz_2}{H(z_2)} W_L^j(z_2) \times \int_0^\infty dk k^2 T_{\Phi+\Psi}(k,z_1) T_{\Phi+\Psi}(k,z_2) P_m(k,z_1,z_2) j_\ell(k\chi(z_1)) j_\ell(k\chi(z_2)).} \quad (6.24)$$

With $W_L^i(z_i)$ being the lensing kernel defined as:

$$W_L^i(\tilde{z}) = \int_{\tilde{z}}^\infty dz p^i(z) \frac{\chi(z)-\chi(\tilde{z})}{\chi(z)\chi(\tilde{z})}. \quad (6.25)$$

In Figure 6.3 the power spectrum for several redshift slices, given by (6.22), is shown. Figure 6.3a gives the spectrum for two slices evaluated at the same redshift. As expected the correlations become stronger with redshift. Figure 6.3b gives the spectrum when considering unequal redshift slices. Due to the convergence effect depending on the full line of sight, the unequal redshift contribution is significant. The spectrum (6.24) is shown in Chapter 8.

6.4 Malmquist bias

In principle we could also have correlations coming from surveys being magnitude limited. This induces a bias known as the Malmquist bias, which affects the distribution $p(z)$. The lensing effects magnify or demagnify supernovae and can thus push stars that are otherwise to faint to observe over the magnification threshold. This effect depends on the large scale

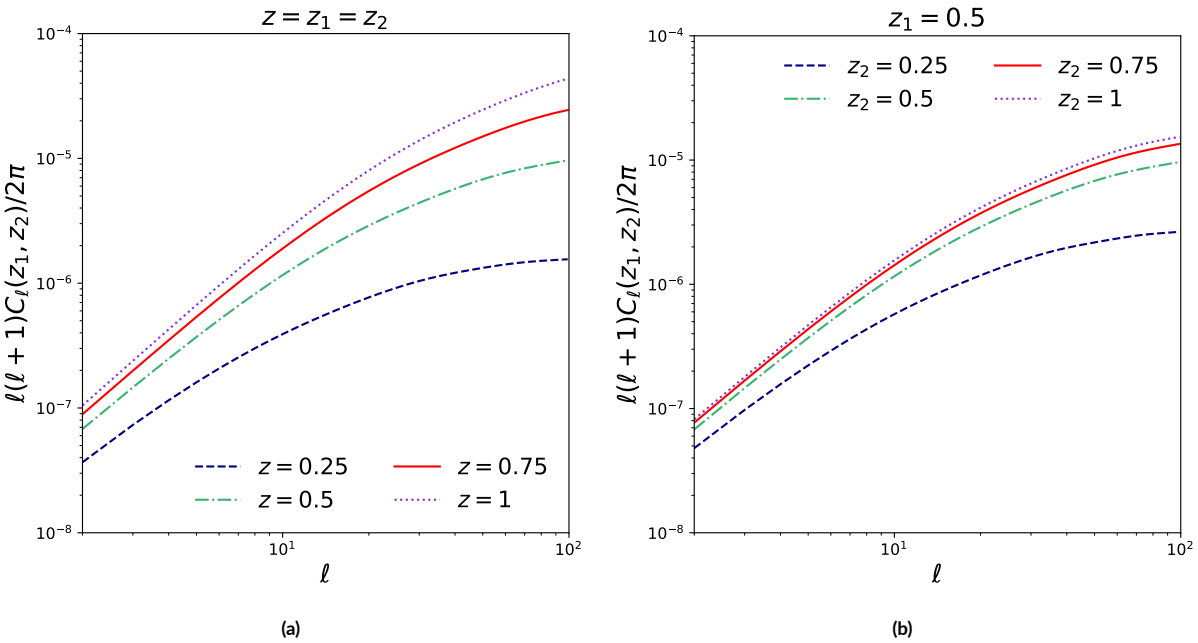

Figure 6.3: The angular power spectrum for the convergence effect, given by (6.22). The left panel considers equal redshift slices, while the right panels considers unequal redshift slices.

structure and thus induces non zero correlations. Specifically the observed number of supernovae N in a redshift shell z would be altered by

$$\frac{N(z,\hat{n})}{\bar{N}(z)} = 1 + 5s\kappa(z,\hat{n}) \tag{6.26}$$

$$\Rightarrow p(z,\hat{n}) = \bar{p}(z)(1 + 5s\kappa(z,\hat{n})), \tag{6.27}$$

where s is the effective number count slope [71, 72] and κ the lensing effects. This would then be a correction to the average distribution $\bar{p}^i(z)$. However, this correction is higher order, as it multiplies (6.1), which is already leading order in perturbation theory. We are therefore justified in considering the average distribution as our distribution.

6.5 The matter spectrum

These integrals can be quite complicated, as the higher ℓ spherical Bessel functions become heavily oscillating. To simplify the computations we use the linear power spectrum at the largest scales instead of the non linear spectrum. This is given by [43],

$$P_L(k,z_1,z_2) = \frac{8\pi^2}{25}\frac{\mathcal{A}_s}{\Omega_M^2}D(z_1)D(z_2)T(k)^2\frac{k^{n_s}}{H_0^4 k_p^{n_s-1}}. \tag{6.28}$$

$\mathcal{A}_s$ is the amplitude of curvature perturbations on the pivot scale k_p. Using the linear power spectrum has the benefit that the redshift dependence of the power spectrum decouples, i.e. $P_L(k,z_1,z_2) \propto D(z_1)D(z_2)k^{n_s}$ and is accurate on large scales.

After $\ell = 15$ we switch to the non linear power spectrum[†]. To still efficiently calculate these integrals we then adopt the Limber approximation [73]. Switching at $\ell = 15$ ensures an almost smooth transition ($< 1\%$) between the calculation methods. The power spectrum, growth rate, growth function and transfer functions are obtained by using the publicly available Core Cosmology Library (CCL [74], v2.1.0), CCL uses CAMB power spectrum [75].

For these quantities we assume the following flat *Planck* ΛCDM cosmology [1]: $\Omega_b = 0.045$, $\Omega_{\rm CDM} = 0.27$, $h = H_0/(100\,{\rm km\,s^{-1}Mpc^{-1}}) = 0.67$, $\mathcal{A}_s = 2.1 \times 10^{-9}$ on a pivot scale of $k_p = 0.05\ {\rm Mpc}^{-1}$ and $n_s = 0.96$. In ΛCDM Ω_b and $\Omega_{\rm CDM}$ are the fractional energy densities of baryonic and cold dark matter, h is the dimensionless Hubble constant, $\mathcal{A}_s$ is the variance of curvature perturbations in a logarithmic wavenumber interval centered around the pivot scale k_p, and n_s is the scalar tilt.

[†]This is the approach we use to calculate the full spectrum integrated over a supernova distribution, these results are shown in Chapter 8. The figures in this chapter, that display the angular spectrum $C_\ell(z, z')$, are obtained by using just the linear approximation.

7

Forecasting and supernovae surveys

To assess whether this effect is measurable, we perform a forecast. The measurability of the effect depends on the astrophysical object one uses to trace the field and are thus survey specific.

An analogy could be made with a more earthly example: when one would observe a perfectly clear river, it would be impossible to see how fast the water in the river is flowing. However, you can focus on a leaf floating in the water and use this as a proxy for the speed of the water. It would then also be important to understand the physics of the leaf, for example their floating abilities as function of speed and environment would be pivotal. Our leafs are supernovae, as supernovae have proven their worth to cosmology [76]. Supernovae are excellent tracers of the expansion of the universe for several reasons; first and foremost, due to their characteristic light curves supernovae make exquisite standard candles, but almost as important, supernovae also form some of the brightest events in the universe, making them visible over enormous distances. However, there are a few complications when doing supernovae cosmology; while a galaxy will be visible on the sky for practically forever on human time scales, a supernovae is only visible for a limited time. It is thus possible to miss it, for example, when your telescope is observing another patch of the sky. For supernova cosmology the survey strategy is thus very important. Another complication comes from the need for accurate spectroscopic redshifts, several modern surveys will perform photometric measurements. Then to obtain accurate measurements, another telescope needs to perform a spectroscopic follow up.

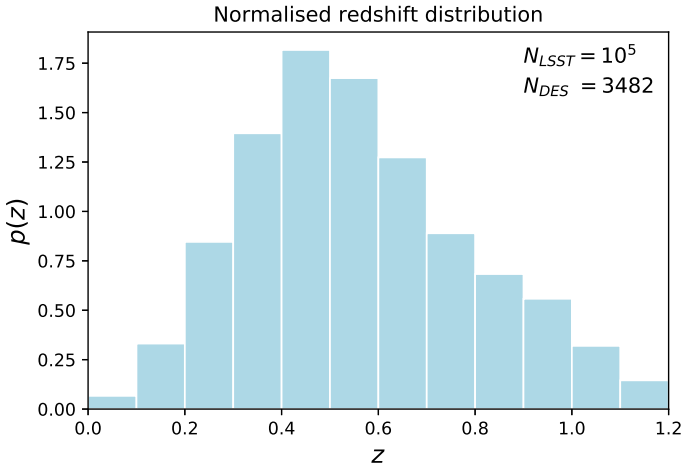

Figure 7.1: The supernova distribution expected to be obtained by the Dark Energy Survey (DES) [78]. This survey will observe 30 square degrees of the sky repeatedly, 6 of wich will be allocated more observing time for so called 'deep drilling'. This survey will be used to make forecasts for the observability of our dark energy signal.

We consider two such surveys, first we consider the ongoing Dark Energy survey (DES y5, [77]), we make predictions for the Y5 data. This will be available in the near future. However, we also make forecasts in a more futuristic setup, as will be produced by the year 10 Legacy Survey of Space and Time (LSST Y10, [32]). Both surveys are described in the following two sections. In the last section we describe the formalism in which we make the forecast.

7.1 The Dark Energy Survey

The dark energy survey is a survey that is conducted by the Victor M. Blanco telescope in Chile. Observations ran from 2013 to 2019. As of today the data from the first three years is available.

We make predictions for the DES Y5 survey which will be released in the near future. The expected characteristics of the supernovae survey are described by [78]. As discussed before, the survey strategy is of pivotal importance. In this case the telescope will visit 10 regions of 3 deg^2, covering a total area of 30 deg^2, corresponding with a fraction of the sky $f_{\rm sky} = 0.0007$. Two of these regions will have a longer exposure times, performing 'deep drills' into redshift space. This strategy is expected to find about 3482 supernovae with accurate redshift measurements. This sample is shown in Figure 7.1. We estimate the intrinsic uncertainty in magnitude $\sigma_m = 0.13$, in accordance with [78].

7.2 Legacy Survey of Space and Time

Separately, we also make forecasts in a more futuristic setup, with the goal of mimicking the year 10 *Legacy Survey of Space and Time* (LSST Y10). This survey will be conducted by the Vera C. Rubin Observatory, located in Chile.

This sample will improve significantly on current samples for several reasons [79]: it will have a significantly higher number count, with an expected number of supernovae with well measured redshift of about 10^5 , almost two orders of magnitudes more than DES. Secondly, LSST will observe a much larger region of the sky, as LSST will produce the first all sky

supernova survey, with $f_{\rm sky} = 0.5$. This will significantly reduce the cosmic variance. We assume the total LSST sample to be similar in shape as the DES sample, therefore we use the same redshift distribution $p(z)$.

Similar to DES we will assume the intrinsic magnitude scatter to be $\sigma_m = 0.13$.

7.3 Forecasting methods

We aim to predict the overall detectability of the signal. To this end we provide a forecast for the signal to noise ratio (SNR). The SNR of an angular power spectrum C_ℓ between two redshift bins i and j is defined as:

$$\mathrm{SNR}^{ij} = \sqrt{\sum_{\ell=\ell_{\rm min}}^{\ell=\ell_{\rm max}} \frac{\left(C_\ell^{ij}\right)^2}{\mathrm{Var}\left[C_\ell^{ij}\right]}}. \tag{7.1}$$

Here, $\mathrm{Var}\left[C_\ell\right]$ is the variance of the power spectrum. Assuming all the perturbations are statistically homogeneous, isotropic and Gaussian the variance of a power spectrum is given by [80]:

$$\mathrm{Var}\left[C_\ell^{ij}\right] = \frac{\tilde{C}_\ell^{ii}\tilde{C}_\ell^{jj} + \tilde{C}_\ell^{ij}\tilde{C}_\ell^{ji}}{(2\ell+1)f_{\rm sky}}, \tag{7.2}$$

where $\tilde{C}_\ell^{ij}$ is the angular power spectrum between two redshift bins including noise and $f_{\rm sky}$ is the observed fraction of the sky. We consider noise for the auto-power spectra and we assume this to be white noise. This noise is a result from the fact that we do not measure a smooth field, but a finite number of supernovae. We refer to this noise as shot noise. For our power spectrum it takes the following form [36]:

$$\tilde{C}_\ell^{ii} = C_\ell^{ii} + \frac{4\pi f_{\rm sky}}{N_{SNe}}\left(\frac{\sigma_{d_L}}{d_L}\right)^2 \tag{7.3}$$

Here N_{SNe} is the amount of supernovae in the redshift bin and $\frac{\sigma_{d_L}}{d_L}$ is the intrinsic dispersion of luminosity distance measurement, this can be related to the intrinsic magnitude dispersion of the supernova via $\frac{\sigma_{d_L}}{d_L} = \frac{\ln 10}{5}\sigma_m$. The intrinsic uncertainty in the magnitude is usually estimated to be roughly 0.1-0.2 [78, 81, 82]. We assume an ℓ range of $2 \leq \ell \leq 100$. However, we explore the dependence of the SNR on ℓ_{min}.

8

Prospects for the measurability

In this Chapter we present the results for the angular power spectra derived in Chapter 5. We analyse which range of the model parameters $H_0 r_0$ and $n_{\rm DE}$ would lead to a possible positive detection, and assess what is the best strategy to detect this signal. We consider the contaminant effects described in Chapter 6 and predict the noise as discussed in Chapter 7. We consider $H_0 r_0$ instead of r_0 as this is a dimensionless quantity, the length scale of the fluctuations with respect to the Hubble length today. We only consider lengths r_0 larger than twice the Hubble length, thus we never reach the regime where the fluctuations saturate. The general shape of the angular power spectrum does not significantly change as the factor $(H_0 r_0)^{-n_{\rm DE}}$ mostly* affects the general amplitude, therefore not changing the form of the spectrum.

Our predictions are made in the context of *Case I*. Generalising the results to *Case II* is in principle straightforward once $\tilde{\sigma}_Q^2$ is fixed. A simple comparison can be made in the following cases, when $\tilde{\sigma}_Q^2 = 2$ the results are the same and when $\tilde{\sigma}_Q^2 < 2$ ($\tilde{\sigma}_Q^2 > 2$) *Case II* would be harder (easier) to detect than the results in this Chapter. An order of magnitude conversion between the two cases could be obtained by rescaling the characteristic length scale of *Case I* by $r_0 \to r_0 \left(\frac{2}{\tilde{\sigma}^2}\right)^{\frac{1}{n_{\rm DE}}}$.†

*It also appears in the contribution from the monopole, however, the monopole only affects the shape of the spectrum on the few percent level.

†This approximation neglects the fact that in principle one would have to calculate the bare quantities $\Omega_{Q,0}$ and H_0 again in *Case II*.

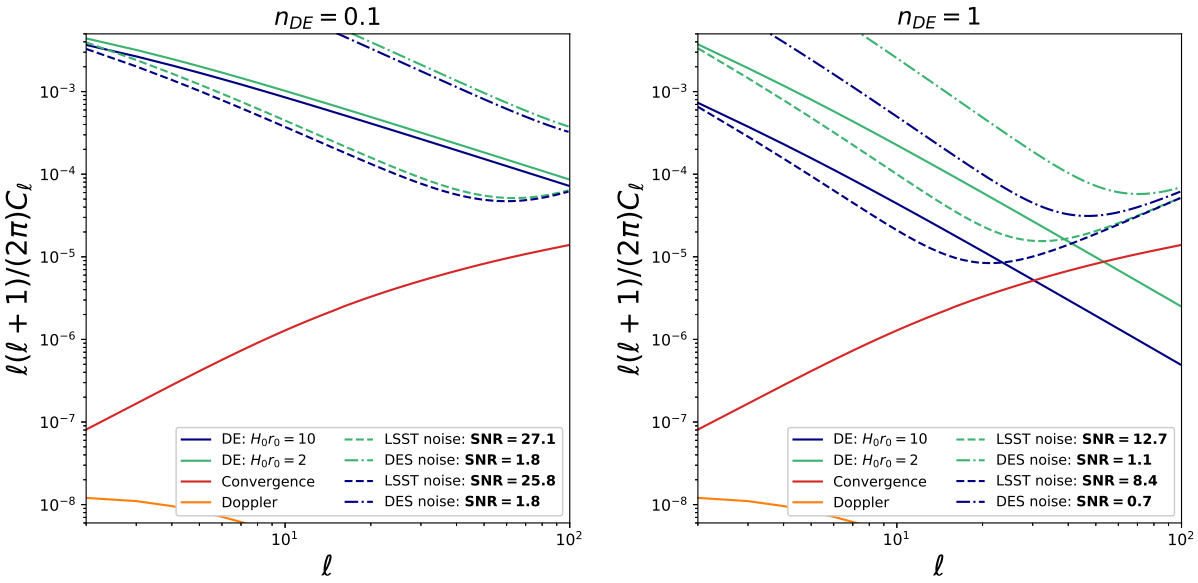

(a) $n_{\mathrm{DE}} = 0.1$ **(b)** $n_{\mathrm{DE}} = 1$

Figure 8.1: The angular power spectra C_ℓ shown with characteristic fluctuation scale $H_0 r_0 = 2$ (solid green line) and 10 (solid blue line). We also show the spectra for the lensing effects (convergence in red and Doppler in orange). The left panel shows the dark energy signal with a spectral slope of $n_{\mathrm{DE}} = 0.1$ and the right panel the spectra for $n_{\mathrm{DE}} = 1$. The figures also include the expected noise, including shot noise and cosmic variance for the two survey set ups (LSST - dashed and DES - dot-dashed). This gives four curves, as the noise depends both on the survey and the power spectrum via (7.2). In the legend the expected signal to noise ratio corresponding to this noise is given in bold.

8.1 Overall detectability

First, we assess the detectability over the full redshift distribution. In Figure 8.1 the angular power spectrum (5.16) is shown. It is clear that the signal is mostly located at the lower ℓ's and then decays very rapidly. This decay is steepest in the case where the spectral index is larger, which is the case shown in Figure 8.1b. We understand the fact that a higher n_{DE} gives a smaller signal as follows: due to always considering large scales, indicated by $H_0 r_0 \geq 2$, the fluctuations contributing are those with a relatively small length scale with respect to r_0. When we consider the profiles of the correlations, Figure 3.1, the profiles with a small spectral index change significantly more rapidly at smaller r. This then results in a higher C_ℓ.

In the low ℓ regime, the main contribution of noise is the cosmic variance. The cosmic variance is especially large for DES due to the small fraction of the sky it includes (only 30 deg^2). LSST does not have this problem as it includes all of the southern hemisphere for the Y10 survey. When comparing the noise for the power spectra (dashed (LSST)/dot-dashed (DES)) with the green and blue lines) we see that the prospects of detecting this effect with the dark energy survey (DES) are very small, as the low ℓ regime is drowned in cosmic variance. Even though the total amount of supernovae observed is significantly larger for LSST, the number density is actually quite similar to DES. The shot noise is thus comparable for both surveys. For LSST the signal rises above the noise for $\ell_{\mathrm{max}} = 20$ when $n_{\mathrm{DE}} \approx 1$ and $\ell_{\mathrm{max}} \approx 100$ when $n_{\mathrm{DE}} = 1$.

In this regime we also observe that both the convergence as the Doppler effect are subdominant to the dark energy spectrum and are thus not a nuisance. In the case $n_{\mathrm{DE}} = 1$, around $\ell \approx 40$ the convergence effect does surpass the dark energy signal; however, in this regime the signal is located below the shot noise, so it would not contribute to a detection. The

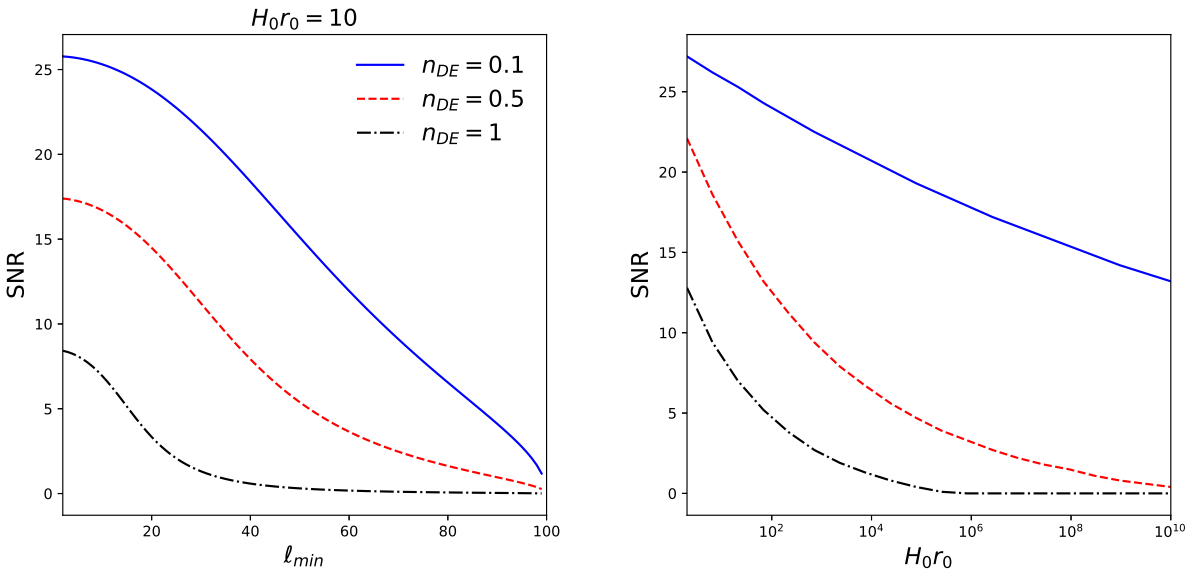

(a) (b)

Figure 8.2: The left panel shows the signal to noise ratio for Y10 LSST depending on the lowest multipole measured. A range of values for the spectral indices $n_{\rm DE}$ is explored, $n_{\rm DE} \in (0.1, 0.5, 1)$ with (blue-solid, red-dashed, black-dot-dashed). We fix the scale of the fluctuations at $H_0 r_0 = 10$. In the right panel we show the dependency of the SNR on the scale of the fluctuations $H_0 r_0$ for LSST Y10. We consider the same spectral indices.

Doppler signal is similar to the dark energy signal as it is mainly relevant at large scales. However, even at these scales it is several orders of magnitude below the dark energy signal and thus can safely be neglected. We also note that in general the lensing effects are below the shot noise[‡], thus in the regime where our signal would be of the same order as the lensing effects (large $H_0 r_0$) the signal is not measurable in any case.

The large scales that we want to probe are challenging to extract from the data. On these scales the details of the survey strategy, survey mask and the galactic foreground can make this signal harder to extract. Because of this we have explored how the signal to noise ratio depends on the lowest multipole probed. This is shown in Figure 8.2a. Here we see that for most of the values for $n_{\rm DE}$ a LSST measurement would also be possible for $\ell_{\rm min} \approx 20$, but for the case where $n_{\rm DE} = 1$ this would be a challenge. In this case it would be worth the effort to constrain these lower multipoles.

We also studied how the signal to noise ratio depends on the scale $H_0 r_0$. This is shown in Figure 8.2b. We observe that as long as the spectral index is not close to one, the signal is measurable even if $H_0 r_0$ becomes relatively large. However, in the case where $n_{\rm DE} = 1$ the signal decays rapidly. Measuring this signal when $H_0 r_0 > 100$ would probably pose a considerable challenge for observationalists.

Overall, comparing the signal to noise predicted in Figure 8.1, we expect a positive measurement in DES would be very challenging. As even in the case with a very small slope and a relatively small typical length scale of $H_0 r_0 = 2$, we still find a signal to noise SNR of 1.8. However, due to the very large area of the sky LSST covers, it does not suffer from these effects and could potentially measure even the 'harder' case with $H_0 r_0 = 10$ and $n_{\rm DE} = 1$.

[‡]Irrespective of our dark energy signal, we note that because of this measuring these relativistic effects with supernovae surveys would be challenging at best.

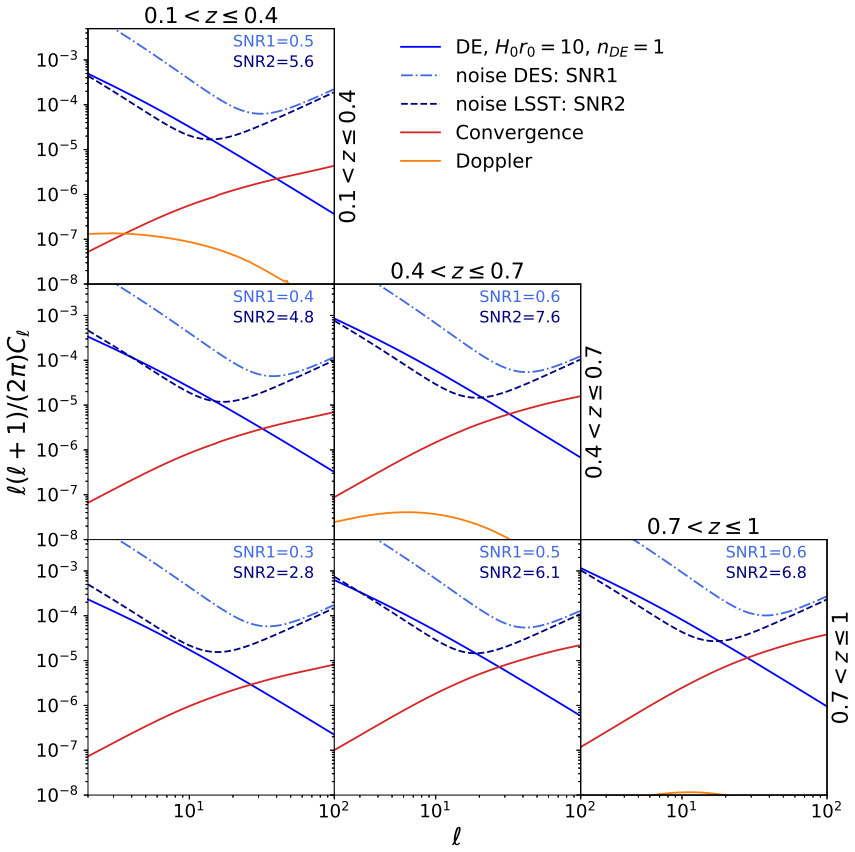

Figure 8.3: The angular power spectra C_ℓ calculated over several redshift bins. We use three bins with width $\Delta z = 0.3$ between $z = 0.1$ and $z = 1$, using these bins we then consider all auto- and cross-correlations. This then gives the six panels shown above. We also include the lensing effects (convergence - red, Doppler - orange) and the noise expected from both surveys (DES - dot-dashed line, LSST - dashed line). In the top right the expected signal to noise ratio corresponding to this noise is given: SNR1 denotes the signal to noise ratio expected for DES, SNR2 gives the SNR expected for LSST Y10.

8.2 Redshift dependence of the signal

We conduct a study into the redshift dependence of the signal. To this end we show the redshift dependence of $\tilde{C}_{\ell=10}(z, z')$, which can be calculated from (5.14). This is shown for several values of the spectral slope n_{DE} in Figure 8.4 (upper panels). We see that the signal is mostly located at equal redshift, however, it is good to note that the signal does not decay rapidly at unequal redshift. This is also clearly visible in Figure 8.3, in which we show the signal calculated over several redshift bins, also including cross-correlations between bins. The relatively strong signal at unequal redshift distinguishes itself from the regular cold dark matter power spectrum, which is strongly peaked at equal redshift. This would be beneficial if the value of $H_0 r_0$ is large enough for this effect to be comparable with the Doppler effect. The Doppler effect is negligible at unequal redshifts, as it requires two objects to be physically close together in order for their velocities to be correlated. This is not true for the convergence spectrum, as this depends on all perturbations along the line of sight and therefore naturally has correlations at unequal redshift. From Figure 8.3 we can also conclude that binning the signal in different redshift bins is not beneficial for the signal to noise, as in every bin the SNR is significantly lower than the SNR obtained for the full distribution (Figure 8.1). We explain this by the fact that the signal has correlations even when considering very different red-

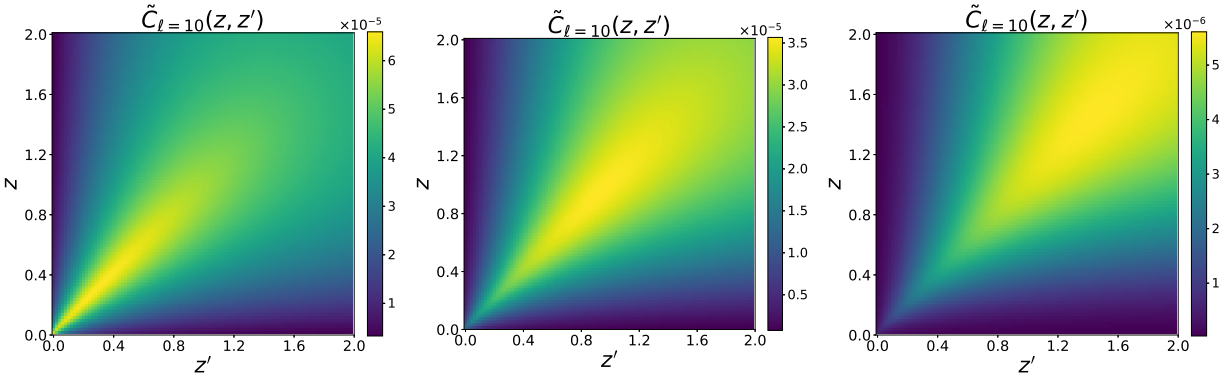

(a) $n_{\rm DE} = 0.1$ **(b)** $n_{\rm DE} = 0.5$ **(c)** $n_{\rm DE} = 1$

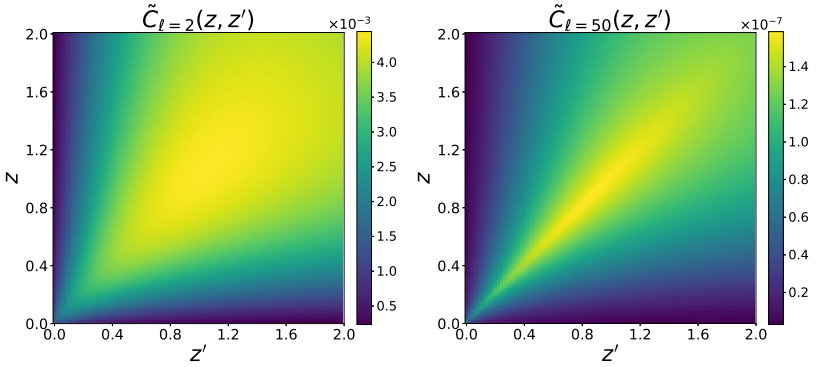

(d) $n_{\rm DE} = 0.5$ **(e)** $n_{\rm DE} = 0.5$

Figure 8.4: The angular power spectrum (5.14) as a function redshift. The upper panels show $\tilde{C}_{\ell=10}(z,z')$ shown for several values of the spectral slope $n_{\rm DE}$: $n_{\rm DE} = 0.1$ (left), 0.5 (middle) and 1 (right). The lower panels show $\tilde{C}_{\ell=2}(z,z')$ and $\tilde{C}_{\ell=50}(z,z')$, with $n_{\rm DE} = 0.5$. These figures are obtained using $H_0 r_0 = 10$ and the power spectrum is calculated for the values $z, z' \in (0,2)$ on a 100×100 grid.

shifts, therefore considering a broad redshift distribution does not water down the signal. This is especially visible on the larger scales, small ℓ, as here the unequal redshift contribution is most prominent. This is evident in Figures 8.4d and 8.4e, here we show the redshift behaviour of two different multipoles ℓ. When $\ell = 2$, corresponding to larger scales, we see that the signal is relatively strong over a broad range of $\Delta z = z - z'$. While at $\ell = 50$ the signal becomes more centered around equal redshift. To obtain the best SNR, the proper strategy would be reducing the shot noise as much as possible by including the full distribution. However, the unequal redshift signal could be used as a cross-check for the detection as we see in the cross-bins in Figure 8.3 can still produce a measurable signal (SNR$>$ 3).

From Figure 8.4 we see that when the spectral index is smaller, the signal resides more at low redshift. Again, this can be understood from Figure 3.1. Low redshift means probing smaller scales, therefore the part that is most relevant is the small r behaviour in Figure 3.1. A small spectral index means that the function $s(r)$ varies more rapidly when r is small, thereby giving a better signal at low redshift.

9

Dark energy from inflation

Up until now we have studied a phenomenological model of spatial correlations in dark energy. We will now switch gears and apply our formalism to a specific model. We will consider the case where the present dark energy traces its origin to the early stages of the universe. In this scenario, the initial conditions of dark energy were quantum and, as a result, can remain quantum even up to late times. We are particularly interested in how the quantum backreaction affects the late-time cosmology. This was investigated by a series of papers [26–31]. Specifically, using perturbative methods, ref. [28] studied a very light non minimally coupled scalar field that is spectator during inflation. They found there is a regime where the backreaction remains small during inflation and becomes relevant at late times, where it effectively behaves as a cosmological constant. However, once the backreaction becomes comparable to the background it can no longer be treated perturbatively. This was solved by ref. [29] by suitable adopting the stochastic formalism [83] and solving the problem self consistently. They found that the backreaction accelerates the universe, driving it towards a de Sitter phase. Therefore providing a new candidate for dark energy. As dark energy originates from quantum fluctuations of matter fields, it can be expected that the dark energy field exhibits spatial correlations. This was studied by ref. [30, 31], in these works the density-density correlators of the dark energy density field were calculated. They found that the spatial correlations imprinted during inflation are indeed inherited by the late time dark energy fluid. This was then applied to the problem of the Hubble tension by [30] (for a review of the Hubble tension, see [14, 15]). Due to the fluctuations of dark energy the Hubble rate itself becomes a fluctu-

ating parameter, if these fluctuations are relevant on sub-Hubble scales, it was found by [30] that this model can relieve the Hubble tension to 1σ. Posing a significant improvement over the ΛCDM tension, currently estimated around 4σ [14, 15].

This Chapter is devoted to giving a brief overview of this model and the most important results. We mostly follow the work by [29] and [30]. We go over the derivations of the one- and two-point energy density functions and discuss the intricate connection between inflation and this dark energy candidate.

9.1 A non minimally coupled scalar field

Following the work by [28–31] we consider a light scalar field with a non minimal coupling. This is then described by the following action

$$S[\Phi] = \int d^4x\sqrt{-g}\left\{-\frac{1}{2}g^{\mu\nu}\partial_\mu\Phi\partial_\nu\Phi - \frac{1}{2}m^2\Phi^2 - \frac{1}{2}\xi R\Phi^2\right\}, \tag{9.1}$$

where R is the Ricci curvature scalar of the metric $g_{\mu\nu}$ and $g = \det\left[g_{\mu\nu}\right]$. Due to the non minimal coupling this field has an effective mass given by $M^2 = m^2 + \xi R$, via the Ricci scalar R this is directly dependent on the cosmological background. We assume a FLRW background and generalise the action to this metric. In this form we obtain:

$$S[\Phi] = \int dt d^3x\mathcal{L}_\Phi = \int \mathrm{d}t\,\mathrm{d}^3x\,a^3 \times \left\{\frac{1}{2}\dot{\Phi}^2 - \frac{1}{2a^2}(\vec{\nabla}\Phi)^2 - \frac{1}{2}\left[m^2 + 6\xi(2-\varepsilon)H^2\right]\Phi^2\right\}, \tag{9.2}$$

where $\varepsilon = -\frac{\dot{H}}{H^2}$, which during inflation is known as the slow roll parameter. It depends on the epochs that we will consider: de Sitter inflation ($\varepsilon = 0$), radiation-domination ($\varepsilon = 2$) and matter-domination ($\varepsilon = 3/2$).

We now wish to proceed with quantizing the model on this background. For this we use the standard way of canonical quantization. We know the canonical momentum as:

$$\Pi(x) = \frac{\partial\mathcal{L}_\Phi}{\partial\dot{\Phi}(x)} = a^3\dot{\Phi}(x). \tag{9.3}$$

The quantum properties can then be studied from the Hamiltonian,

$$H[\Phi, t] = \int d^3x\left[\Pi(t,\vec{x})\dot{\Phi}(t,\vec{x}) - \mathcal{L}_\Phi\right] \tag{9.4}$$

$$= \int d^3x\left\{\frac{1}{2a^3}\Pi^2 + \frac{a}{2}\left(\vec{\nabla}\Phi\right)^2 + \frac{a^3}{2}\left[m^2 + 6\xi(2-\varepsilon)\right]\right\}. \tag{9.5}$$

These fields can be quantized via the regular procedure by promoting the fields to operators and turning their Poisson brackets into equal-time commutation relations:

$$\left[\hat{\Phi}(t,\vec{x}), \hat{\Pi}\left(t,\vec{x}'\right)\right] = i\partial^3\left(\vec{x} - \vec{x}'\right), \quad \left[\hat{\Phi}(t,\vec{x}), \hat{\Phi}\left(t,\vec{x}'\right)\right] = 0 = \left[\hat{\Pi}(t,\vec{x}), \hat{\Pi}\left(t,\vec{x}'\right)\right] \tag{9.6}$$

The Heisenberg equations of motions associated with the Hamiltonian (9.4) are then,

$$\frac{d}{dt}\hat{\Phi}(t,\vec{x}) - a^{-3}\hat{\Pi}(t,\vec{x}) = 0, \tag{9.7}$$

$$a^{-3}\frac{d}{dt}\hat{\Pi}(t,\vec{x}) - \frac{\nabla^2}{a^2}\Phi(t,\vec{x}) + M^2(t)\hat{\Phi}(t,\vec{x}) = 0. \tag{9.8}$$

Here, the effective mass M^2 is defined by:

$$M^2(t) = m^2 + \xi R(t) = m^2 + 6\xi(2-\varepsilon)H^2. \tag{9.9}$$

The fields are then expanded in creation and annihilation operators $\hat{b}$ and $\hat{b}^\dagger$,

$$\hat{\Phi}(t,\vec{x}) = \int \frac{d^3k}{(2\pi)^{\frac{3}{2}}}\left\{e^{i\vec{k}\cdot\vec{x}}\varphi(t,k)\hat{b}(\vec{k}) + e^{-i\vec{k}\cdot\vec{x}}\varphi^*(t,k)\hat{b}^\dagger(\vec{k})\right\}, \tag{9.10}$$

$$\hat{\Pi}(t,\vec{x}) = \int \frac{d^3k}{(2\pi)^{\frac{3}{2}}}\left\{e^{i\vec{k}\cdot\vec{x}}\pi(t,k)\hat{b}(\vec{k}) + e^{-i\vec{k}\cdot\vec{x}}\pi^*(t,k)\hat{b}^\dagger(\vec{k})\right\}. \tag{9.11}$$

Due to the symmetries of the background, the mode functions φ and π only depend on the modulus of the comoving momentum $k = \|\vec{k}\|$. The standard commutation relations for the ladder operators are,

$$[\hat{b}(\vec{k}), \hat{b}^\dagger(\vec{k}')] = \delta^3(\vec{k}-\vec{k}'), \qquad [\hat{b}(\vec{k}), \hat{b}(\vec{k}')] = [\hat{b}^\dagger(\vec{k}), \hat{b}^\dagger(\vec{k}')] = 0. \tag{9.12}$$

These are only consistent with the canonical commutation relations (9.6) when the Wronskian normalization condition is satisfied by the mode functions:

$$\varphi(t,k)\pi^*(t,k) - \pi(t,k)\varphi^*(t,k) = i. \tag{9.13}$$

We can now rewrite the Heisenberg equations of motion (9.7,9.8) in terms of the mode functions. This then gives a second order equation for $\varphi(t,k)$,

$$\ddot{\varphi}(t,k) + 3H\dot{\varphi}(t,k) + \left[\frac{k^2}{a^2} + M^2(t)\right]\varphi(t,k) = 0. \tag{9.14}$$

Hereafter, the Hilbert space of states is generated in the usual way, by defining a vacuum state $|\Omega\rangle$ that is destroyed by every annihilation operator $\hat{b}|\Omega\rangle = 0$. Following that, creation operators acting on $|\Omega\rangle$ construct the remaining part of the state space.

The effect of the scalar field on the cosmology is determined by the energy momentum tensor, defined as $\frac{-2}{\sqrt{-g}}\frac{\partial S}{\partial g^{\mu\nu}}$. In operator form this is given by:

$$\hat{T}_{\mu\nu} = \partial_\mu\hat{\Phi}\partial_\nu\hat{\Phi} - \frac{1}{2}g_{\mu\nu}g^{\alpha\beta}\partial_\alpha\hat{\Phi}\partial_\beta\hat{\Phi} - \frac{m^2}{2}g_{\mu\nu}\hat{\Phi}^2 + \xi\left[G_{\mu\nu} - \nabla_\mu\nabla_\nu + g_{\mu\nu}\Box\right]\hat{\Phi}^2. \tag{9.15}$$

Here, $\Box$ is the box operator or d'Alembertian. The state average with respect to a homogeneous and isotropic state then

takes the perfect fluid form, therefore the energy density is given by the 00 element of the energy momentum tensor, we then specify (9.15) to FLRW and neglect the spatial gradients*. We obtain,

$$\hat{\rho}_Q(t,\vec{x}) \equiv -\hat{T}^0_0(t,\vec{x}) = \frac{H^2}{2}\left\{\left[\left(\frac{m}{H}\right)^2 + 6\xi\right]\hat{\Phi}^2(t,\vec{x}) + \frac{6\xi}{a^3H}\{\hat{\Phi}(t,\vec{x}),\hat{\Pi}(t,\vec{x})\} + \frac{1}{a^6H^2}\hat{\Pi}^2(t,\vec{x})\right\} \tag{9.16}$$

Similarly, the pressure follows from the ii components:

$$\hat{p}_Q\delta^i_j = \hat{T}^i{}_j = \frac{H^2}{2}\left\{\frac{1-4\xi}{a^6H^2}\hat{\Pi}^2(t,\vec{x}) + \frac{2\xi}{a^3H}\{\hat{\Phi}(t,\vec{x}),\hat{\Pi}(t,\vec{x})\} + \left[-2\xi(3-2\varepsilon) + 24\xi^2(2-\varepsilon) - \left(\frac{m}{H}\right)^2(1-4\xi)\right]\hat{\Phi}^2(t,\vec{x})\right\}\delta^i_j, \tag{9.17}$$

where the Heisenberg EOM (9.7, 9.8) were used to simplify the result. The relevant expectation values to obtain $\langle\hat{\rho}_Q\rangle$ and $\langle\hat{p}_Q\rangle$ are the coincident correlators, $\left\langle\hat{\Phi}^2(t,\vec{x})\right\rangle$, $\left\langle\hat{\Pi}^2(t,\vec{x})\right\rangle$ and $\left\langle\{\hat{\Phi}(t,\vec{x}),\hat{\Pi}(t,\vec{x})\}\right\rangle$, where $\{\hat{A},\hat{B}\} \equiv \hat{A}\hat{B} + \hat{B}\hat{A}$. These were calculated by [29], we will give a short summary of this calculation in the next section.

However, we are also interested in the spatial correlations inherited by dark energy. For these we need to consider the density-density correlator, which is a 4-point function built from the field and momentum operators. This was studied by [30, 31].

9.2 Stochastic Formalism

Ref. [29] adopted the stochastic formalism introduced by [83] to evolve the density of the dark energy fluid. The stochastic formalism is a useful way of describing the long (super-horizon) modes of the light field. In this formalism the short wavelength modes enter as stochastic sources due to the migration of modes out or inside the Hubble sphere. During inflation, the Hubble radius shrinks and therefore the modes leave the Hubble sphere, while during the other epochs the the Hubble radius grows leading to modes entering the Hubble sphere over time. The main contribution to the correlators of a light scalar field during inflation comes from the super horizon modes ($k < 1/aH$). It was shown by [27, 28] that this is also true in the radiation and matter era. This is formalized by splitting the fields into long and short wavelength modes:

$$\hat{\Phi}(t,\vec{x}) = \hat{\varphi}(t,\vec{x}) + \hat{\varphi}_s(t,\vec{x}), \quad \hat{\Pi}(t,\vec{x}) = \hat{\pi}(t,\vec{x}) + \hat{\pi}_s(t,\vec{x}) \tag{9.18}$$

The modes are separated at a comoving scale of μaH, with $0 < \mu < 1$ being the control parameter of the splitting. μ is a UV cutoff, it selects the lowest scale at the beginning of inflation for which the modes are still nearly scale invariant. In Fourier

*This assumption is analysed in more detail in ref. [31].

space, this is easiest incorporated, where for the long wavelength:

$$\hat{\varphi}(t,\vec{x}) = \int \frac{d^3k}{(2\pi)^{\frac{3}{2}}}\theta(\mu aH - \|\vec{k}\|)\left\{e^{i\vec{k}\cdot\vec{x}}\varphi(t,k)\hat{b}(\vec{k}) + e^{-i\vec{k}\cdot\vec{x}}\varphi^*(t,k)\hat{b}^\dagger(\vec{k})\right\}, \tag{9.19}$$

$$\hat{\pi}(t,\vec{x}) = \int \frac{d^3k}{(2\pi)^{\frac{3}{2}}}\theta(\mu aH - \|\vec{k}\|)\left\{e^{i\vec{k}\cdot\vec{x}}\pi(t,k)\hat{b}(\vec{k}) + e^{-i\vec{k}\cdot\vec{x}}\pi^*(t,k)\hat{b}^\dagger(\vec{k})\right\}, \tag{9.20}$$

and for the short wavelengths:

$$\hat{\varphi}_s(t,\vec{x}) = \int \frac{d^3k}{(2\pi)^{\frac{3}{2}}}\theta(\|\vec{k}\| - \mu aH)\left\{e^{i\vec{k}\cdot\vec{x}}\varphi(t,k)\hat{b}(\vec{k}) + e^{-i\vec{k}\cdot\vec{x}}\varphi^*(t,k)\hat{b}^\dagger(\vec{k})\right\}, \tag{9.21}$$

$$\hat{\pi}_s(t,\vec{x}) = \int \frac{d^3k}{(2\pi)^{\frac{3}{2}}}\theta(\|\vec{k}\| - \mu aH)\left\{e^{i\vec{k}\cdot\vec{x}}\pi(t,k)\hat{b}(\vec{k}) + e^{-i\vec{k}\cdot\vec{x}}\pi^*(t,k)\hat{b}^\dagger(\vec{k})\right\}. \tag{9.22}$$

As a window function we have used the Heaviside θ-function for simplicity. In this form we can split the equations of motions (9.7 and 9.8) in a long and short wavelength part. This gives us:

$$\frac{d}{dt}\hat{\varphi}(t,x) - a^{-3}\hat{\pi}(t,x) = \hat{f}_\varphi(t,x), \tag{9.23}$$

$$a^{-3}\frac{d}{dt}\hat{\pi}(t,x) + M^2(t)\hat{\varphi}(t,x) = a^{-3}\hat{f}_\pi(t,x) \tag{9.24}$$

The sources $\hat{f}_\pi$ and $\hat{f}_\varphi$ arise from the time derivatives on the short wavelength field window functions. They thus incorporate the modes that cross the horizon. Using that $\frac{d}{dt}\theta(\|\vec{k}\|-\mu aH) = -\delta(\|\vec{k}\|-\mu aH)\mu\frac{d}{dt}(aH) = -\mu aH^2(1-\varepsilon)\delta(\|\vec{k}\|-\mu aH)$ gives us:

$$\hat{f}_\varphi(t,\vec{x}) = \mu aH^2(1-\varepsilon)\int \frac{d^3k}{(2\pi)^{\frac{3}{2}}}\delta(\|\vec{k}\| - \mu aH)\left\{e^{i\vec{k}\cdot\vec{x}}\varphi(t,k)\hat{b}(\vec{k}) + e^{-i\vec{k}\cdot\vec{x}}\varphi^*(t,k)\hat{b}^\dagger(\vec{k})\right\}, \tag{9.25}$$

$$\hat{f}_\pi(t,\vec{x}) = \mu a^4H^2(1-\varepsilon)\int \frac{d^3k}{(2\pi)^{\frac{3}{2}}}\delta(\|\vec{k}\| - \mu aH)\left\{e^{i\vec{k}\cdot\vec{x}}\dot{\varphi}(t,k)\hat{b}(\vec{k}) + e^{-i\vec{k}\cdot\vec{x}}\dot{\varphi}^*(t,k)\hat{b}^\dagger(\vec{k})\right\}. \tag{9.26}$$

These sources can be interpreted as stochastic, making (9.23) and (9.24) stochastic differential equations. The latter parts of this Chapter will be about recasting these equations in terms of 2- or 4-point correlations functions and subsequently solving these.

9.3 Two-point correlators

It is convenient to rescale the previously introduced infrared (IR) operators in the following way,

$$\Delta_{\varphi\varphi}(t) \equiv \left\langle\hat{\varphi}^2(t,\vec{x})\right\rangle, \tag{9.27}$$

$$\Delta_{\varphi\pi}(t) \equiv \frac{1}{a^3(t)H(t)}\langle\{\hat{\varphi}(t,\vec{x}),\hat{\pi}(t,\vec{x})\}\rangle, \tag{9.28}$$

$$\Delta_{\pi\pi}(t) \equiv \frac{1}{a^6(t)H^2(t)}\left\langle\hat{\pi}^2(t,\vec{x})\right\rangle. \tag{9.29}$$

Using these definitions the equations of motion, (9.7) and (9.8), can be written as follows,

$$n_{\varphi\varphi} = \frac{d}{dN}\Delta_{\varphi\varphi} - \Delta_{\varphi\pi}, \tag{9.30}$$

$$n_{\varphi\pi} = \frac{d}{dN}\Delta_{\varphi\pi} + (3-\varepsilon)\Delta_{\varphi\pi} - 2\Delta_{\pi\pi} + 2\left(\frac{M}{H}\right)^2\Delta_{\varphi\varphi}, \tag{9.31}$$

$$n_{\pi\pi} = \frac{d}{dN}\Delta_{\pi\pi} + 2(3-\varepsilon)\Delta_{\pi\pi} + \left(\frac{M}{H}\right)^2\Delta_{\varphi\pi}. \tag{9.32}$$

Here, we switched the time variable for the number of e-folds N, using that $\frac{d}{dt} = H(t)\frac{d}{dN}$. For some period in time period between t and t_0 this is defined as $N(t) = \log\frac{a(t)}{a_0}$. The stochastic noise quantities f appear in the quantities n, these are defined as follows,

$$n_{\varphi\varphi} \equiv \frac{1}{H(t)}\left\langle\left\{\hat{f}_\varphi(t,x),\hat{\varphi}(t,x)\right\}\right\rangle, \tag{9.33}$$

$$n_{\varphi\pi} \equiv \frac{1}{a^3(t)H^2(t)}\left[\left\langle\left\{\hat{f}_\varphi(t,x),\hat{\pi}(t,x)\right\}\right\rangle + \left\langle\left\{\hat{f}_\pi(t,x),\hat{\varphi}(t,x)\right\}\right\rangle\right], \tag{9.34}$$

$$n_{\pi\pi} \equiv \frac{1}{a^6(t)H^3(t)}\left\langle\left\{\hat{f}_\pi(t,x),\hat{\pi}(t,x)\right\}\right\rangle. \tag{9.35}$$

To obtain predictions for the correlators at late times, the correlators need to be evolved through the different cosmological epochs: inflation, radiation domination and matter domination.

To obtain the sources expressions for the sources n, we need an expression for the mode function φ. During inflation we can use the Chernikov-Tagirov-Bunch-Davies (CTBD) mode function, which can be derived in exact de Sitter space by solving (9.14). A derivation can be found in *e.g.* ref. [45].

$$\varphi(t,k) = \sqrt{\frac{\pi}{4a^3H_I}}H^{(1)}_{\nu_I}\left(\frac{k}{aH_I}\right), \qquad \nu_I = \sqrt{\frac{9}{4} - 12\xi - \left(\frac{m}{H_I}\right)^2}. \tag{9.36}$$

Using this mode function, the factors n can be calculated [29, 31]. Then, we can evolve the correlators through time using the equations of motion, (9.30-9.32). In the regime that $\xi < 0$ and $\left(\frac{m}{H_I}\right)^2 \ll |\xi| \ll 1$ it was shown by ref. [29] that the correlators take the following form at the end of inflation:

$$\Delta_2(N_I) \equiv \left(\Delta_{\varphi\varphi},\Delta_{\varphi\pi},\Delta_{\pi\pi}\right) \simeq \frac{H_I^2}{32\pi^2|\xi|}e^{8|\xi|N_I}\left(1, 8|\xi|, 16\xi^2\right). \tag{9.37}$$

With N_I the amount of inflationary e-folds. Using (9.16) we can rewrite the density in terms of the correlators as:

$$\langle\hat{\rho}_Q\rangle \approx \frac{H^2}{2}\left\{\Delta_{\pi\pi} + 6\xi\Delta_{\varphi\pi} + \left[6\xi + \left(\frac{m}{H}\right)^2\right]\Delta_{\varphi\varphi}\right\}, \tag{9.38}$$

we can neglect the other correlators apart from $\Delta_{\varphi,\varphi}$ as they are suppressed with a factor ξ. This gives [29]:

$$\langle\hat{\rho}_Q\rangle(N_I) = \frac{H^2}{2}\left[\left(\frac{m}{H}\right)^2 - 6|\xi|\right]\frac{H_I^2}{32\pi^2|\xi|}e^{8|\xi|N_I} \tag{9.39}$$

Similarly, we can also write down the expression for the pressure $\langle\hat{p}_Q\rangle$ in terms of the relevant correlators,

$$\langle\hat{p}_Q\rangle \approx \frac{H^2}{2}\left((1-4\xi)\Delta_{\pi\pi} + 2\xi\Delta_{\varphi\pi} + \left[-2\xi(3-2\varepsilon) + 24\xi^2(2-\varepsilon) - \left(\frac{m}{H}\right)^2(1-4\xi)\right]\Delta_{\varphi\varphi}\right). \tag{9.40}$$

Under our assumptions this can be simplified to [29],

$$\langle\hat{p}_Q\rangle(N_I) = -\langle\hat{\rho}_Q\rangle(N_I) \tag{9.41}$$

Therefore at the end of inflation, the energy-momentum tensor of the field behaves like a cosmological constant: $p = -\rho$.

The correlators, (9.37), then serve as initial conditions for the equations of motions during the radiation dominated era. Again, the mode functions can be calculated during radiation era and proceed in similar fashion again. However, we are in luck. It was shown by ref. [29] that the stochastic terms are subdominant and can therefore be neglected during radiation domination. By subsequently solving the remaining equations in the limit of small mass and minimal coupling one can conclude that the $\Delta_{\varphi\varphi}$ correlator stays constant during radiation domination, while the other correlators are suppressed [29][†]. Hereafter, we assume a period of matter domination. Then, before the backreaction of the scalar field on the background metric becomes too important, one should proceed by solving the Friedmann equations self consistently using numerics, as was done by [29]. They found that, indeed, at late times this model can produce dark energy.

However, some simplified analytical understanding can be obtained by assuming a period of pure matter after radiation domination up to late times[‡], which produces some error at the later e-folds. Recently it was realized that, in agreement with [28], there is also some growth during this era [31]. This growth is similar to the growth during inflation and results in the following correlator in the matter-dominated epoch [31],

$$\Delta_{\varphi\varphi}(N_M) = \frac{H_I^2}{32\pi^2|\xi|}e^{8|\xi|N_I + 4|\xi|N_M}, \tag{9.42}$$

where N_M is the number of e-folds passed after matter-radiation equality. Therefore, using $\varepsilon = \frac{3}{2}$, the density (9.38) and pressure fields (9.40) can be approximated in this epoch by [31]:

$$\boxed{\begin{aligned}\langle\hat{\rho}_Q(N_M)\rangle &= \frac{H^2}{2}\left[\left(\frac{m}{H}\right)^2 - 6|\xi|\right]\Delta_{\varphi\varphi}(N_M), &(9.43)\\ \langle\hat{p}_Q(N_M)\rangle &= -\frac{m^2}{2}\Delta_{\varphi\varphi}(N_M). &(9.44)\end{aligned}}$$

[†]This does not mean the pressure and density stay the same, due to the different ε in this epoch the quantum energy density contains a cosmological constant like part and a relativistic component at the end of the radiation epoch.

[‡]Another way of evaluating these correlators at late times is evaluating the last part of the expansion in a background containing a cosmological constant and dark energy, as was done by [31].

Which is valid at leading order in $|\xi|$ and $\frac{m^2}{H(N_M)^2}$. The first part of the energy density scales as $\langle\hat{\rho}_Q\rangle = -\langle\hat{p}_Q\rangle$. This is exactly the behaviour of a cosmological constant. Apart from this it also includes a contribution behaving as dark matter with negative energy scaling as the background. The cosmological constant like term must explain the amount of dark energy we observe today, therefore the following relation must be true:

$$\frac{m^2}{2}\Delta_{\varphi\varphi}(t_0) = 3M_P^2H_0^2\Omega_\Lambda, \tag{9.45}$$

where t_0 means it is evaluated today and Ω_Λ is the required energy density fraction of dark energy observed today. This then gives a constraint for the length of inflation, as inflation needs to take long enough to produce the required amount of dark energy [29, 31].

$$\boxed{N_I = \frac{1}{8|\xi|}\ln\left[24\pi|\xi|\left(\frac{m_P}{H_I}\right)^2\left(\frac{H_{DE}}{m}\right)^2\right] - \frac{1}{2}\ln\left(\frac{\Omega_M}{\Omega_R}\right).} \tag{9.46}$$

Here we used that today $N_M(t_0) = \ln\left(\frac{\Omega_M}{\Omega_R}\right)$ where Ω_M and Ω_R are the energy fractions in matter and radation today. For notational convienence we defined $H_{DE}^2 = \Omega_\Lambda H_0^2$ and $m_P = M_P\sqrt{8\pi}$ is the Planck mass. This then forms a fundamental link between inflation and this dark energy candidate.

For this scenario to unfold a few constraints need to be satisfied,

$$|\xi| < \frac{1}{6}\left(\frac{m}{H_{\rm DE}}\right)^2, \quad \xi < 0 \quad \text{and} \quad m/H_{\rm DE} < 1. \tag{9.47}$$

The first constraint is the result from the need that the cosmological constant-like part of $\langle\hat{\rho}_Q\rangle$ has to dominate over the dark matter-like part. The assumptions of light field and negative non-minimal coupling are those which allow a better enhancement of quantum fluctuations [29, 31] . This can be seen from the effective potential of the scalar field $V(\varphi) = \frac{1}{2}\mathcal{M}^2\varphi^2$ with $\mathcal{M}^2 = m^2 + 6\xi(2-\varepsilon)H^2$. A light field and negative non-minimal coupling are the conditions for which a minimum length of inflation is needed to amplify the quantum fluctuations of the scalar field, which will later manifest as dark energy in matter-dominated epoch and eventually lead the expansion.

9.4 Four-point correlators

We now extend our interest to the four-point correlator, describing the (spatial) correlations. These can be calculated using similar methods [30, 31], however, now the calculation becomes much more complicated. The full system is now described by six coupled differential equations, instead of the previous three. For the complete calculation we will refer the reader to the work by [30] and [31] and quote some of their main results.

We are interested in the spatial correlations at late times. These are encoded in the two-point function of the density $\hat{\rho}_Q$. These are described by the four-point correlators in terms of the quantum fields. Similar to the behaviour of the two-point functions of the quantum fields, the main contribution comes from the correlators built from the fields, where the momentum correlators are suppressed by higher orders of ξ. This can also be observed in the four-point correlator in matter

domination, which is derived in [31][§],

$$\Delta_4(N_M, r) \equiv \left(\Delta_{\varphi^2,\varphi^2}, \Delta_{\varphi^2,\varphi\pi}, \Delta_{\varphi\pi,\varphi\pi}, \Delta_{\varphi^2,\pi^2}, \Delta_{\varphi\pi,\pi^2}, \Delta_{\pi^2,\pi^2}\right) \simeq \Delta^2_{\varphi\varphi}(N_M)s(r)\left(1, 8|\xi|, 16\xi^2, 8\xi^2, 32|\xi|^3, 16\xi^4\right). \quad (9.48)$$

Here, r is the comoving distance between the two coordinates and $\Delta_{\varphi\varphi}$ is the two-point correlations function during matter domination as given by (9.42). The spatial dependence is encoded in the function $s(r)$, which is given by

$$s(r) \simeq \begin{cases} 3, & \text{if } 0 \leq \mu a_{\text{in}} H_I r < \mathrm{e}^{-N_I}, \\ 3 - 2\left(\mu a_{\text{in}} H_I r\right)^{16|\xi|} & \text{if } \mathrm{e}^{-N_I} < \mu a_{\text{in}} H_I r < 1, \\ 1 & \text{if } \mu a_{\text{in}} H_I r \geq 1. \end{cases} \quad (9.49)$$

Which depends on the scale $r_0 = (\mu a_{\text{in}} H_I)^{-1}$, which is (up to μ^{-1}) the comoving Hubble length at the beginning of inflation. Similar to the previous section, we can write the the density-density correlator in terms of the field correlators [30, 31]:

$$\langle\hat{\rho}_Q(t,\vec{x})\hat{\rho}_Q(t,\vec{x}')\rangle \approx \frac{H^4}{4}\left\{\left[\left(\frac{m}{H}\right)^2 + 6\xi\right]\Delta_{\varphi^2,\varphi^2} + 6\xi\left[\left(\frac{m}{H}\right)^2 + 6\xi\right]\Delta_{\varphi^2,\varphi\pi} + 36\xi^2\Delta_{\varphi\pi,\varphi\pi} + \left[\left(\frac{m}{H}\right)^2 + 6\xi\right]\Delta_{\varphi^2,\pi^2} + 6\xi\Delta_{\varphi\pi,\pi^2} + \Delta_{\pi^2,\pi^2}\right\}. \quad (9.50)$$

Then, when combining (9.38), (9.48) and (9.50) and considering leading order in $|\xi|$ and $\frac{m^2}{H(N_M)^2}$ gives us [30, 31],

$$\boxed{\langle\hat{\rho}_Q(N_M,\vec{x})\hat{\rho}_Q(N_M,\vec{y})\rangle = \langle\rho_Q(N_M)\rangle^2 s(r),} \quad (9.51)$$

which is the precise form of the phenomenological model we discussed before. Specifically this model can be mapped onto *Case I* in Chapter 3. Therefore we can use the formalism developed in the previous Chapters to study this model. This will be the topic of the following Chapter.

9.5 Effect of a reduced speed of sound

In the previous sections we considered a model with a speed of sound c_s equal to the speed of light, *i.e.* $c_s = 1$, as was done by [29] and [30]. The speed of sound denotes the speed of propagation of the field fluctuations. Recently, this dark energy model has also been studied in a more general setup with a reduced speed of sound [31]. This turns out to significantly affect the measurability of this model, as we will show in the following Chapter. Therefore, following the work of [31] we give a brief outline of how a reduced a speed of sound affects this model. A reduced speed of sound appears in various models. For example, it typically emerges in the effective field theory of dark energy [84] or, similarly, in the setting of inflation [85]. In our quantum dark energy model we will treat it as an independent model parameter, which for simplicity stays constant throughout the evolution of the universe [31].

[§]The derivation and exact definitions of these correlators, which are similar to the ones defined in (9.27), can be found in [31]

A reduced speed of sound enters the equation of motion for the mode function as a rescaling of the wavevector k, thereby taking a slightly different from (9.14) [31],

$$\ddot{\varphi}(t,k) + 3H\dot{\varphi}(t,k) + \left[c_s^2\frac{k^2}{a^2} + M^2(t)\right]\varphi(t,k) = 0. \tag{9.52}$$

This leads to the mode functions (9.36) being rescaled in the same way,

$$\varphi(t,k) = \sqrt{\frac{\pi}{4a^3H_I}}H^{(1)}_{\nu_I}\left(\frac{c_s k}{aH_I}\right), \qquad \nu_I = \sqrt{\frac{9}{4} - 12\xi - \left(\frac{m}{H_I}\right)^2}. \tag{9.53}$$

The mode functions enters the quantum equation of motion via the stochastic sources (9.33-9.35). Going through the same treatment as before results in the correlator in the matter epoch being rescaled roughly by a factor c_s^{-3} [31]:

$$\Delta_{\varphi\varphi}(N_M) = c_s^{-3}\frac{H_I^2}{32\pi^2|\xi|}e^{8|\xi|N_I + 4|\xi|N_M}, \tag{9.54}$$

Resulting in the following energy density,

$$\boxed{\langle\hat{\rho}_Q(N_M)\rangle = \frac{H^2}{2}\left[\left(\frac{m}{H}\right)^2 + 6\xi\right]c_s^{-3}\frac{H_I^2}{32\pi^2|\xi|}e^{8|\xi|N_I + 4|\xi|N_M}}, \tag{9.55}$$

valid at leading order in $|\xi|$ and $\frac{m^2}{H(N_M)^2}$. This will then be matched to the value of dark energy today, using (9.45), resulting in a value for the necessary amount of inflationary e-fold N_I to produce enough dark energy. When considering a reduced speed of sound this required amount is decreased [31],

$$\boxed{N_I = \frac{1}{8|\xi|}\ln\left[24\pi|\xi|\left(\frac{m_P}{H_I}\right)^2\left(\frac{H_{DE}}{m}\right)^2 c_s^3\right] - \frac{1}{2}\ln\left(\frac{\Omega_M}{\Omega_R}\right)}, \tag{9.56}$$

therefore, inflation can take less e-folds and still be able to produce enough dark energy to explain the accelerated expansion of the universe. This can be understood by the following argument. A speed of sound rescales the wavevector $k \to c_s k$, if we assume the speed of sound to be reduced ($c_s < 1$) then the same wavevector k contributes as a longer wavelength (smaller k) as compared to the case where $c_s = 1$. This then acts as an enhancement due to the quantum correlators being mostly built from long wavelength modes [28, 31].

10

Observational consequences of inflationary dark energy

We now want to assess whether this model of quantum dark energy will leave any substantial imprint on our observables. To this end we will derive suitable predictions for $\Omega_Q(z)$, $H(z)$, n_{DE} and $H_0 r_0$ in terms of the models bare Lagrangian parameters ξ and m. Hereafter we will make predictions for the angular power spectrum as a function of the Lagrangian parameters and assess the signal to noise ratio to be expected from this.

10.1 The model parameters

We can parameterize the classical and quantum energy densities as energy fractions Ω:

$$\Omega_Q(z) = \frac{\langle\hat{\rho}_Q\rangle(z)}{3M_P^2\bar{H}^2(z)}, \qquad \Omega_c(z) = \frac{\rho_c(z)}{3M_P^2\bar{H}^2(z)}. \tag{10.1}$$

Due to the Friedmann equation, (4.1), these then have to sum to unity. We derive the redshift dependence $\langle\hat{\rho}_Q\rangle$ from (9.55) and (9.56). It is given by:

$$\frac{\langle\hat{\rho}_Q\rangle(z)}{\langle\hat{\rho}_Q\rangle(0)} = \frac{\Omega_\Lambda - \frac{1}{\alpha}\frac{\bar{H}^2(z)}{H_0^2}}{\Omega_\Lambda - \frac{1}{\alpha}}, \tag{10.2}$$

Where we neglected the growth in matter domination. Here, $\Omega_\Lambda = 1 - \Omega_M$ is the energy fraction in dark energy today, which can be expressed in terms of the energy fraction in dark matter today Ω_M. For notational convenience we defined α as a rescaled mass parameter $\alpha = \frac{1}{6|\xi|}\left(\frac{m}{H_{DE}}\right)^2$. In terms of this parameter the constraints given by (9.47) require

$$|\xi| < \frac{1}{6\alpha}, \qquad \alpha > 1, \qquad \xi < 0. \tag{10.3}$$

The reasons for which are explained around (9.47). We assume that the classical matter scales as non-relativistic matter, as it includes the cold dark matter and baryonic matter contributions. We can then use that the energy fractions sum up to unity and use (10.2) to obtain:

$$1 = \Omega_c(z) + \Omega_Q(z) = \Omega_{0,c}(1+z)^3 \frac{H_0^2}{\bar{H}^2(z)} + \left[\Omega_\Lambda \frac{H_0^2}{\bar{H}^2(z)} - \frac{1}{\alpha}\right]. \tag{10.4}$$

This can be rewritten in terms of the Hubble rate to yield,

$$\frac{\bar{H}^2(z)}{H_0^2} = \frac{\left(\Omega_M + \frac{1}{\alpha}\right)(1+z)^3 + \Omega_\Lambda}{1 + \frac{1}{\alpha}}. \tag{10.5}$$

We used that $\Omega_{0,c} = \Omega_M + \frac{1}{\alpha}$, which follows from (9.55), (9.56), (10.1) and $\Omega_M = 1 - \Omega_\Lambda$. In the limit where $\alpha \to \infty$, indicating the minimally coupled limit, this indeed reduces to the regular Friedmann equation.

Using (10.1), (10.2) and (10.5) we also obtain the following expression for $\Omega_Q(z)$:

$$\Omega_Q(z) = \frac{\Omega_\Lambda - \frac{1}{\alpha}\left(\Omega_M + \frac{1}{\alpha}\right)(1+z)^3}{\Omega_\Lambda + \left(\Omega_M + \frac{1}{\alpha}\right)(1+z)^3} \tag{10.6}$$

10.2 Spatial correlations

This model produces spatial correlations of the same form as *Case I* using the following identifications [30], comparing with (3.4), we see that the spectral slope can be related to the non minimal coupling by $n_{\mathrm{DE}} = 16|\xi|$ and the reference scale r_0 is connected to the energy scale of inflation by $r_0 = \frac{1}{\mu a_I H_I}$:

$$s(\|\vec{x} - \vec{y}\|) = \begin{cases} 3 - 2\left(\mu a_I H_I r\right)^{16|\xi|}, & \mu a_I H_I r < 1, \\ 1, & \mu a_I H_I r > 1. \end{cases} \tag{10.7}$$

Here, a_I and H_I are the scale factor and Hubble parameter at the start of inflation.

We will now want to relate the lengths scale $\left(\mu a_{in} H_I\right)^{-1} = r_0$ in terms of predictable quantities. For this we need the scale factor during inflation a_{in}. When assuming an instant reheating after inflation we have the following Friedmann equation,

$$\frac{H_I^2}{H_0^2} = \Omega_R a_e^{-4} + \Omega_M a_e^{-3} + \Omega_\Lambda. \tag{10.8}$$

	H_0 [km s^{-1}Mpc^{-1}]	Ω_M
$\alpha = 10$	116.6	0.03
$\alpha = 25$	116.8	0.08
$\alpha = 50$	116.9	0.1

Table 10.1: The values for the bare energy fraction of non-relativistically scaling matter and the bare Hubble constant, calculated for several values of the model constant α.

We denoted the scale factor at the end of inflation with a_e, this can be related to the scale factor at the start of inflation by $a_e = a_{in}e^{N_I}$. As at the end of inflation $a_e \ll 1$ we can safely neglect the matter and cosmological constant contributions. Then we obtain,

$$a_{in} = \Omega_R \left(\frac{H_I}{H_0}\right)^{-\frac{1}{2}} e^{-N_I}. \tag{10.9}$$

We then obtain for the characteristic length scale [30],

$$H_0 r_0 = \mu^{-1} e^{N_I} \left(\frac{H_I}{H_0}\right)^{-\frac{1}{2}} \Omega_R^{-\frac{1}{4}}. \tag{10.10}$$

Here, Ω_R is the energy fraction in radiation today, which we take as $9.1 \cdot 10^{-5}$.

Similar to *Case I* in the previous sections, the quantities Ω_M and H_0 are still the unobservable bare quantities. To obtain values for these we match them analogously to the phenomenological model in section 4.3, with the difference being that for $\bar{H}(z)$ and $\Omega_Q(z)$ we now use (10.5) and (10.6). As the redshift dependence is determined by the model parameters, we expand up to the deceleration parameter.

$$\frac{1}{H_L} = \frac{1}{4H_0\alpha^2}\left(3 + 6\alpha(\Omega_M - 1) + \alpha^2(7 + 3(\Omega_M - 2)\Omega_M)\right), \tag{10.11}$$

$$\begin{aligned}\frac{1}{2H_L}\left[1 - q_L\right] = \left(16H_0\alpha^2(1+\alpha)\right)^{-1}\left(3 + \alpha(42 - 39\Omega_M) + \alpha^2(3\Omega_M(48 - 29\Omega_M) - 53) + \right.\\ \left. \alpha^3(28 - 3\Omega_M(27 + \Omega_M(15\Omega_M - 34))\right).\end{aligned} \tag{10.12}$$

We then solve these equations numerically in the the bare variables H_0 and Ω_Q for several values of α. The results are shown in Table 10.1. Values smaller than $\alpha = 8$ result in a negative Ω_M, thus we choose α larger than this. Again, we stress that this is not a fit to data, but merely a way of estimating our parameters to make predictions for the SNR.

Using this knowledge we can calculate the C_ℓ's. For this model (5.16) takes the following form:

$$\begin{aligned}C_\ell^{i,j} = &-\pi^{\frac{3}{2}}\Omega_{Q,0}^2 H_0^4 \frac{2^{-\ell}\,(-8|\xi|)_\ell}{\Gamma(\frac{3}{2}+\ell)} \\ &\times \int_0^\infty dz \int_0^\infty dz' \left\{ \frac{W^{i,j}(z,z')}{\bar{H}(z)^3 \bar{H}(z')^3}\left[1 - (z+z')\frac{3}{1+\alpha}\frac{1+\alpha\Omega_M}{\alpha(1-\Omega_M)-1}\right]\right. \\ &\left.\times \left(\frac{\chi(z)^2 + \chi(z')^2}{r_0^2}\right)^{8|\xi|} \mu_0(z,z')^{-\ell}\, {}_2F_1\left(\frac{\ell}{2} - 4|\xi|, \frac{1}{2} + \frac{\ell}{2} - 4|\xi|; \frac{3}{2} + \ell; \mu_0(z,z')^{-2}\right)\right\}.\end{aligned} \tag{10.13}$$

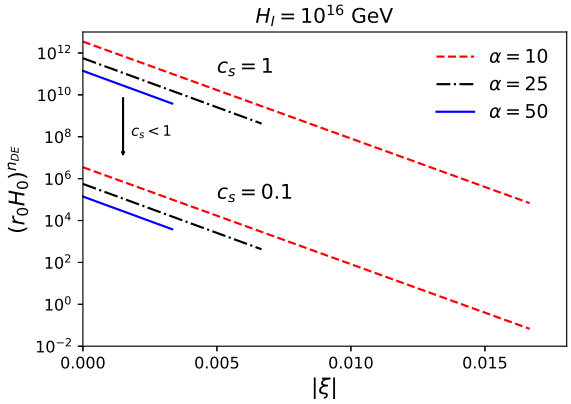

Figure 10.1: The figure shows the factor $(H_0 r_0)^{n_{\rm DE}}$ shown as a function of $|\xi|$. We keep the scale of inflation fixed at $H_I = 10^{16}$ GeV and explore several values of α and c_s. We only show the values that are allowed by the constraint $|\xi| \leq (6\alpha)^{-1}$.

10.3 Prospects for measurability

Before calculating the C_ℓ's it is useful to work on the factor $(H_0 r_0)^{-16|\xi|}$, as this term can be factored out of the power spectrum, see (10.13), and acts as an effective amplitude. Combining (9.56) and (10.10) yields the following expression:

$$(H_0 r_0)^{16|\xi|} = c_s^6 \left(\frac{4\pi}{\alpha}\frac{m_p^2}{H_I^2}\right)^2 \left(\frac{H_0\sqrt{\Omega_R}}{H_I \Omega_M}\right)^{8|\xi|}, \tag{10.14}$$

where we have taken $\mu = 1$ for simplicity. For H_I we adopt the value of 10^{16} GeV, this is around the GUT scale and still below the observational constraint of about 2×10^{16} GeV [43, 86]. The signal is only measurable when $(H_0 r_0)^{n_{\rm DE}}$ is not too big, as if this factor becomes too large the signal starts to be drowned in the shot noise. From (10.14) we see that this is mostly determined by the ratio between the Hubble rate today and during inflation, with exponential dependence on $|\xi|$. We also note that $|\xi|$ is limited by α via $|\xi| \leq \frac{1}{6\alpha}$. This turns out to be very restricting.

We first consider the case where the speed of sound is equal to the speed of light, *i.e.* $c_s = 1$, as was the case studied by the original model [29, 30]. Then, the regime where $(H_0 r_0)^{n_{\rm DE}}$ lies between 2 and 10^4 mostly lies in the range that is forbidden by this constraint, as can be seen in Figure 10.1 (upper lines). The factor $(H_0 r_0)^{n_{\rm DE}}$ grows exponentially with $|\xi|$, effectively pushing the signal to scales we cannot probe anymore with upcoming surveys such as LSST. This is confirmed by Figure 10.2 (lower lines). In this Figure one can observe that in the best case a SNR of 0.48 can be obtained, which means that it would not be measurable by LSST Y10. A smaller α would free up the parameter space to ranges where the signal would be measurable; however, a smaller α leads to a negative Ω_M in our matching. Alternatively, if the scale of inflation H_I was higher, it would also be possible to obtain a measurable result. Yet, this range of H_I would already have led to a positive detection of the tensor spectrum, therefore this range is already ruled out by observations.

From this we conclude the following. To match the results of the $\langle \hat{d}_L \rangle(z)$, the amount of negative matter that this model predicts has to be small, this then leads to a relatively large α. To still be able to ensure that the mass of the field m stays small throughout the evolution of the universe, the non minimal coupling ξ also has to be small. Then, to be able to produce

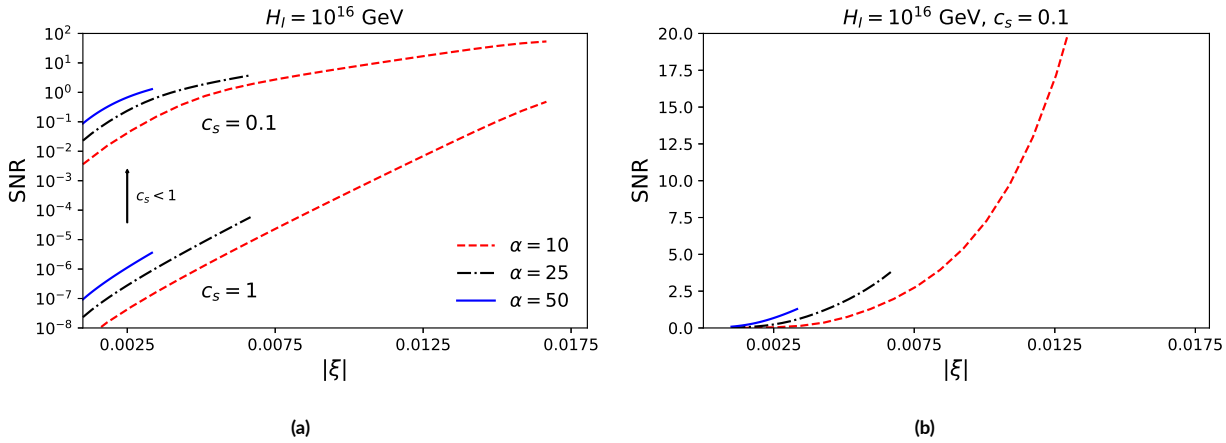

Figure 10.2: The SNR of the model, calculated for the LSST y10 survey.We keep the scale of inflation fixed at $H_I = 10^{16}$ GeV and explore several values of α. We only show the values that are allowed by the constrained $|\xi| \leq (6\alpha)^{-1}$. The left panel shows the SNR on a logarithmic scale, with both $c_s = 1$ and $c_s = 0.1$, the right panel shows the SNR in the case $c_s = 0.1$ on a linear scale.

enough dark energy to match the required amount today, inflation has to take a long time. As our characteristic length scale $H_0 r_0$ grows with the length of inflation this then leads to scales we cannot probe with upcoming experiments, therefore, in this case this model would not be testable by LSST Y10.

However, we can also consider the case with a reduced speed of sound $c_s < 1$, taken constant for simplicity. The speed of sound denotes the speed of propagation of the field fluctuations and appears in several models of dark energy (some of which are mentioned in section 9.5). Lowering it reduces $(H_0 r_0)^{16\xi}$ with a factor c_s^6, as can be seen in (10.14). This enhances the signal significantly, as is demonstrated in Figure 10.2. When $c_s = 0.1$, both the cases $\alpha = 10$ and $\alpha = 25$ are possibly detectable. We note that when the SNR becomes larger, the cosmic variance becomes a relevant noise contribution, resulting in the upper SNR lines exhibiting a bend.

We also point out that the redshift evolution of the model discussed in this section was tested by [87]. They found that this model is slightly favored over ΛCDM, although not at a statistically significant level.

11

Conclusion and outlook

11.1 Conclusion

In this thesis we explored the effect of spatial correlations in dark energy. These spatial correlations can arise when dark energy fluctuates. We considered a phenomenological model where these fluctuations come from an underlying (quantum) field. We explored two cases, assuming that the energy density of dark energy depends either quadratically (*Case I*) or linearly (*Case II*) on a single underlying field $\hat{\varphi}$ with Gaussian statistics.

Due to the fluctuating nature of dark energy in our model, the Hubble rate itself becomes a fluctuating quantity, described by the operator (4.1). We then considered the effect these fluctuations have on the luminosity distance. To this end we studied the properties of the luminosity distance operator (4.3). We first considered the one-point statistics of this operator. We find that due to the fluctuations in dark energy the luminosity distance becomes dressed by the fluctuations, thereby differing from standard ΛCDM. In *Case I* this difference can be predicted by using Wick's theorem and is found to be relatively large. As a consequence of this difference the parameters measured by experiments such as *Planck* [1] or SH0ES [3] do not match the parameters describing the underlying FLRW universe of our model. We therefore have to make a distinction between the local parameters measured and the 'bare' parameters describing the underlying FLRW universe. To estimate these parameters we matched our model to local ladder measurements that are model independent [2]. The idea that

parameters measured do not equal the underlying parameters is not a new idea, as it was previously studied in the context of relativistic universes containing inhomogeneities [34, 62]. But to our knowledge it has to this date not yet been studied from a quantum perspective, where the fluctuations arise due to quantum effects.

Spatial correlations also result in a signal for the luminosity distance correlator. To study this we constructed the power spectrum for the fluctuations in the luminosity distance. Using this power spectrum we assessed its measurability for DES and LSST, taking into account contaminants from relativistic effects such as the Doppler effect and the convergence effect. From Figure 8.1 we found that detecting this signal with DES would be very challenging: the signal is mostly located at the largest scales, making cosmic variance a significant noise contribution. DES only observes a very small patch of the sky, resulting in a large contribution of cosmic variance. On the other hand, LSST will observe the full sky on the southern hemisphere, which greatly reduces the cosmic variance. We then find that depending on the scale of the fluctuations r_0 and the spectral index of dark energy n_{DE}, defined in (3.4), the signal would be measurable. From Figure 8.2b we conclude that when $n_{\mathrm{DE}} = 1$, the signal is measurable when $H_0 r_0 \lesssim 10^2$, while for $n_{\mathrm{DE}} = 0.1$ the signal would still easily be measurable when $H_0 r_0 \approx 10^{10}$. For the case that $n_{\mathrm{DE}} = 1$ it would be useful to go through the effort of measuring the lowest multipoles ℓ, as the signal is mostly located in the lower ℓ region (see Figure 8.2a). The contaminant signal, coming from relativistic effects, does not alter these conclusions. In the regime where these effects become of the same order of our signal, the signal is not measurable as it would be located well below the shot noise contribution (see Figure 8.1). We also find that this model has relatively strong correlations at unequal redshift, this could be used as a cross-check for the signal in a tomographic approach.

With these conclusions in mind we then considered a specific model for dark energy fluctuations [26–31]. In this model dark energy is linked to a non minimally coupled spectator field during inflation and has subsequently quantum fluctuations imprinted in it. We explored the parameter space of this model. We find that if we want this model to be consistent, the allowed values are such that inflation needs be long (see (10.14) and (9.46)), thereby pushing the signal to scales we cannot probe anymore with upcoming experiments such as LSST, as can be seen in Figure 10.2a. Taking into account a speed of sound $c_s < 1$ lowers the characteristic length scale $H_0 r_0$ [31] and could thereby make it measurable (see Figure 10.2).

To summarize, we found that a fluctuating Hubble rate due to a fluctuating dark energy fluid can have some profound implications for the luminosity distance. As a result of the fluctuating Hubble rate, the luminosity distance itself becomes a fluctuating parameter. Even at the level of the one-point function, the luminosity distance becomes dressed by the fluctuations, resulting in a difference from ΛCDM. The spatial correlations in the dark energy fluid become visible in the two-point correlator of the luminosity distance. We constructed the angular power spectrum for these fluctuations and studied its detectability. We find that these fluctuations are mostly visible on very large scales ($\ell \leq 50$) and that for a large part of the models parameter space, this model would be testable by LSST Y10 data.

11.2 Outlook

We can propose several avenues in continuing this research. In our work we calculated the relativistic effects in the context of perturbed ΛCDM to obtain an estimate of this effect. Implicitly this assumes that fluctuating dark energy does not alter this effect. A complete treatment would calculate these effects in our model. For this, one would need to know how the gravitational potential is affected by quantum fields containing spatial correlations. This would be an interesting extension of our work. Similarly, it would be interesting to study how the growth of structure would be affected by such models. In the light of the σ_8 tension, a tension between the CMB [1] and shear measurements [4, 5] of σ_8, being a major problem in ΛCDM, we would be interested to see whether it would persist in a model with a fluctuating dark energy candidate. Recently it was shown that such models can alleviate the Hubble tension [30], which is one of the most pressing issues in current cosmology [14, 15]. This shows promise for the σ_8 tension as well.

In principle, not only dark energy, but also dark matter could have a quantum nature. It would be interesting to see how this would influence causal observables such as the luminosity distance. There has been some progress on the study of dark matter from a fundamental field theoretic perspective [88–90], but as of yet, a study of such effects on the luminosity distance has not been carried out to our knowledge. Another interesting route would be studying how a coupling between dark matter and dark energy would affect our analysis.

We would also be interested in the effect this model has on gravitational waves. In general this would be interesting in the light of upcoming gravitational wave experiments. This would also have another advantage, because the relativistic lensing effects affect both the electromagnetic luminosity distance and the gravitational wave luminosity distance. By considering the difference between the electromagnetic distance and the gravitational wave distance, these would thus drop out [36].

The implications of this model on other observables is also a natural route to consider. Observables directly related to the Hubble parameter would be especially promising, for example, time delays from strongly lensed objects. Other interesting probes would be the cosmic microwave background or lensing studies.

A

Distance measurements in cosmology

In this Appendix we derive the classical expression of the luminosity distance. We start with this expression in Chapter 4 and then upgrade it to operator form. This is a derivation found in most cosmology textbooks, we follow the approach of Weinbergs book [91].

Distance measurements have historically been very important in cosmology. Hubble's distance measurements of galaxies [39] can arguably be seen as the start of observational cosmology and more recently the distance measurements of Type Ia supernovae formed the first evidence of an accelerating universe [6, 7]. Distance measurements work in the following way: from other means one knows the luminosity of a certain astrophysical object, for example, the light curves of type Ia supernovae are linked to their luminosity. These light curves can be measured independently from the distance. From measurements on earth one can then infer the flux of this standard candle. With these two quantities the luminosity distance can then be obtained:

$$d_L = \sqrt{\frac{L}{4\pi F}} \tag{A.1}$$

This is nothing more than the dispersion of photons over the surface of a sphere with radius d_L. This can be connected to the cosmology. To make this concrete, we modify the standard $L = 4\pi d^2 F$ for three reasons:

- In the time the photon reaches the earth the universe has expanded by a certain amount, therefore increasing the area

where they are dispersed over. This changes d to the cosmological distance $a(t_0)\chi$, where χ is the comoving distance which we define hereafter.

- Due to the expansion of the universe the rate of arrival of individual photons is lowered by the redshift factor.
- For the same reason, the energy of the photons is also lower due to the redshift factor.

Taking all of this into account we can write down a definition for the flux F:

$$F = \frac{L}{4\pi\chi^2(1+z)^2} \tag{A.2}$$

Comparing this with (A.1) we find that the luminosity distance is given by:

$$d_L = a(t_0)\chi(1+z) \tag{A.3}$$

The comoving distance can be derived from (2.1). For light-like geodesics over the radial direction this gives

$$d\chi = \frac{dt}{a(t)}. \tag{A.4}$$

This can be integrated and recast in terms of the redshift to obtain:

$$\chi = \int_0^z \frac{dz'}{H(z')}. \tag{A.5}$$

When we normalise the scale factor such that $a(t_0) = 1$ we then have for the luminosity distance,

$$\boxed{d_L = (1+z)\int_0^z \frac{dz'}{H(z')},} \tag{A.6}$$

we see that the luminosity distance indeed depends on the cosmology via the integrated Hubble parameter.

It is customary to write distances not in terms of luminosity, but in terms of magnitude. Therefore results are usually given in terms of the *distance modulus*. This is defined as:

$$\mu = 5\log_{10} d_L(\text{Mpc}) + 25. \tag{A.7}$$

Which is a logarithmic counterpart to the luminosity. We will mostly be interested in distance measurements using type Ia supernovae as a standard candle, an elaborate review on supernovae cosmology has been written by [76].

B

Gaussian fields

In cosmology we often deal with fields obeying certain statistics. Often, the relevant statistics are Gaussian statistics. Those statistics arise when the field is the sum of a large number of fluctuating terms, a statement formally captured by the *central limit theorem*. In cosmology these statistics are especially relevant as the perturbations in the cosmic microwave background are believed to be nearly Gaussian. A fact that can be traced back to inflation, where they arise as the quantum fluctuations of a nearly free field. In this thesis Gaussian fields form the bedrock of our method, as we assume the underlying quantum density fields of our dark energy candidate to be Gaussian.

The underlying probability distribution of Gaussian fields is the famous normal distribution, defined as:

$$\boxed{P(\varphi) = \frac{1}{\sqrt{2\pi}\sigma} e^{-\frac{(\varphi - \langle\varphi\rangle)^2}{2\sigma^2}}}, \tag{B.1}$$

where $\sigma^2 = \langle\varphi^2\rangle - \langle\varphi\rangle^2$ is the variance of the field.

B.1 Gaussian fields and Wicks Theorem

One of the advantages of Gaussian fields is that they satisfiy Wick's theorem, in fact, one could define Gaussian fields as the fields that satisfy this theorem. Wick's theorem states the following: consider a random variable $\varphi(x)$, which is governed by a

Gaussian distribution function and depends on the D dimensional coordinate x. Then, The average of an even number φ's is equal to the sum over all ways of pairing φ's with each other of a product of the average values of the pairs:

$$\boxed{\langle \varphi(x_1)\varphi(x_2)\ldots\rangle = \sum_{\text{pairings}} \prod_{\text{pairs}} \langle \varphi\varphi\rangle.} \tag{B.2}$$

As there is no way of pairing up odd numbers of fields, therefore for Gaussian fields these correlators must vanish.

C

Three dimensional power spectrum

Often times in cosmology predictions are made in terms of 3D power spectra. We will derive the 3D power spectrum for our theory. This can be derived from the s-functions derived in Chapter 3. In principle the function s has the following form : $a - b(r/r_0)^{n_{\rm DE}}$. We will ignore the factor at coincidence, a, as this will directly give a delta function, and set the factor b to one for simplicity. The remaining correlation function is then,

$$\xi(r) = -\left(\frac{r}{r_0}\right)^{n_{\rm DE}}. \tag{C.1}$$

The power spectrum is the Fourier transform of the correlation function. It is therefore given by,

$$P(k) = \frac{1}{(2\pi)^3}\int d^3x \xi(r) e^{i\vec{x}\cdot\vec{k}} \tag{C.2}$$

$$= \frac{1}{2\pi^2}\int_0^\infty dr \xi(r)\frac{\sin(kr)}{kr}r^2. \tag{C.3}$$

Here we integrated out the angular dependence. It will now be useful to switch coordinates to $u = kr$:

$$\frac{1}{2\pi^2}\int dr\xi(r)\frac{\sin(kr)}{kr}r^2 = -\frac{1}{2\pi^2}\frac{1}{k^3}\frac{1}{(r_0k)^{n_{\rm DE}}}\int_0^\infty duu^{n_{\rm DE}+1}\sin(u) \tag{C.4}$$

$$= -\frac{1}{2\pi^2}\frac{1}{k^3}\frac{1}{(r_0k)^{n_{\rm DE}}}\,{\rm Im}\left[\int_0^\infty duu^{n_{\rm DE}+1}e^{iu}\right]. \tag{C.5}$$

We can Wick rotate this integral, evaluating it from 0 to $i\infty$:

$$P(k) = -\frac{1}{2\pi^2}\frac{1}{k^3}\frac{1}{(r_0k)^{n_{\rm DE}}}\,{\rm Im}\left[\int_0^{i\infty} duu^{n_{\rm DE}+1}e^{iu}\right]. \tag{C.6}$$

Then, we write this in terms of Eulers Gamma function by substituting $u = iv$:

$${\rm Im}\left[\int_0^\infty duu^{n_{\rm DE}+1}e^{iu}\right] = {\rm Im}\left[(i)^{n_{\rm DE}+2}\int_0^{i\infty} dvv^{n_{\rm DE}+1}e^{-v}\right] \tag{C.7}$$

$$= {\rm Im}\left[e^{\frac{i\pi}{2}(n_{\rm DE}+2)}\Gamma(n_{\rm DE}+2)\right] \tag{C.8}$$

$$= -\sin(\frac{\pi n_{\rm DE}}{2})\Gamma(n_{\rm DE}+2). \tag{C.9}$$

Using this, we obtain the following expression for the power spectrum,

$$P(k) = \frac{1}{2\pi^2}\frac{1}{(r_0k)^{n_{\rm DE}}}\frac{1}{k^3}\sin(\frac{\pi n_{\rm DE}}{2})\Gamma(n_{\rm DE}+2). \tag{C.10}$$

As a dimensionless power spectrum this is then:

$$\boxed{\Delta(k) = \frac{k^3}{2\pi^2}P(k) \propto (kr_0)^{-n_{\rm DE}}}, \tag{C.11}$$

which is similar to the power spectrum from inflation. When considering $n_{\rm DE} > 0$, as we do in the main text, we note that the spectrum red-tilted, as in this case there is more energy in the long wavelength modes. The spectrum from inflation, (2.12), is also slightly red-tilted when considering the *Planck* measurement of $n_s \approx 0.96$ [1].

D

Resummed derivation of the luminosity distance

In Chapter 4 we derived the following expression for the luminosity distance, (4.4),

$$\frac{\langle \hat{d}_L \rangle(z)}{1+z} = \int_0^z dz' \left\langle \frac{1}{\hat{H}(z',\hat{n})} \right\rangle = \int_0^z \frac{dz'}{\bar{H}(z')} \left\langle \frac{1}{\sqrt{1+\frac{\delta\hat{\rho}_Q(z',\hat{n})}{\rho_{\rm tot}(z')}}} \right\rangle . \tag{D.1}$$

We then proceeded with expanding in fluctuations $\delta\hat{\rho}_Q$. However, this formal series expansion has a zero radius of convergence in both our cases. Using Newtons binomium we have:

$$\left\langle \left(1+\frac{\delta\hat{\rho}_Q(z,\hat{n})}{\rho_{\rm tot}(z)}\right)^{-\frac{1}{2}} \right\rangle = \sum_{m=0}^{\infty} \binom{-\frac{1}{2}}{m} \left\langle \left(\frac{\delta\hat{\rho}_Q(z',\hat{n})}{\rho_{\rm tot}(z')}\right)^m \right\rangle . \tag{D.2}$$

To understand until which order we can trust this expansion, and to obtain some insights in the non perturbative behaviour of these fluctuations we will derive an exact analytic solution for the dressed luminosity distance in both cases by exploiting the Gaussian statistics of the fundamental fields $\hat{\varphi}$.

D.1 Case I

In *Case I* we assume the density relies on the fields squared, *i.e.* $\hat{\rho}_Q(z) = B(z)\hat{\varphi}(z,\hat{n})^2$. Here, $B(z)$ is a proportionality constant depending on the specifics of the model. For example, in the quantum origin model discussed in Chapter 9 we have an expression, (9.43), for this constant depending on the model parameters ξ and m. In terms of the field $\hat{\varphi}$ we can rewrite (D.2) as:

$$\left\langle \left(1+\frac{\delta\hat{\rho}_Q(z,\hat{n})}{\rho_{\text{tot}}(z)}\right)^{-\frac{1}{2}} \right\rangle = \sum_{m=0}^{\infty} \binom{-\frac{1}{2}}{m} \left(\frac{B(z)}{\rho_{\text{tot}}}\right)^m \left\langle \left(\hat{\varphi}^2(z) - A(z)\right)^m \right\rangle . \tag{D.3}$$

Here, $A(z) = \langle\hat{\varphi}\rangle(z)^2$, gives the squared average of the field. The factor in brackets can now be simplified using Wick's theorem, stating that every m point function can be decomposed in $(2m-1)!!$ two-point functions*. This gives us

$$\left\langle \left(\varphi^2(z) - A(z)\right)^m \right\rangle = \sum_{k=0}^{m} \binom{m}{k} \left\langle \hat{\varphi}^{2k} \right\rangle (-A(z))^{m-k} \tag{D.4}$$

$$= \sum_{k=0}^{m} \binom{m}{k} (-1)^{m-k}(2k-1)!!(A(z))^m \tag{D.5}$$

$$= (2m-1)!!\,{}_1F_1(-m;\frac{1}{2}-m;-\frac{1}{2})(A(z))^m, \tag{D.6}$$

where we used that the confluent hypergeometric function can be expressed as,

$${}_1F_1(-m;\frac{1}{2}-m;-\frac{1}{2}) = \sum_{k=0}^{m} \binom{m}{k} (-1)^{m-k} \frac{(2k-1)!!}{(2m-1)!!}. \tag{D.7}$$

Substituting (D.6) in (D.3) we obtain an expression for the fluctuations, given as a sum over the confluent hypergeometric funtion:

$$\left\langle \left(1+\frac{\delta\hat{\rho}_Q(z,\hat{n})}{\rho_{\text{tot}}(z)}\right)^{-\frac{1}{2}} \right\rangle = \sum_{m=0}^{\infty} \binom{-\frac{1}{2}}{m} \left(\frac{B(z)A(z)}{\rho_{\text{tot}}}\right)^m (2m-1)!!\,{}_1F_1(-m;\frac{1}{2}-m;-\frac{1}{2}) \tag{D.8}$$

$$= \sum_{m=0}^{\infty} \binom{-\frac{1}{2}}{m} (2m-1)!!\,\Omega_Q(z)^m\,{}_1F_1(-m;\frac{1}{2}-m;-\frac{1}{2}). \tag{D.9}$$

Here, we used that $\Omega_Q(z) = \frac{A(z)B(z)}{\rho_{\text{tot}}(z)}$. This series diverges due to of the amount of Wick contractions rapidly increasing. Per example, we have shown the first 10 terms in this expansion.

$$\left\langle \left(1+\frac{\delta\hat{\rho}_Q(z,\hat{n})}{\rho_{\text{tot}}(z)}\right)^{-\frac{1}{2}} \right\rangle \overset{\text{Series}}{=} 1 + \frac{3}{4}\Omega_Q^2 - \frac{5}{2}\Omega_Q^3 + \frac{525}{32}\Omega_Q^4 - \frac{1071}{8}\Omega_Q^5 + \frac{174405}{128}\Omega_Q^6 - \frac{1059201}{64}\Omega_Q^7$$
$$+ \frac{478873395}{2048}\Omega_Q^8 - \frac{964560025}{256}\Omega_Q^9 + \frac{558742466997}{8192}\Omega_Q^{10} + \mathcal{O}\left(\Omega_Q^{11}\right). \tag{D.10}$$

A first observation is that there are also odd terms in this expansion, a result of the non Gaussian nature of $\hat{\rho}_Q$ in *Case I*.

*The double factorial is defined as follows: $n!! = n(n-2)(n-4)\ldots$, with $(-1)!! \equiv 1$

We will now apply another method to obtain, via a non perturbative route, an expression for the fluctuations. In the spirit of the stochastic formalism [83], we will define a classical stochastic variable φ whose statistical properties are the same as those of the quantum operator $\hat{\varphi}$. We know this field obeys Gaussian statistics with vacuum expectation value $\langle\varphi\rangle(z) = 0$ and variance $\sigma^2(z) = \langle\varphi^2\rangle(z) - \langle\varphi\rangle^2(z) = A(z)$. Therefore, we can use this knowledge and replace the ensemble brackets by an integral over the Gaussian distribution,

$$\left\langle \left(1 + \frac{\delta\hat{\rho}_Q(z,\hat{n})}{\rho_{\text{tot}}(z)}\right)^{-\frac{1}{2}} \right\rangle = \frac{1}{\sqrt{2\pi A(z)}} \int_{-\infty}^{\infty} d\varphi \frac{e^{-\frac{1}{2}\frac{\varphi^2(z)}{A(z)}}}{\sqrt{1 + \frac{B(z)}{\rho_{\text{tot}}(z)}\left(\varphi^2(z) - A(z)\right)}} \tag{D.11}$$

We can make a change of variables $\varphi(x) = \sqrt{A(z)}\psi(x)$ and recognize that $\frac{A(z)B(z)}{\rho_{\text{tot}}(z)} = \frac{\langle\rho_Q\rangle(z)}{\rho_{\text{tot}}(z)} = \Omega_Q(z)$. Then we obtain,

$$\left\langle \left(1 + \frac{\delta\hat{\rho}_Q(z,\hat{n})}{\rho_{\text{tot}}(z)}\right)^{-\frac{1}{2}} \right\rangle = \frac{\sqrt{A(z)}}{\sqrt{2\pi A(z)}} \int_{-\infty}^{\infty} d\psi \frac{e^{-\frac{1}{2}\psi^2}}{\sqrt{1 + \Omega_Q(z)\left(\psi^2 - 1\right)}} \tag{D.12}$$

$$= \frac{1}{\sqrt{2\pi\Omega_Q(z)}} \int_{-\infty}^{\infty} d\psi \frac{e^{-\frac{1}{2}\psi^2}}{\sqrt{\frac{1}{\Omega_Q(z)} - 1 + \psi^2}}. \tag{D.13}$$

When $\Omega_Q(z) \in [0,1)$ this integral can be solved as a Bessel function yielding,

$$\boxed{\left\langle \left(1 + \frac{\delta\hat{\rho}_Q(z,\hat{n})}{\rho_{\text{tot}}(z)}\right)^{-\frac{1}{2}} \right\rangle = \frac{1}{\sqrt{2\pi\Omega_Q(z)}} e^{\frac{1}{4}\left(\frac{1}{\Omega_Q(z)} - 1\right)} K_0\left(\frac{1}{4}\left(\frac{1}{\Omega_Q(z)} - 1\right)\right).} \tag{D.14}$$

K_0 denotes the modified Bessel function of the second kind. We note that to obtain this result we did not make an assumptions except for the range of Ω_Q and the Gaussian nature of the underlying field $\hat{\varphi}$.

In Figure D.1 we show both the perturbative and the non perturbative result and compare the two. We see that the relative error is at most 10 percent, which justifies using our expansion. As a second check we can calculate the formal series expansion of (D.14), as the magnitude of the fluctuations is determined by $\Omega_Q(z)$ we can perform an expansion in this quantity. This then yields exactly (D.10), showing that the answer results in the same formal series.

D.2 Case II

We will now extend our treatment to *Case II*, where the energy density field $\hat{\rho}_Q$ depends linearly on the underlying field, $\hat{\rho}_Q = B(z)\hat{\varphi}$. We note that this $B(z)$ is in principle a different function from *Case I* as they describe different theories. In this

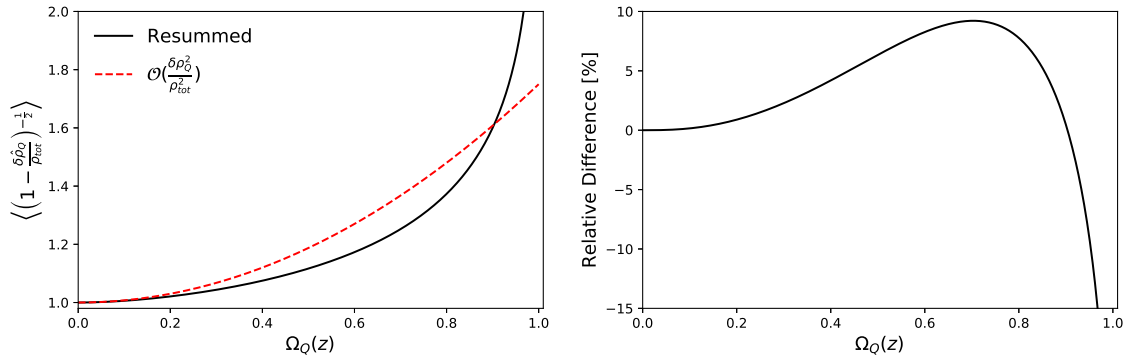

(a) (b)

Figure D.1: The left panel shows both the non perturbative and the perturbative results for the fluctuations. We note that in a universe without perturbations this factor is one. The panel on the right shows the relative error of the perturbative result, which we observe to be at most rougly 10 percent.

case, (D.2) takes the following form:

$$\left\langle\left(1+\frac{\delta\hat{\rho}_Q(z,\hat{n})}{\rho_{\rm tot}(z)}\right)^{-\frac{1}{2}}\right\rangle = \sum_{m=0}^{\infty}\binom{-\frac{1}{2}}{m}\left(\frac{B(z)}{\rho_{\rm tot}(z)}\right)^m\langle(\hat{\varphi}(z)-\langle\hat{\varphi}\rangle)^m\rangle\,. \tag{D.15}$$

$$= \sum_{m=0}^{\infty}\binom{-\frac{1}{2}}{2m}\left(\frac{B(z)}{\rho_{\rm tot}(z)}\right)^{2m}\left\langle\delta\hat{\varphi}^{2m}(z)\right\rangle\,. \tag{D.16}$$

$$= \sum_{m=0}^{\infty}\binom{-\frac{1}{2}}{2m}(2m-1)!!\left(\frac{\sigma_Q}{\rho_{\rm tot}(z)}\right)^{2m}\,. \tag{D.17}$$

In the second line we made use of the fact that all the odd contributions vanish as a consequence of the Gaussian nature of the fields, and in the last line we used Wick's theorem again and expressed the result in terms of the variance of $\hat{\rho}_Q$, which is denoted by σ_Q^2. This sum also diverges, as can be seen clearly by writing it out up to $\mathcal{O}(\frac{\sigma_Q^{10}}{\rho_{\rm tot}^{10}})$.

$$\left\langle\left(1+\frac{\delta\hat{\rho}_Q(z,\hat{n})}{\rho_{\rm tot}(z)}\right)^{-\frac{1}{2}}\right\rangle \overset{\text{Series}}{=} 1+\frac{3}{8}\left(\frac{\sigma_Q^2}{\rho_{\rm tot}^2}\right)+\frac{105}{128}\left(\frac{\sigma_Q^2}{\rho_{\rm tot}^2}\right)^2+\frac{3465}{1024}\left(\frac{\sigma_Q^2}{\rho_{\rm tot}^2}\right)^3+\frac{675675}{32768}\left(\frac{\sigma_Q^2}{\rho_{\rm tot}^2}\right)^4+\frac{43648605}{262144}\left(\frac{\sigma_Q^2}{\rho_{\rm tot}^2}\right)^5\,. \tag{D.18}$$

Again, it is clear that this is a diverging series, in fact, the radius of convergence of this series is 0 again. We can also note that when $\sigma_Q^2 = 2\langle\hat{\rho}_Q\rangle^2$, as is the case in *Case I*, indeed the first term matches the expansion (D.10). Which was expected as in this case the function $s_i(\|\vec{x}-\vec{y}\|)$ is the same. However, it is now also clear that this does not mean that the theories are the same at higher order, as the two expansions differ significantly when considering the higher order contributions.

Similar to *Case I*, we will now calculate a non perturbative expression by assuming the field $\hat{\varphi}$ is Gaussian. If $\hat{\varphi}$ obeys Gaussian statistics, then $\delta\hat{\rho}_Q = B(z)\,(\hat{\varphi}-\langle\varphi\rangle)$ will also obey Gaussian statistics. In this case the expectation value is given

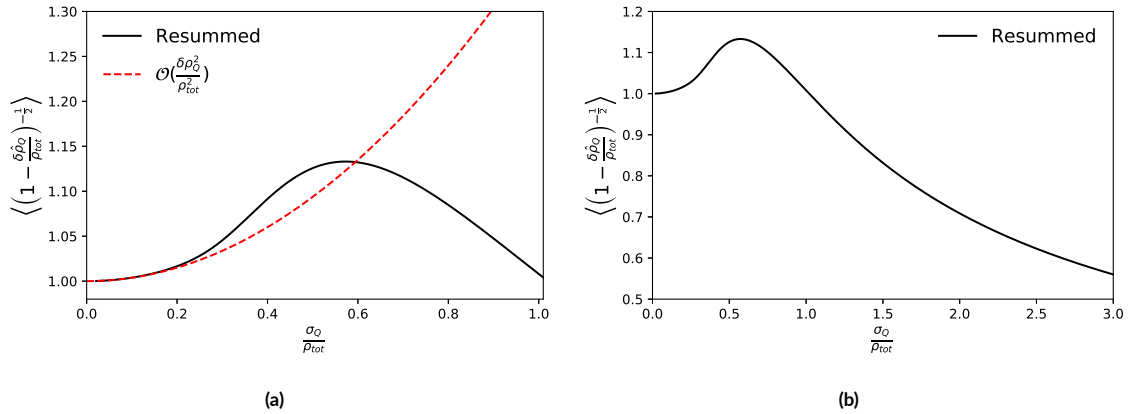

Figure D.2: The term describing the enhancement or decrease due to the fluctuations in the case where the density depends on the fields in a linear fashion (*Case II*). The left panel gives the comparison with our expansion, the black line shows (D.22), the red line shows $1+\frac{3}{8}\frac{\sigma_Q^2}{\rho_{tot}^2}$ (see (4.7)). The right panel shows (D.22) for a large range of $\frac{\sigma_Q}{\rho_{\text{tot}}}$.

by:

$$\left\langle\left(1+\frac{\delta\hat{\rho}_Q(z,\hat{n})}{\rho_{\text{tot}}(z)}\right)^{-\frac{1}{2}}\right\rangle=\frac{1}{\sqrt{2\pi}\sigma_Q}\int_{-\infty}^{\infty}d\left(\delta\rho_Q\right)\frac{1}{\sqrt{1+\frac{\delta\rho_Q}{\rho_{\text{tot}}}}}e^{-\frac{1}{2}\frac{\delta\rho_Q^2}{\sigma_Q^2}}. \tag{D.19}$$

However, we note that the lower limit is actually restricted as values where the square root becomes negative are prohibited due to $H^2\geq 0$. Changing the limits gives us:

$$\left\langle\left(1+\frac{\delta\hat{\rho}_Q(z,\hat{n})}{\rho_{\text{tot}}(z)}\right)^{-\frac{1}{2}}\right\rangle=\frac{1}{\sqrt{2\pi}\sigma_Q}\int_{-\rho_{\text{tot}}}^{\infty}d\left(\delta\rho_Q\right)\frac{1}{\sqrt{1+\frac{\delta\rho_Q}{\rho_{\text{tot}}}}}e^{-\frac{1}{2}\frac{\delta\rho_Q^2}{\sigma_Q^2}}. \tag{D.20}$$

Changing the lower limit in this way is allowed when the Gaussian is strongly peaked, i.e. $\frac{\sigma_Q^2}{\rho_{tot}}^2\ll 1$. We can observe that in the case where $\sigma_Q\to 0$, which is classical limit of this theory, the Gaussian distribution becomes the Dirac delta function $\delta(\delta\rho_Q)$. As a consequence the integral reduces to one, matching the classical result. Now we substitute $x=\frac{\delta\rho_Q}{\rho_{\text{tot}}}+1$ such that we obtain,

$$\left\langle\left(1+\frac{\delta\hat{\rho}_Q(z,\hat{n})}{\rho_{\text{tot}}(z)}\right)^{-\frac{1}{2}}\right\rangle=\frac{1}{\sqrt{2\pi c}}\int_0^{\infty}dx x^{-\frac{1}{2}}e^{-\frac{(x-1)^2}{2c}}. \tag{D.21}$$

Here, the constant c is the ratio between the total amount of matter and the fluctuations $c=\left(\frac{\sigma_Q}{\rho_{\text{tot}}}\right)^2$. This integral can also be solved in terms of Bessel functions, this then yields the following:

$$\boxed{\left\langle\left(1+\frac{\delta\hat{\rho}_Q(z,\hat{n})}{\rho_{\text{tot}}(z)}\right)^{-\frac{1}{2}}\right\rangle=\sqrt{\frac{\pi}{8}}\frac{\rho_{\text{tot}}}{\sigma_Q}e^{-\frac{\rho_{\text{tot}}^2}{4\sigma_Q^2}}\left(I_{-\frac{1}{4}}(\frac{\rho_{\text{tot}}^2}{4\sigma_Q^2})+I_{\frac{1}{4}}(\frac{\rho_{\text{tot}}^2}{4\sigma_Q^2})\right).} \tag{D.22}$$

Where I_n is the modified Bessel function of the first kind. The behaviour of this function is shown in Figure D.2b. We see that, indeed, it starts at one. We also notice that when the variance becomes sufficiently large, the fluctuations actually make

the effective Hubble parameter larger. However, as this is outside the regime where the variance is small, this result might not be trustworthy. From Figure D.2a we see that the quadratic order expansion is very good when the variance is relatively small, up to about $\frac{\sigma}{\rho_{\text{tot}}} \approx 0.2$. Hereafter the lines start to diverge.

As in the previous case, we can show that expanding (D.22) results in the same series as (D.18). To do this it is more convenient to define the variable $x = \frac{1}{c}$ and then use the asymptotic expansion at $x = \infty$. This then gives us:

$$\left\langle \left(1 + \frac{\delta\hat{\rho}_Q(z,\hat{n})}{\rho_{\text{tot}}(z)}\right)^{-\frac{1}{2}} \right\rangle \overset{\text{Series}}{=} \left(1 + \frac{3}{8x} + \frac{105}{128x^2} + \frac{3465}{1024x^3} + \frac{675675}{32768x^4} + \frac{43648605}{262144x^5}\right) + \mathcal{O}\left(\frac{1}{x^6}\right) \tag{D.23}$$

Which is the same as (D.18).

E

Unequal time correlator

In our ansatz (3.1) we assumed an equal time correlator for the density-density correlations. However, as our perturbations span very large scales, it is also possible to have correlations at different times. It is thus important to calculate the effects of the correlator at different times, a so called 'unequal time' correlator. In this Appendix we derive this correlator, which in the main text is used to obtain (4.12).

This unequal time correlator would be a way of distinguishing from perturbed ΛCDM. In ΛCDM the dark matter power spectrum $P_m(k, z, z')$ decays very rapidly with $\Delta z = z - z'$ [92], hence unequal time correlations differ from ΛCDM*.

To obtain such a correlator in our theory we expand the equal time correlator around $t = t_0$.

$$\langle \hat{\rho}_Q(t_1, \hat{n}_1)\hat{\rho}_Q(t_2, \hat{n}_2)\rangle = \langle \hat{\rho}_Q(t_0, \hat{n}_1)\hat{\rho}_Q(t_0, \hat{n}_2)\rangle + \Delta t_1 \langle \dot{\hat{\rho}}_Q(t_0, \hat{n}_1)\hat{\rho}_Q(t_0, \hat{n}_2)\rangle + \Delta t_2 \langle \hat{\rho}_Q(t_0, \hat{n}_1)\dot{\hat{\rho}}_Q(t_0, \hat{n}_2)\rangle. \tag{E.1}$$

where $\Delta t = t_1 - t_0$, t_i denotes the cosmological time, the subscript o means it is evaluated today (therefore t_0 is equal to the age of the universe). This expansion is good even if $t(z) - t_0$ becomes relatively large, this as dark energy varies very slowly with time and thus the correlator between $\dot{\hat{\rho}}_{Q,0}$ and $\hat{\rho}_{Q,0}$ will be small.

*This is only true on the level of the matter power spectrum itself, in ΛCDM there are also correlations depending on the line of sight, therefore also including correlations over different redshift bins. The lensing effect is discussed in more detail in Chapter 6.

Analogous to (3.1), we can define an ansatz for the unequal time correlator,

$$\langle \dot{\hat{\rho}}_Q(t,n)\hat{\rho}_Q(t,n')\rangle = \langle \hat{\rho}_Q(t,n)\dot{\hat{\rho}}_Q(t,n')\rangle = B(t)\langle\hat{\rho}_Q(t)\rangle\langle\hat{\rho}_Q(t)\rangle s_i(\|\vec{x}-\vec{y}\|). \tag{E.2}$$

Using the Leibniz rule we can obtain,

$$\partial_t\langle \hat{\rho}_Q(t,n)\hat{\rho}_Q(t,n')\rangle = \langle \dot{\hat{\rho}}_Q(t,n)\hat{\rho}_Q(t,n')\rangle + \langle \hat{\rho}_Q(t,n)\dot{\hat{\rho}}_Q(t,n')\rangle \tag{E.3}$$

$$= 2B(t)\langle\hat{\rho}_Q(t)\rangle\langle\hat{\rho}_Q(t)\rangle s_i(\|\vec{x}-\vec{y}\|). \tag{E.4}$$

However, we can calculate the left hand side by inserting (3.1) in the equal time operator. This yields,

$$\partial_t\langle \hat{\rho}_Q(t,n)\hat{\rho}_Q(t,n')\rangle = \left(2\frac{\langle\dot{\hat{\rho}}_Q(t)\rangle}{\langle\hat{\rho}_Q(t)\rangle}\right)\langle\hat{\rho}_Q\rangle(t)^2 s_i(\|\vec{x}-\vec{y}\|). \tag{E.5}$$

We can now obtain $B(t)$ by comparing (E.4) and (E.5). This gives us:

$$B(t) = \frac{\langle\dot{\hat{\rho}}_Q(t)\rangle}{\langle\hat{\rho}_Q(t)\rangle}. \tag{E.6}$$

In total we then get as our result for the correlator in (E.1):

$$\boxed{\langle\hat{\rho}_Q(t_1,\hat{n}_1)\hat{\rho}_Q(t_2,\hat{n}_2)\rangle \approx \langle\hat{\rho}_Q(t_0,\hat{n}_1)\hat{\rho}_Q(t_0,\hat{n}_2)\rangle\cdot\left(1+(\Delta t_1+\Delta t_2)\frac{\langle\dot{\hat{\rho}}_Q\rangle(t_0)}{\langle\hat{\rho}_Q\rangle(t_0)}\right).} \tag{E.7}$$

Indeed, as long as the dark energy field is a slowly varying field with time, this expansion will be very good and can be trusted even at $z \approx \mathcal{O}(1)$. Later it will be more useful to use redshift as a time coordinate instead of time. To linear order in time or redshift these can be related with the simple relation $t_0 - t \approx -H_0 z$, the coefficient on the RHS of (E.7) then becomes

$$\left(1+(\Delta t_1+\Delta t_2)\frac{\langle\dot{\hat{\rho}}_Q\rangle(t_0)}{\langle\hat{\rho}_Q\rangle(t_0)}\right) = \left(1+(z_1+z_2)\frac{\langle\hat{\rho}'_Q\rangle(z=0)}{\langle\hat{\rho}_Q\rangle(z=0)}\right), \tag{E.8}$$

the prime now denotes a derivative w.r.t. redshift. When the quantum fluid would obey a simple equation of state $p = w\rho$ the unequal time correlator (E.7) can be simplified some more,

$$\langle\hat{\rho}_Q(t_1,\hat{n}_1)\hat{\rho}_Q(t_2,\hat{n}_2)\rangle \approx \langle\hat{\rho}_Q(t_0,\hat{n}_1)\hat{\rho}_Q(t_0,\hat{n}_2)\rangle\cdot(1+3(z_1+z_2)\delta w). \tag{E.9}$$

Here, we defined $\delta w = w + 1$ as the difference from the equation of state a cosmological constant would give. Indeed, we see that if this is a small quantity, this expansion will be quite good also at intermediate redshift.

F

Angular and ensemble averages

We derived an expression for the spectrum corresponding to tracer defined by (5.2). In practice observations are done over the past light cone, measuring instead the spectrum corresponding to $\frac{\hat{d}_L(z,\hat{n})-\bar{d}_L(z)}{\bar{d}_L(z)}$. The bar denotes angular averaging, defined as:

$$\bar{d}_L = \int \frac{d^2\hat{n}}{4\pi} \hat{d}_L(z,\hat{n}). \tag{F.1}$$

This is still a stochastic quantity: a measurement on a different location could give a different value, as our measurement could be influenced by fluctuations. The relationship between an angular average $\bar{d}_L$ and the ensemble average $\langle d_L \rangle$ is in principle complicated and depends on the specific observable [93–96]. Differences between these two can have several origins; A state average is for example defined over a hyper surface of constant time, while the angular average averages of the past light cone. However, we will focus on another aspect, namely the fact that due to cosmic variance the average we observe is different from the true background average. The true background average is in principle not measurable, due to the fact that we can only access our past light-cone. We therefore have no way of knowing if our measured average is the true one, as for this we would have to do different measurements at different positions. This problem was discussed in the context of the Cosmic Microwave Background by [95], we extend this treatment and apply it to our own case.

Formally we can write the error made by assuming the two methods are the same by $\bar{d}_L = \langle \hat{d}_L \rangle + \left(\bar{d}_L - \langle \hat{d}_L \rangle \right)$. Where

the term in brackets is not necessarily zero. We can now define the cosmic variance*,

$$\delta_{cv} = \frac{\bar{d}_L}{\langle \hat{d}_L \rangle} - 1. \tag{F.2}$$

If $\delta_{cv} = 0$ the two averages are the same. The ensemble average of the cosmic variance is also zero, due to the fact that $\langle \bar{d}_L \rangle = \langle \hat{d}_L \rangle$. Using the cosmic variance we can write down a relation between the two distances: $\bar{d}_L = \langle \hat{d}_L \rangle (\delta_{cv} + 1)$.

We are interested in the observational accessible average, therefore we want to make predictions for the fluctuations with respect to the angular mean $\bar{d}_L$, theoretically we have predictions for the fluctuations with respect to the ensemble average $\langle \hat{d}_L \rangle$. The different Δ's look as follows in the two cases:

$$\tilde{\Delta}(z, \hat{n}) = \frac{\hat{d}_L(z, \hat{n})}{\bar{d}_L(z)} - 1, \qquad \Delta(z, \hat{n}) = \frac{\hat{d}_L}{\langle d_L \rangle} - 1. \tag{F.3}$$

Fluctuations become visible in the two-point functions, for these two quantities these are given by:

$$\langle \tilde{\Delta}(z, \hat{n}) \tilde{\Delta}(z', \hat{m}) \rangle = \frac{\langle \hat{d}_L(z, \hat{n}) \hat{d}_L(z', \hat{m}) \rangle}{\bar{d}_L(z) \bar{d}_L(z')} - 1, \tag{F.4}$$

$$\langle \Delta(z, \hat{n}) \Delta(z', \hat{m}) \rangle = \frac{\langle \hat{d}_L(z, \hat{n}) \hat{d}_L(z', \hat{m}) \rangle}{\langle d_L \rangle(z) \langle d_L \rangle(z')} - 1. \tag{F.5}$$

The task at hand is then expressing the first quantity in terms of the observable quantity on the left the theoretically available quantity on the right. To this end we can express Δ in terms of $\tilde{\Delta}$ and the cosmic variance δ_{cv},

$$\Delta(z, \hat{n}) = \tilde{\Delta}(z, \hat{n}) + \delta_{cv}(z) + \tilde{\Delta}(z, \hat{m}) \delta_{cv}(z) \tag{F.6}$$

Using this we can express the ensemble correlator in terms of correlation functions including $\tilde{\Delta}$ and δ_{cv}:

$$\begin{aligned} \langle \Delta(z, \hat{n}) \Delta(z', \hat{m}) \rangle = & \langle \tilde{\Delta}(z, \hat{n}) \tilde{\Delta}(z', \hat{m}) \rangle + \langle \tilde{\Delta}(z, \hat{n}) \delta_{cv}(z') \rangle + \langle \tilde{\Delta}(z', \hat{m}) \delta_{cv}(z) \rangle \\ & + \langle \delta_{cv}(z) \delta_{cv}(z') \rangle + \langle \tilde{\Delta}(z, \hat{n}) \delta_{cv}(z') \tilde{\Delta}(z', \hat{m}) \rangle \\ & + \langle \tilde{\Delta}(z', \hat{m}) \delta_{cv}(z) \tilde{\Delta}(z, \hat{n}) \rangle + \langle \delta_{cv}(z) \tilde{\Delta}(z, \hat{n}) \delta_{cv}(z') \rangle \\ & + \langle \delta_{cv}(z') \tilde{\Delta}(z', \hat{m}) \delta_{cv}(z) \rangle + \langle \tilde{\Delta}(z, \hat{n}) \delta_{cv}(z) \tilde{\Delta}(z', \hat{m}) \delta_{cv}(z') \rangle. \end{aligned} \tag{F.7}$$

We now assume Wick's theorem. Wick's theorem is valid for Gaussian distributed functions. This is in principle not true for our $\hat{d}_L$ correlators, however, we may assume that they are approximately Gaussian. Because $\langle \tilde{\Delta} \rangle = \langle \delta_{cv} \rangle = 0$ the three-

*This cosmic variance is conceptually related, but not the same, to the previously mentioned cosmic variance that arises during the averaging procedure for the C_ℓ.

point functions vanish. The four-point function can be expressed in three products of two-point functions. This yields:

$$\begin{aligned}\langle\Delta(z,\hat{n})\Delta(z',\hat{m})\rangle \approx &\langle\tilde{\Delta}(z,\hat{n})\tilde{\Delta}(z',\hat{m})\rangle + \langle\tilde{\Delta}(z,\hat{n})\delta_{cv}(z')\rangle + \langle\tilde{\Delta}(z',\hat{m})\delta_{cv}(z)\rangle \\ &+ \langle\delta_{cv}(z)\delta_{cv}(z')\rangle + \langle\delta_{cv}(z')\tilde{\Delta}(z',\hat{m})\rangle\langle\delta_{cv}(z)\tilde{\Delta}(z,\hat{n})\rangle \\ &+ \langle\delta_{cv}(z')\tilde{\Delta}(z,\hat{n})\rangle\langle\delta_{cv}(z)\tilde{\Delta}(z',\hat{m})\rangle + \langle\delta_{cv}(z)\delta_{cv}(z')\rangle\langle\tilde{\Delta}(z,\hat{n})\tilde{\Delta}(z',\hat{m})\rangle.\end{aligned} \tag{F.8}$$

The remaining task is now finding the suitable expressions for the $\langle\delta_{cv}(z)\delta_{cv}(z')\rangle$ and $\langle\tilde{\Delta}(z,\hat{n})\delta_{cv}(z')\rangle$ correlators. We start with the auto correlation. We first expand the definition to obtain:

$$\langle\delta_{cv}(z)\delta_{cv}(z')\rangle = \left\langle\left(\frac{\bar{d}_L(z)}{\langle\hat{d}_L\rangle(z)} - 1\right)\left(\frac{\bar{d}_L(z')}{\langle\hat{d}_L\rangle(z')} - 1\right)\right\rangle = \frac{\langle\bar{d}_L(z)\bar{d}_L(z')\rangle}{\langle\hat{d}_L\rangle(z)\langle\hat{d}_L\rangle(z')} - 1 \tag{F.9}$$

We can now factor the angular averaging integrals out of the ensemble brackets. This gives us:

$$\langle\delta_{cv}(z)\delta_{cv}(z')\rangle = \int\frac{d^2\hat{n}}{4\pi}\int\frac{d^2\hat{m}}{4\pi}\left[\frac{\langle\hat{d}_L(z,\hat{n})\hat{d}_L(z',\hat{m})\rangle}{\langle\hat{d}_L\rangle(z)\langle\hat{d}_L\rangle(z')} - 1\right] \tag{F.10}$$

$$= \frac{1}{2}\int_{-1}^{1} d\mu\left[\frac{\langle\hat{d}_L(z)\hat{d}_L(z')\rangle(\mu)}{\langle\hat{d}_L\rangle(z)\langle\hat{d}_L\rangle(z')} - 1\right] \tag{F.11}$$

$$= \frac{C_0(z,z')}{4\pi}, \tag{F.12}$$

where we used the fact that the correlator only depends on the relative angle. This angle is contained in $\mu = \hat{n}\cdot\hat{m} = \cos(\theta)$ with θ being the relative angle. In the last step we recognised the angular power spectrum as defined in (5.5). We stress that this is an exact result, we have not assumed anything to obtain it. It tells us that the cosmic variance correlator is given in terms of the monopole C_0. In the case that the ensemble and angular average would be the same, the monopole is zero. As is shown later in this section. This agrees with our result, as in this case the cosmic variance should be zero. We also note that C_0 is possible to calculate within our framework, therefore we can quantify this result.

Inserting this in (F.8) we obtain:

$$\begin{aligned}\langle\Delta(z,\hat{n})\Delta(z',\hat{m})\rangle \approx &\langle\tilde{\Delta}(z,\hat{n})\tilde{\Delta}(z',\hat{m})\rangle\left(1 + \frac{C_0(z,z')}{4\pi}\right) + \langle\tilde{\Delta}(z,\hat{n})\delta_{cv}(z')\rangle \\ &+ \langle\tilde{\Delta}(z',\hat{m})\delta_{cv}(z)\rangle + \frac{C_0(z,z')}{4\pi} + \langle\delta_{cv}(z')\tilde{\Delta}(z',\hat{m})\rangle\langle\delta_{cv}(z)\tilde{\Delta}(z,\hat{n})\rangle \\ &+ \langle\delta_{cv}(z')\tilde{\Delta}(z,\hat{n})\rangle\langle\delta_{cv}(z)\tilde{\Delta}(z',\hat{m})\rangle.\end{aligned} \tag{F.13}$$

At this point we still have the correlators, $\langle\tilde{\Delta}\delta_{cv}\rangle$, which we cannot readily calculate. However, we know that the angular

averaged power spectrum should have a zero monopole, $\tilde{C}_0(z,z') = 0$. This can be seen as follows:

$$\frac{\tilde{C}_0(z,z')}{4\pi} = \int \frac{d^2\hat{n}}{4\pi}\int \frac{d^2\hat{m}}{4\pi}\langle\tilde{\Delta}(z,\hat{n})\tilde{\Delta}(z',\hat{m})\rangle \tag{F.14}$$

$$= \left\langle \left(\int \frac{d^2\hat{n}}{4\pi}\tilde{\Delta}(z,\hat{n})\right)\left(\int \frac{d^2\hat{m}}{4\pi}\tilde{\Delta}(z',\hat{m})\right)\right\rangle . \tag{F.15}$$

We can then note that the terms in brackets will be zero as:

$$\int \frac{d^2\hat{n}}{4\pi}\tilde{\Delta}(z,\hat{n}) = \frac{\int \frac{d^2\hat{n}}{4\pi}\hat{d}_L(z,\hat{n})}{\bar{d}_L(z)} - 1 = 0. \tag{F.16}$$

The last equality follows from the definition of the angular averaged luminosity distance (F.1). We can now use this to make some progress. If we multiply (F.13) by $2\pi\mathcal{P}_\ell$ and integrate over the relative angle, we obtain C_ℓ on the left hand side. The correlators $\langle\tilde{\Delta}\delta_{cv}\rangle$ do not depend on an angle[†] and are therefore proportional to $\mathcal{P}_0$, resulting in Kronecker delta's. This gives us the constraint equation:

$$C_\ell(z,z') = \tilde{C}_\ell(z,z')\left(1+\frac{C_0(z,z')}{4\pi}\right) + C_0(z,z')\delta_{\ell,0} + 4\pi\left[\langle\tilde{\Delta}(z,\hat{n})\delta_{cv}(z')\rangle + \langle\tilde{\Delta}(z',\hat{m})\delta_{cv}(z)\rangle + \langle\delta_{cv}(z')\tilde{\Delta}(z',\hat{m})\rangle\langle\delta_{cv}(z)\tilde{\Delta}(z,\hat{n})\rangle\right]\delta_{\ell,0}. \tag{F.17}$$

Considering $\ell = 0$ and using the $\tilde{C}_0 = 0$ we can deduce that the cross correlation terms have to be zero. Without these terms we can rewrite (F.13) in terms of power spectra as:

$$C_\ell(z,z') = \tilde{C}_\ell(z,z')\left(1+\frac{C_0(z,z')}{4\pi}\right) + C_0(z,z')\delta_{\ell,0} \tag{F.18}$$

The complete expression for $\tilde{C}_\ell(z,z')$ in terms of our predicted power spectrum $C_\ell(z,z')$ is then:

$$\boxed{\tilde{C}_\ell(z,z') = \frac{C_\ell(z,z') - C_0(z,z')\delta_{\ell,0}}{1+\frac{C_0(z,z')}{4\pi}}}. \tag{F.19}$$

We can understand this as follows: if the background average per steradian $C_0/4\pi$ is non zero, the size of the fluctuations as given by $\tilde{C}_\ell$ will be smaller. This makes intuitive sense, as relative to the background the fluctuations are smaller due to the background average being larger. We conclude two things about this result: First, indeed for $\ell = 0$ this gives zero. This does not come as a surprise as we constructed it this way. Second, we can account for the different normalisation of our power spectrum by dividing (5.12) by a factor $1+\frac{C_0(z,z')}{4\pi}$.

In principle this result is independent of our specific model. However, we are interested in its effect on our model. Therefore we calculate the effect is has in our case. The Legendre polynomial with $\ell = 0$ is simply one. Therefore we obtain via

[†]Only Δ has angular dependence and this angular dependence disappears when taking the ensemble average.

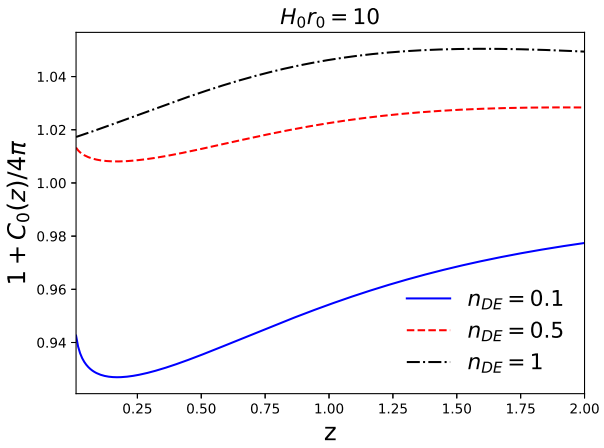

Figure F.1: The relevant contribution from the monopole in (F.18). We show this result for *Case I*. Several spectral indices $n_{\rm DE}$ are shown and $H_0 r_0 = 10$.

(5.12),

$$C_0(z, z') = 2\pi \int_{-1}^{1} d\mu \langle \Delta(z)\Delta(z')\rangle(\mu). \tag{F.20}$$

Inserting the Δ's using (4.12) then gives us:

$$\begin{aligned} C_0(z_1, z_2) = 2\pi \frac{(1+z_1)(1+z_2)}{\langle \hat{d}_L\rangle(z_1)\langle \hat{d}_L\rangle(z_2)} \int_{-1}^{1} d\mu \int_0^{z_1} dz \int_0^{z_2} dz' \frac{1}{\bar{H}(z)\bar{H}(z')} \Bigg[1 + \frac{3}{8}\left(\Omega_Q(z)^2 + \Omega_Q^2(z')\right)(s_i(0) - 1) \\ + \frac{1}{4}\left(\frac{\bar{H}_0^4}{\bar{H}(z)^2\bar{H}(z')^2}\Omega_{Q,0}^2 \left(1 + (\Delta t(z) + \Delta t(z'))\frac{\langle \dot{\hat{\rho}}_Q\rangle_0}{\langle \hat{\rho}_Q\rangle_0}\right) s_i(\|\vec{x} - \vec{y}\|) - \Omega_Q(z)\Omega_Q(z')\right)\Bigg] - 4\pi. \end{aligned} \tag{F.21}$$

We calculate the monopole in the context of *Case I*. The contribution of the extra factor $1 + \frac{C_0(z,z')}{4\pi}$ is shown in Figure F.1.

We see that the factor changes the result at most with roughly 1-5 percent.

F.1 Alternative method

We will now derive (F.19) in an independent way. The correlator between the variance and the tracer is:

$$\langle \tilde{\Delta}(z, \hat{n})\delta_{cv}(z')\rangle = \left\langle \left(\frac{\hat{d}_L(z, \hat{n})}{\bar{d}_L(z)} - 1 \right) \delta_{cv}(z') \right\rangle \tag{F.22}$$

$$= \left\langle \left(\frac{\hat{d}_L(z, \hat{n})}{\langle d_L\rangle(z)(1 + \delta_{cv}(z))} + 1 \right) \delta_{cv}(z') \right\rangle \tag{F.23}$$

$$\approx \left\langle \left(\frac{\hat{d}_L(z, \hat{n})}{\langle d_L\rangle(z)}(1 - \delta_{cv}(z)) - 1 \right) \delta_{cv}(z') \right\rangle + \mathcal{O}(\delta_{cv}^3). \tag{F.24}$$

Here, we expanded the cosmic variance up to linear order, assuming it is small. We can now rewrite (F.24) in terms of the tracers again,

$$\langle \tilde{\Delta}(z,\hat{n})\delta_{cv}(z')\rangle \approx \left\langle \left(\frac{d_L(z,\hat{n})}{\langle d_L\rangle(z)}(1-\delta_{cv}(z)) - 1 \right) \delta_{cv}(z') \right\rangle + \mathcal{O}(\delta_{cv}^3) \tag{F.25}$$

$$= \langle \Delta(z,\hat{n})\delta_{cv}(z')\rangle - \langle \delta_{cv}(z)\delta_{cv}(z')\rangle + \langle \Delta(z,\hat{n})\delta_{cv}(z)\delta_{cv}(z')\rangle + \mathcal{O}(\delta_{cv}^3). \tag{F.26}$$

Now we drop the three-point function as a consequence of their assumed Gaussianity. We can also derive an expression for the $\langle \Delta\delta_{cv}\rangle$ correlator by using the same trick as in deriving (F.10). We factor out the angular integral out of the ensemble brackets to obtain:

$$\langle \Delta(z,\hat{n})\delta_{cv}(z')\rangle = \int \frac{d^2\hat{m}}{4\pi} \left[\frac{\langle \hat{d}_L(z,\hat{n})\hat{d}_L(z',\hat{m})\rangle}{\langle \hat{d}_L\rangle(z)\langle \hat{d}_L\rangle(z')} - 1 \right] \tag{F.27}$$

$$= \frac{1}{2}\int_{-1}^{1} d\mu \left[\frac{\langle d_L(z)d_L(z')\rangle(\mu)}{\langle \hat{d}_L\rangle(z)\langle \hat{d}_L\rangle(z')} - 1 \right] \tag{F.28}$$

$$= \frac{C_0(z,z')}{4\pi}. \tag{F.29}$$

This is precisely the same as (F.10). Inserting both (F.10) and (F.29) in (F.26) then gives us:

$$\langle \tilde{\Delta}(z,\hat{n})\delta_{cv}(z')\rangle = 0. \tag{F.30}$$

Using this to simplify (F.13) and then rewriting it as power spectra then also results in (F.19). We note that we have now obtained that the angular averaged monopole is zero without demanding this.

G

A hypergeometric integral

In the main text we arrived at the following integral when calculating the angular power spectrum for the dark energy signal, see (5.10). The integral is over a relative angle μ and the Legendre polynomials $\mathcal{P}_\ell$,

$$I = \int_{-1}^{1} d\mu \left(\frac{r(z_1, z_2, \mu)^{n_{\rm DE}}}{r_0^{n_{\rm DE}}} \right) \mathcal{P}_\ell(\mu), \tag{G.1}$$

r being the comoving distance between two points. We can rewrite $r(z_1, z_2, \mu)^{n_{\rm DE}} = \left(\chi_1^2 + \chi_2^2 - 2\chi_1\chi_2\mu\right)^{\frac{n_{\rm DE}}{2}}$, where $\chi_i = \chi(z_i)$, the comoving distance to the point z_i and $\mu = \cos\theta$ with θ the relative angle between the two points. We can then rewrite the integral as

$$I = \left(2\chi_1\chi_2\right)^{\frac{n_{\rm DE}}{2}} \frac{\mu_0^{\frac{n_{\rm DE}}{2}}}{r_0^{n_{\rm DE}}} \int_{-1}^{1} d\mu \left(1 - \frac{\mu}{\mu_0}\right)^{\frac{n_{\rm DE}}{2}} \mathcal{P}_\ell(\mu) = \frac{\left(2\chi_1\chi_2\right)^{\frac{n_{\rm DE}}{2}}}{r_0^{n_{\rm DE}}} \tilde{I}. \tag{G.2}$$

Here, we defined $\tilde{I}$ as the integral over μ and $\mu_0 = \frac{\chi_1^2+\chi_2^2}{2\chi_1\chi_2}$. As the ratio $\frac{\mu}{\mu_0}$ is always smaller than one we can write it as a series expansion. As this function is nicely behaved, we can subsequently commute the sum and the integral,

$$\tilde{I} = \mu_0^{\frac{n_{\rm DE}}{2}} \int_{-1}^{1} d\mu (1 - \frac{\mu}{\mu_0})^{\frac{n_{\rm DE}}{2}} \mathcal{P}_\ell(\mu) = \mu_0^{\frac{n_{\rm DE}}{2}} \sum_{n=0}^{\infty} \binom{\frac{n_{\rm DE}}{2}}{n} \frac{1}{(-\mu_0)^n} \int_{-1}^{1} d\mu \mu^n \mathcal{P}_\ell(\mu), \tag{G.3}$$

We have now replaced our integral with a summation and a more tractable integral: $\int_{-1}^{1} d\mu x^n \mathcal{P}_\ell(\mu)$. A very similar integral is given by ref. [97]:

$$\int_0^1 d\mu x^n \mathcal{P}_\ell(\mu) = \frac{\sqrt{\pi}}{2^{1+n}} \frac{\Gamma(1+n)}{\Gamma(1+\frac{n-\ell}{2})\Gamma(\frac{3}{2}+\frac{n+\ell}{2})}. \tag{G.4}$$

Here, $\Gamma(z)$ is Eulers Gamma function. To calculate the integral on the other half of its domain we make use of the fact that $\mathcal{P}_\ell(-x) = (-1)^\ell \mathcal{P}_\ell(x)$. For the complete domain the integral is then given by

$$\int_{-1}^1 d\mu x^n \mathcal{P}_\ell(\mu) = \left(1+(-1)^{\ell+n}\right) \frac{\sqrt{\pi}}{2^{1+n}} \frac{\Gamma(1+n)}{\Gamma(1+\frac{n-\ell}{2})\Gamma(\frac{3}{2}+\frac{n+\ell}{2})}. \tag{G.5}$$

We can insert this in (G.3), yielding

$$\tilde{I} = \frac{\mu_0^{\frac{n_{\mathrm{DE}}}{2}}\sqrt{\pi}}{2} \sum_{n=0}^{\infty} \binom{\frac{n_{\mathrm{DE}}}{2}}{n} \left(1+(-1)^{\ell+n}\right) \left(-\frac{1}{2\mu_0}\right)^n \frac{\Gamma(1+n)}{\Gamma(1+\frac{n-\ell}{2})\Gamma(\frac{3}{2}+\frac{n+\ell}{2})}. \tag{G.6}$$

We can now rewrite the Binomial coefficients in a form more useful to us:

$$\Gamma(1+n)\binom{\frac{n_{\mathrm{DE}}}{2}}{n} = \frac{\Gamma(1+\frac{n_{\mathrm{DE}}}{2})}{\Gamma(1-n+\frac{n_{\mathrm{DE}}}{2})} = (-1)^n \frac{\Gamma(n-\frac{n_{\mathrm{DE}}}{2})}{\Gamma(-\frac{n_{\mathrm{DE}}}{2})}. \tag{G.7}$$

Substituting this in (G.6) then gives us,

$$\tilde{I} = \frac{\mu_0^{\frac{n_{\mathrm{DE}}}{2}}\sqrt{\pi}}{2\Gamma(-\frac{n_{\mathrm{DE}}}{2})} \sum_{n=0}^{\infty} \left(1+(-1)^{\ell+n}\right) \left(\frac{1}{2\mu_0}\right)^n \frac{\Gamma(n-\frac{n_{\mathrm{DE}}}{2})}{\Gamma(1+\frac{n-\ell}{2})\Gamma(\frac{3}{2}+\frac{n+\ell}{2})}. \tag{G.8}$$

To get rid of the factor $\left(1+(-1)^{\ell+n}\right)$, we can consider separately the even and odd cases for ℓ.

G.1 ℓ is even

In the even case this factor can be conveniently written as,

$$\left(1+(-1)^{\ell+n}\right) = \begin{cases} 0, & n = \text{odd}, \\ 2, & n = \text{even} \end{cases} \tag{G.9}$$

Using this we obtain in the case that ℓ is even,

$$\tilde{I}_{\text{even}} = \frac{\mu_0^{\frac{n_{\mathrm{DE}}}{2}}\sqrt{\pi}}{\Gamma(-\frac{n_{\mathrm{DE}}}{2})} \sum_{n=0}^{\infty} \left(\frac{1}{2\mu_0}\right)^{2n} \frac{\Gamma(2n-\frac{n_{\mathrm{DE}}}{2})}{\Gamma(1+n-\frac{\ell}{2})\Gamma(\frac{3}{2}+n+\frac{\ell}{2})} \tag{G.10}$$

Our goal is to rewrite this in terms of Pochammer symbols, $(a)_n = \frac{\Gamma(a+n)}{\Gamma(a)}$. However, these do not contain factors $2n$. To remove these we will use Gauss' multiplication theorem (see e.g. [64]),

$$\Gamma(2n - \frac{n_{\text{DE}}}{2}) = \Gamma(2(n - \frac{n_{\text{DE}}}{4})) = \frac{2^{2n-\frac{n_{\text{DE}}}{2}-1}}{\sqrt{\pi}}\Gamma(n - \frac{n_{\text{DE}}}{4})\Gamma(n - \frac{n_{\text{DE}}}{4} + \frac{1}{2}). \tag{G.11}$$

Using this to rewrite the Gamma functions containing factors $2n$ yields:

$$\tilde{I}_{\text{even}} = \frac{\mu_0^{\frac{n_{\text{DE}}}{2}} 2^{-\frac{n_{\text{DE}}}{2}-1}}{\Gamma(-\frac{n_{\text{DE}}}{2})} \sum_{n=0}^{\infty} \left(\frac{1}{\mu_0^2}\right)^n \frac{\Gamma(n - \frac{n_{\text{DE}}}{4})\Gamma(n - \frac{n_{\text{DE}}}{4} + \frac{1}{2})}{\Gamma(1 + n - \frac{\ell}{2})\Gamma(\frac{3}{2} + n + \frac{\ell}{2})}. \tag{G.12}$$

Now we may note that $\Gamma(1 + n - \frac{\ell}{2})$ hits a pole if $\frac{\ell}{2} \geq 1 + n$, which means that all terms up to and including $n = \frac{\ell}{2} - 1$ do not contribute. This allows us to relabel the starting index of the summation to $n = \frac{\ell}{2}$, after this we can relabel everything to make the summation start at 0 again. This then results in,

$$\tilde{I}_{\text{even}} = \frac{\mu_0^{\frac{n_{\text{DE}}}{2}-\ell} 2^{-\frac{n_{\text{DE}}}{2}-1}}{\Gamma(-\frac{n_{\text{DE}}}{2})} \sum_{n=0}^{\infty} \frac{\left(\frac{1}{\mu_0^2}\right)^n}{n!} \frac{\Gamma(n + \frac{\ell}{2} - \frac{n_{\text{DE}}}{4})\Gamma(n + \frac{\ell}{2} - \frac{n_{\text{DE}}}{4} + \frac{1}{2})}{\Gamma(\frac{3}{2} + n + \ell)} \tag{G.13}$$

Gauss' hypergeometric function is defined as follows,

$${}_2F_1(a, b; c; z) = \sum_{n=0}^{\infty} \frac{(a)_n (b)_n}{(c)_n} \frac{z^n}{n!}, \qquad \text{where } (a)_n = \frac{\Gamma(a+n)}{\Gamma(a)} \tag{G.14}$$

Using that $\Gamma(a + n) = (a)_{(n)}\Gamma(a)$,we can now rewrite (G.13) as hypergeometric function. This gives the following expression,

$$\tilde{I}_{\text{even}} = \frac{\mu_0^{\frac{n_{\text{DE}}}{2}-\ell} 2^{-\frac{n_{\text{DE}}}{2}-1}}{\Gamma(-\frac{n_{\text{DE}}}{2})} \frac{\Gamma(\frac{\ell}{2} - \frac{n_{\text{DE}}}{4})\Gamma(\frac{1}{2} + \frac{\ell}{2} - \frac{n_{\text{DE}}}{4})}{\Gamma(\frac{3}{2} + \ell)} {}_2F_1\left(\frac{\ell}{2} - \frac{n_{\text{DE}}}{4}, \frac{1}{2} + \frac{\ell}{2} - \frac{n_{\text{DE}}}{4}; \frac{3}{2} + \ell; \frac{1}{\mu_0^2}\right) \tag{G.15}$$

G.2 ℓ is odd

We now wish to calculate the odd ℓ's with a similar approach. Then we have:

$$\left(1 + (-1)^{\ell+n}\right) = \begin{cases} 2, & n = \text{odd}, \\ 0, & n = \text{even}. \end{cases} \tag{G.16}$$

Using this we get:

$$\tilde{I}_{\text{odd}} = \frac{\mu_0^{\frac{n_{\text{DE}}}{2}} \sqrt{\pi}}{\Gamma\left(-\frac{n_{\text{DE}}}{2}\right)} \sum_{n=0}^{\infty} \left(\frac{1}{2\mu_0}\right)^{2n+1} \frac{\Gamma\left(2n + 1 - \frac{n_{\text{DE}}}{2}\right)}{\Gamma\left(\frac{3}{2} + n - \frac{\ell}{2}\right)\Gamma\left(2 + n + \frac{\ell}{2}\right)}. \tag{G.17}$$

Which we can, similar as in the other case, simplify using the Gauss' multiplication formula. Resulting in

$$\tilde{I}_{\text{odd}} = \frac{2^{-\frac{n_{\text{DE}}}{2}-1}\mu_0^{\frac{n_{\text{DE}}}{2}-1}}{\Gamma\left(-\frac{n_{\text{DE}}}{2}\right)} \sum_{n=0}^{\infty} \left(\frac{1}{\mu_0^2}\right)^n \frac{\Gamma\left(n+\frac{1}{2}-\frac{n_{\text{DE}}}{4}\right)\Gamma\left(n+1-\frac{n_{\text{DE}}}{4}\right)}{\Gamma\left(\frac{3}{2}+n-\frac{\ell}{2}\right)\Gamma\left(2+n+\frac{\ell}{2}\right)}. \tag{G.18}$$

From studying the Gamma function in the denominator, $\Gamma(\frac{3}{2}+n-\frac{\ell}{2})$, we see that the terms up to and including $n = \frac{\ell}{2}-\frac{3}{2}$ do not contribute. We thus start counting at $n = \frac{\ell}{2}-\frac{1}{2}$:

$$\tilde{I}_{\text{odd}} = \frac{2^{-\frac{n_{\text{DE}}}{2}-1}\mu_0^{\frac{n_{\text{DE}}}{2}-1}}{\Gamma\left(-\frac{n_{\text{DE}}}{2}\right)} \sum_{n=\frac{\ell}{2}-\frac{1}{2}}^{\infty} \left(\frac{1}{\mu_0^2}\right)^n \frac{\Gamma\left(n+\frac{1}{2}-\frac{n_{\text{DE}}}{4}\right)\Gamma\left(n+1-\frac{n_{\text{DE}}}{4}\right)}{\Gamma\left(\frac{3}{2}+n-\frac{\ell}{2}\right)\Gamma\left(2+n+\frac{\ell}{2}\right)}. \tag{G.19}$$

Shifting the summation index again,

$$\tilde{I}_{\text{odd}} = \frac{2^{-\frac{n_{\text{DE}}}{2}-1}\mu_0^{\frac{n_{\text{DE}}}{2}-1}}{\Gamma\left(-\frac{n_{\text{DE}}}{2}\right)} \sum_{n=0}^{\infty} \left(\frac{1}{\mu_0^2}\right)^{n+\frac{l-1}{2}} \frac{\Gamma\left(n+\frac{\ell}{2}-\frac{n_{\text{DE}}}{4}\right)\Gamma\left(n+\frac{1}{2}+\frac{\ell}{2}-\frac{n_{\text{DE}}}{4}\right)}{\Gamma\left(1+n\right)\Gamma\left(\frac{3}{2}+n+\ell\right)} \tag{G.20}$$

$$= \frac{2^{-\frac{n_{\text{DE}}}{2}-1}\mu_0^{\frac{n_{\text{DE}}}{2}-l}}{\Gamma\left(-\frac{n_{\text{DE}}}{2}\right)} \sum_{n=0}^{\infty} \frac{\left(\frac{1}{\mu_0^2}\right)^n}{n!} \frac{\Gamma\left(n+\frac{\ell}{2}-\frac{n_{\text{DE}}}{4}\right)\Gamma\left(n+\frac{1}{2}+\frac{\ell}{2}-\frac{n_{\text{DE}}}{4}\right)}{\Gamma\left(\frac{3}{2}+n+\ell\right)}. \tag{G.21}$$

Which is remarkably precisely the same as (G.13). We thus conclude that (G.15) is also a solution for the odd case. Then, we can use Gauss' multiplication theorem again to simplify the prefactor of (G.15), yielding our final result,

$$\boxed{I = \frac{\left(2\chi_1\chi_2\right)^{\frac{n_{\text{DE}}}{2}}}{r_0^{n_{\text{DE}}}} \sqrt{\pi}\mu_0^{\frac{n_{\text{DE}}}{2}-\ell} 2^{-\ell} \frac{\Gamma\left(-\frac{n_{\text{DE}}}{2}+\ell\right)}{\Gamma(-\frac{n_{\text{DE}}}{2})\Gamma(\frac{3}{2}+\ell)} {}_2F_1\left(\frac{\ell}{2}-\frac{n_{\text{DE}}}{4}, \frac{1}{2}+\frac{\ell}{2}-\frac{n_{\text{DE}}}{4}; \frac{3}{2}+\ell; \frac{1}{\mu_0^2}\right)}. \tag{G.22}$$

G.3 Limiting case

We can study the limit where $\mu_0 \to 1$ to check our result. From [97] we know that in this limit the integral should reduce to,

$$\int_{-1}^{1} d\mu (1-\mu)^{\frac{n_{\text{DE}}}{2}} \mathcal{P}_\ell(\mu) = (-1)^\ell 2^{1+\frac{n_{\text{DE}}}{2}} \frac{\Gamma(1+\frac{n_{\text{DE}}}{2})^2}{\Gamma(1+\frac{n_{\text{DE}}}{2}-\ell)\Gamma(2+\ell+\frac{n_{\text{DE}}}{2})}. \tag{G.23}$$

In this case we can use Gauss summation theorem (see e.g. [64]) that states,

$${}_2F_1(a,b;c;1) = \frac{\Gamma(c)\Gamma(c-a-b)}{\Gamma(c-a)\Gamma(c-b)}. \tag{G.24}$$

Applying this to (G.22) in the limit $\mu_0 \to 1$ then yields,

$$\tilde{I}(\mu_0 \to 1) = \sqrt{\pi} 2^{-\ell} \frac{\Gamma\left(-\frac{n_{\text{DE}}}{2}+\ell\right)\Gamma(1+\frac{n_{\text{DE}}}{2})}{\Gamma(-\frac{n_{\text{DE}}}{2})\Gamma(\frac{3}{2}+\frac{\ell}{2}+\frac{n_{\text{DE}}}{4})\Gamma(1+\frac{\ell}{2}+\frac{n_{\text{DE}}}{4})}. \tag{G.25}$$

we combine the denominator using Gauss multiplication theorem to obtain,

$$\tilde{I}(\mu_0 \to 1) = 2^{1+\frac{n_{\rm DE}}{2}} \frac{\Gamma\left(-\frac{n_{\rm DE}}{2}+\ell\right)\Gamma(1+\frac{n_{\rm DE}}{2})}{\Gamma(-\frac{n_{\rm DE}}{2})\Gamma(2+\ell+\frac{n_{\rm DE}}{2})}. \tag{G.26}$$

We can simplify this some more by using Euler's reflection theorem (see e.g. [64]). Eulers reflection theorem applied to our case states,

$$\Gamma(-\frac{n_{\rm DE}}{2}) = \frac{\pi}{\sin(-\frac{n_{\rm DE}\pi}{2})}\frac{1}{\Gamma(1+\frac{n_{\rm DE}}{2})} \quad \text{and} \quad \Gamma(-\frac{n_{\rm DE}}{2}+\ell) = \frac{\pi}{\sin(-\frac{n_{\rm DE}\pi}{2}+\ell\pi)}\frac{1}{\Gamma(1+\frac{n_{\rm DE}}{2}-\ell)}, \tag{G.27}$$

we can divide the right equation by the left equation and simplify the sine terms to $(-1)^\ell$,

$$\frac{\Gamma(-\frac{n_{\rm DE}}{2}+\ell)}{\Gamma(-\frac{n_{\rm DE}}{2})} = \frac{\sin\left(-\frac{n_{\rm DE}\pi}{2}\right)}{\sin\left(-\frac{n_{\rm DE}\pi}{2}+\ell\pi\right)}\frac{\Gamma(1+\frac{n_{\rm DE}}{2})}{\Gamma(1+\frac{n_{\rm DE}}{2}-\ell)} = (-1)^\ell\frac{\Gamma(1+\frac{n_{\rm DE}}{2})}{\Gamma(1+\frac{n_{\rm DE}}{2}-\ell)}. \tag{G.28}$$

This gives us the following expression for the integral in the limit,

$$\tilde{I}(\mu_0 \to 1) = (-1)^\ell 2^{1+\frac{n_{\rm DE}}{2}} \frac{\Gamma(1+\frac{n_{\rm DE}}{2})^2}{\Gamma(1+\frac{n_{\rm DE}}{2}-\ell)\Gamma(2+\ell+\frac{n_{\rm DE}}{2})} \tag{G.29}$$

Which matches the result obtained by [97].

Acknowledgments

With this master's thesis, I will have finished my degree in theoretical physics. For this I have many people to thank.

First, I am grateful to my daily supervisor Enis Belgacem. He spent a lot of time and detail on my supervision. He was always willing to make extra time for me when I was stuck, leading to many discussions in his office. I genuinely enjoyed these discussions and they greatly improved my understanding of cosmology. Thank you Enis, it has been a pleasure!

I am also indebted to my supervisor Elisa Chisari, who introduced me to Enis, and thereby this project, and was also actively involved. I am grateful to have done both my bachelor's as master's thesis with her involved. Her critical insights and knowledge of (observational) cosmology were very helpful and a valuable contribution to this work. I also directly felt at home in her group, which I was happy to be a part of. I would also like to thank my second supervisor Tomislav Prokopec. 'Second' supervisor does not do justice to his role in this project, as he actively participated in our meetings, offering many insights or ideas. I could always count on his unwavering enthusiasm for theoretical physics and his creative way of thinking.

I would also like to thank the members of the Large Scale Structure group; I always enjoyed the weekly updates and I learned a lot about the various aspects of (observational) cosmology from the discussions we had.

On a more personal note, I would like to thank my study group during this master, consisting of Iris, Thijs, Justus, Franca, Olaf, Lucas, Margot and Salma, for their support over the last two years. Especially during lockdown times, our teams calls kept me sane. On a similar note, I would like to thank my friends Iman and Eva. I was lucky enough to write my thesis around the same time as them. Their company was a stable factor during this thesis and the many coffee and lunch breaks kept me motivated.

Last but not least, I would like to thank Laura, for moral support and for always believing in me.

References

[1] N. Aghanim et al. Planck 2018 results. *Astronomy & Astrophysics*, 641:A6, Sep 2020.

[2] Adam G. Riess et al. A 2.4% determination of the local value of the Hubble Constant. *The Astrophysical Journal*, 826(1):56, jul 2016.

[3] Adam G. Riess et al. Cosmic distances calibrated to 1% precision with gaia EDR3 parallaxes and hubble space telescope photometry of 75 milky way cepheids confirm tension with LCDM. *The Astrophysical Journal Letters*, 908(1):L6, feb 2021.

[4] Catherine Heymans et al. KiDS-1000 cosmology: Multi-probe weak gravitational lensing and spectroscopic galaxy clustering constraints. *Astronomy and Astrophysics*, 646:A140, feb 2021.

[5] T. M. C. Abbott et al. Dark energy survey year 3 results: Cosmological constraints from galaxy clustering and weak lensing. *Physical Review D*, 105(2), jan 2022.

[6] Adam G. Riess et al. Observational Evidence from Supernovae for an Accelerating Universe and a Cosmological Constant. *The Astronomical Journal*, 116(3):1009–1038, Sep 1998.

[7] S. Perlmutter et al. Measurements of Omega and Lambda from 42 High-Redshift Supernovae. *Astrophysical Journal*, 517(2):565–586, June 1999.

[8] Steven Weinberg. The cosmological constant problem. *Rev. Mod. Phys.*, 61:1–23, Jan 1989.

[9] Austin Joyce, Lucas Lombriser, and Fabian Schmidt. Dark energy versus modified gravity. *Annual Review of Nuclear and Particle Science*, 66(1):95–122, Oct 2016.

[10] Shinji Tsujikawa. Quintessence: a review. *Classical and Quantum Gravity*, 30(21):214003, Oct 2013.

[11] Tessa Baker, Pedro G. Ferreira, and Constantinos Skordis. The parameterized post-Friedmann framework for theories of modified gravity: Concepts, formalism, and examples. *Physical Review D*, 87(2), Jan 2013.

[12] Varun Sahni and Alexei A. Starobinsky. The Case for a positive cosmological Lambda term. *Int. J. Mod. Phys. D*, 9:373–444, 2000.

[13] C. Armendariz-Picon, Viatcheslav F. Mukhanov, and Paul J. Steinhardt. A Dynamical solution to the problem of a small cosmological constant and late time cosmic acceleration. *Phys. Rev. Lett.*, 85:4438–4441, 2000.

[14] Licia Verde, Tommaso Treu, and Adam G. Riess. Tensions between the early and late universe. *Nature Astronomy*, 3(10):891–895, sep 2019.

[15] Eleonora Di Valentino et al. In the realm of the Hubble tension—a review of solutions. *Classical and Quantum Gravity*, 38(15):153001, jul 2021.

[16] Eleonora Di Valentino, Alessandro Melchiorri, and Joseph Silk. Reconciling planck with the local value of h_0 in extended parameter space. *Physics Letters B*, 761:242–246, oct 2016.

[17] Eleonora Di Valentino, Alessandro Melchiorri, Olga Mena, and Sunny Vagnozzi. Interacting dark energy in the early 2020s: A promising solution to the H_0 and cosmic shear tensions. *Physics of the Dark Universe*, 30:100666, December 2020.

[18] Xiaolei Li, Arman Shafieloo, Varun Sahni, and Alexei A. Starobinsky. Revisiting metastable dark energy and tensions in the estimation of cosmological parameters. *The Astrophysical Journal*, 887(2):153, dec 2019.

[19] Kyriakos Vattis, Savvas M. Koushiappas, and Abraham Loeb. Dark matter decaying in the late universe can relieve the H_0 tension. *Phys. Rev. D*, 99:121302, Jun 2019.

[20] J. Colin Hill, Evan McDonough, Michael W. Toomey, and Stephon Alexander. Early dark energy does not restore cosmological concordance. *Physical Review D*, 102(4), aug 2020.

[21] Tanvi Karwal and Marc Kamionkowski. Dark energy at early times, the Hubble parameter, and the string axiverse. *Physical Review D*, 94(10), nov 2016.

[22] Vivian Poulin, Tristan L. Smith, Tanvi Karwal, and Marc Kamionkowski. Early dark energy can resolve the hubble tension. *Physical Review Letters*, 122(22), jun 2019.

[23] Karsten Jedamzik and Levon Pogosian. Relieving the Hubble Tension with Primordial Magnetic Fields. *Physical Review Letters*, 125(18), oct 2020.

[24] Will J. Percival et al. The Shape of the Sloan Digital Sky Survey Data Release 5 Galaxy Power Spectrum. *The Astrophysical Journal*, 657(2):645–663, mar 2007.

[25] Daniel Baumann. TASI Lectures on Inflation, 2009.

[26] D. Glavan, T. Prokopec, and V. Prymidis. Backreaction of a massless minimally coupled scalar field from inflationary quantum fluctuations. *Physical Review D*, 89(2), Jan 2014.

[27] D. Glavan, T. Prokopec, and D.C. van der Woude. Late-time quantum backreaction from inflationary fluctuations of a nonminimally coupled massless scalar. *Physical Review D*, 91(2), Jan 2015.

[28] D. Glavan, T. Prokopec, and T. Takahashi. Late-time quantum backreaction of a very light nonminimally coupled scalar. *Physical Review D*, 94(8), Oct 2016.

[29] D Glavan, T Prokopec, and A. A. Starobinsky. Stochastic dark energy from inflationary quantum fluctuations. *The European Physical Journal C*, 78(5), May 2018.

[30] Enis Belgacem and Tomislav Prokopec. Quantum origin of dark energy and the Hubble tension. *Physics Letters B*, 831:137174, August 2022.

[31] Enis Belgacem and Tomislav Prokopec. Spatial correlations of dark energy from quantum fluctuations in inflation. *arXiv e-prints*, page arXiv:2209.01601, September 2022.

[32] Željko Ivezić et al. LSST: From Science Drivers to Reference Design and Anticipated Data Products. *Astrophysical Journal*, 873(2):111, March 2019.

[33] Misao Sasaki. The magnitude-redshift relation in a perturbed Friedmann universe. *MNRAS*, 228:653–669, October 1987.

[34] Camille Bonvin, Ruth Durrer, and M. Alice Gasparini. Fluctuations of the luminosity distance. *Physical Review D*, 73(2), jan 2006.

[35] Sang Gyu Biern and Jaiyul Yoo. Correlation function of the luminosity distances. *Journal of Cosmology and Astroparticle Physics*, 2017(09):026–026, sep 2017.

[36] Alice Garoffolo et al. Detecting dark energy fluctuations with gravitational waves. *Physical Review D*, 103(8), apr 2021.

[37] Asantha Cooray, Daniel E Holz, and Robert Caldwell. Measuring dark energy spatial inhomogeneity with supernova data. *Journal of Cosmology and Astroparticle Physics*, 2010(11):015–015, nov 2010.

[38] C. J. G. Vedder, E. Belgacem, N. E. Chisari, and T. Prokopec. Fluctuating Dark Energy and the Luminosity Distance. *arXiv e-prints*, page arXiv:2209.00440, September 2022.

[39] Edwin Hubble. A Relation between Distance and Radial Velocity among Extra-Galactic Nebulae. *Proceedings of the National Academy of Science*, 15(3):168–173, March 1929.

[40] Alan H. Guth. Inflationary universe: A possible solution to the horizon and flatness problems. *Phys. Rev. D*, 23:347–356, Jan 1981.

[41] A. D. Linde. A new inflationary universe scenario: A possible solution of the horizon, flatness, homogeneity, isotropy and primordial monopole problems. *Physics Letters B*, 108(6):389–393, February 1982.

[42] Andreas Albrecht and Paul J. Steinhardt. Cosmology for grand unified theories with radiatively induced symmetry breaking. *Phys. Rev. Lett.*, 48:1220–1223, Apr 1982.

[43] Scott Dodelson and Fabian Schmidt. *Modern cosmology*. Academic Press, 2020.

[44] Antonio Riotto. Inflation and the theory of cosmological perturbations. *ICTP Lect. Notes Ser.*, 14:317–413, 2003.

[45] Daniel Baumann. TASI Lectures on Primordial Cosmology, 2018.

[46] Adam G. Riess et al. Large Magellanic Cloud Cepheid Standards Provide a 1 percent Foundation for the Determination of the Hubble Constant and Stronger Evidence for Physics beyond ΛCDM. *The Astrophysical Journal*, 876(1):85, May 2019.

[47] G. E. Addison, D. J. Watts, C. L. Bennett, M. Halpern, G. Hinshaw, and J. L. Weiland. Elucidating ΛCDM: Impact of Baryon Acoustic Oscillation Measurements on the Hubble Constant Discrepancy. *Astrophys. J.*, 853(2):119, 2018.

[48] Nils Schöneberg, Julien Lesgourgues, and Deanna C. Hooper. The BAO+BBN take on the Hubble tension. *Journal of Cosmology and Astroparticle Physics*, 2019(10):029–029, oct 2019.

[49] Éric Aubourg et al. Cosmological implications of baryon acoustic oscillation measurements. *Phys. Rev. D*, 92(12):123516, 2015.

[50] Licia Verde, Jose Luis Bernal, Alan F. Heavens, and Raul Jimenez. The length of the low-redshift standard ruler. *Mon. Not. Roy. Astron. Soc.*, 467(1):731–736, 2017.

[51] T. M. C. Abbott et al. Dark Energy Survey Year 1 Results: A Precise H0 Estimate from DES Y1, BAO, and D/H Data. *Mon. Not. Roy. Astron. Soc.*, 480(3):3879–3888, 2018.

[52] Kenneth C. Wong et al. HoLiCOW – XIII. A 2.4 per cent measurement of H0 from lensed quasars: 5.3σ tension between early- and late-Universe probes. *Mon. Not. Roy. Astron. Soc.*, 498(1):1420–1439, 2020.

[53] Wendy L. Freedman, Barry F. Madore, Taylor Hoyt, In Sung Jang, Rachael Beaton, Myung Gyoon Lee, Andrew Monson, Jill Neeley, and Jeffrey Rich. Calibration of the Tip of the Red Giant Branch (TRGB). 2 2020.

[54] Caroline D. Huang et al. A Near-infrared Period–Luminosity Relation for Miras in NGC 4258, an Anchor for a New Distance Ladder. *Astrophys. J.*, 857(1):67, 2018.

[55] Pablo Lemos, Elizabeth Lee, George Efstathiou, and Steven Gratton. Model independent H(z) reconstruction using the cosmic inverse distance ladder. *MNRAS*, 483(4):4803–4810, March 2019.

[56] Stephen M. Feeney et al. Prospects for Resolving the Hubble Constant Tension with Standard Sirens. *Physical Review Letters*, 122(6), feb 2019.

[57] Mikhail M. Ivanov, Evan McDonough, J. Colin Hill, Marko Simonović, Michael W. Toomey, Stephon Alexander, and Matias Zaldarriaga. Constraining Early Dark Energy with Large-Scale Structure. *Phys. Rev. D*, 102(10):103502, 2020.

[58] Rong-Gen Cai, Zong-Kuan Guo, Li Li, Shao-Jiang Wang, and Wang-Wei Yu. Chameleon dark energy can resolve the Hubble tension. *Physical Review D*, 103(12), jun 2021.

[59] Valerio Marra and Leandros Perivolaropoulos. Rapid transition of Geff at zt$\simeq$0.01 as a possible solution of the Hubble and growth tensions. *Physical Review D*, 104(2), jul 2021.

[60] George Efstathiou. To H0 or not to H0? *Monthly Notices of the Royal Astronomical Society*, 505(3):3866–3872, jun 2021.

[61] Wendy L. Freedman. Measurements of the Hubble Constant: Tensions in Perspective. *ApJ*, 919(1):16, September 2021.

[62] Enrico Barausse, Sabino Matarrese, and Antonio Riotto. Effect of inhomogeneities on the luminosity distance-redshift relation: Is dark energy necessary in a perturbed universe? *Physical Review D*, 71(6), mar 2005.

[63] Matt Visser. Jerk and the cosmological equation of state. *Class. Quant. Grav.*, 21:2603–2616, 2004.

[64] *NIST Digital Library of Mathematical Functions*. http://dlmf.nist.gov/, Release 1.1.5 of 2022-03-15, 2022. F. W. J. Olver, A. B. Olde Daalhuis, D. W. Lozier, B. I. Schneider, R. F. Boisvert, C. W. Clark, B. R. Miller, B. V. Saunders, H. S. Cohl, and M. A. McClain, eds.

[65] Jaiyul Yoo, A. Liam Fitzpatrick, and Matias Zaldarriaga. New perspective on galaxy clustering as a cosmological probe: General relativistic effects. *Physical Review D*, 80(8), oct 2009.

[66] Jaiyul Yoo. General relativistic description of the observed galaxy power spectrum: Do we understand what we measure? *Physical Review D*, 82(8), oct 2010.

[67] Camille Bonvin. Isolating relativistic effects in large-scale structure. *Classical and Quantum Gravity*, 31(23):234002, nov 2014.

[68] R. Sachs. Gravitational Waves in General Relativity. VI. The Outgoing Radiation Condition. *Proceedings of the Royal Society of London Series A*, 264(1318):309–338, November 1961.

[69] Camille Bonvin. Effect of peculiar motion in weak lensing. *Physical Review D*, 78(12), dec 2008.

[70] David J. Bacon, Sambatra Andrianomena, Chris Clarkson, Krzysztof Bolejko, and Roy Maartens. Cosmology with doppler lensing. *Monthly Notices of the Royal Astronomical Society*, 443(3):1900–1915, jul 2014.

[71] T. J. Broadhurst, A. N. Taylor, and J. A. Peacock. Mapping cluster mass distributions via gravitational lensing of background galaxies. *The Astrophysical Journal*, 438:49, jan 1995.

[72] R. Moessner, B. Jain, and J. V. Villumsen. The effect of weak lensing on the angular correlation function of faint galaxies. *Monthly Notices of the Royal Astronomical Society*, 294(2):291–298, feb 1998.

[73] D. Nelson Limber. The Analysis of Counts of the Extragalactic Nebulae in Terms of a Fluctuating Density Field. *The Astrophysical Journal*, 117:134, January 1953.

[74] Nora Elisa Chisari et al. Core Cosmology Library: Precision Cosmological Predictions for LSST. *The Astrophysical Journal Supplement Series*, 242(1):2, may 2019.

[75] Antony Lewis and Anthony Challinor. CAMB: Code for Anisotropies in the Microwave Background. Astrophysics Source Code Library, record ascl:1102.026, February 2011.

[76] Ariel Goobar and Bruno Leibundgut. Supernova cosmology: Legacy and future. *Annual Review of Nuclear and Particle Science*, 61(1):251–279, Nov 2011.

[77] The Dark Energy Survey Collaboration. The Dark Energy Survey, 2005.

[78] J. P. Bernstein et al. Supernova Simulations and Strategies for the Dark Energy Survey. *Astrophysical Journal*, 753(2):152, July 2012.

[79] Rachel Mandelbaum et al. The LSST Dark Energy Science Collaboration (DESC) Science Requirements Document. *arXiv preprint arXiv:1809.01669*, 2018.

[80] Jacobo Asorey, Martin Crocce, Enrique Gaztañaga, and Antony Lewis. Recovering 3D clustering information with angular correlations. *Monthly Notices of the Royal Astronomical Society*, 427(3):1891–1902, nov 2012.

[81] D. M. Scolnic, D. O. Jones, A. Rest, Y. C. Pan, et al. The Complete Light-curve Sample of Spectroscopically Confirmed SNe Ia from Pan-STARRS1 and Cosmological Constraints from the Combined Pantheon Sample. *ApJ*, 859(2):101, June 2018.

[82] R. Amanullah, E. Mörtsell, and A. Goobar. Correcting for lensing bias in the hubble diagram. *Astronomy and Astrophysics*, 397(3):819–823, jan 2003.

[83] A. A. Starobinsky. Stochastic de sitter (inflationary) stage in the early universe. In *Field Theory, Quantum Gravity and Strings*, pages 107–126. Springer Berlin Heidelberg, 1986.

[84] Giulia Gubitosi, Federico Piazza, and Filippo Vernizzi. The Effective Field Theory of Dark Energy. *JCAP*, 02:032, 2013.

[85] Clifford Cheung, Paolo Creminelli, A. Liam Fitzpatrick, Jared Kaplan, and Leonardo Senatore. The Effective Field Theory of Inflation. *JHEP*, 03:014, 2008.

[86] Michele Maggiore. *Gravitational Waves: Volume 2: Astrophysics and Cosmology*. Oxford University Press, 2018.

[87] Marek Demianski and Ester Piedipalumbo. Observational tests of the Glavan, Prokopec and Starobinsky model of dark energy. *The European Physical Journal C*, 79(7), jul 2019.

[88] Pavel Friedrich and Tomislav Prokopec. Scalar field dark matter in hybrid approach. *Physical Review D*, 96(8), oct 2017.

[89] Pavel Friedrich and Tomislav Prokopec. Kinetic theory and classical limit for real scalar quantum field in curved spacetime. *Physical Review D*, 98(2), jul 2018.

[90] Pavel Friedrich and Tomislav Prokopec. Field-theoretic approach to large-scale structure formation. *Physical Review D*, 100(10), nov 2019.

[91] Steven Weinberg. *Cosmology*. OUP Oxford, 2008.

[92] Nora Elisa Chisari and Andrew Pontzen. Unequal time correlators and the zel'dovich approximation. *Physical Review D*, 100(2), jul 2019.

[93] Camille Bonvin, Chris Clarkson, Ruth Durrer, Roy Maartens, and Obinna Umeh. Cosmological ensemble and directional averages of observables. *Journal of Cosmology and Astroparticle Physics*, 2015(07):040–040, jul 2015.

[94] Pierre Fleury, Chris Clarkson, and Roy Maartens. How does the cosmic large-scale structure bias the Hubble diagram? *Journal of Cosmology and Astroparticle Physics*, 2017(03):062–062, mar 2017.

[95] Jaiyul Yoo, Ermis Mitsou, Yves Dirian, and Ruth Durrer. $\bar{T}$: A New Cosmological Parameter? *Physical Review D*, 100(6), sep 2019.

[96] Jaiyul Yoo, Ermis Mitsou, Nastassia Grimm, Ruth Durrer, and Alexandre Refregier. Cosmological information contents on the light-cone. *Journal of Cosmology and Astroparticle Physics*, 2019(12):015–015, dec 2019.

[97] Izrail Solomonovich Gradshteyn and Iosif Moiseevich Ryzhik. *Table of integrals, series, and products*. Academic press, 2014.